Gating of the ClC-1 Chloride Channel

Michael Duffield

Discipline of Physiology

School of Molecular and Biomedical Science

University of Adelaide

Submitted for the degree of

Doctor of Philosophy

Table of Contents

Table of Figures

Abstract

The ClC-1 chloride channel, a dimeric channel with two ion conducting pores, has two unique gating processes. The 'fast' gating processes open and close each pore independently, whereas the 'common' gate acts on both pores simultaneously. Although the crystal structure of two prokaryotic ClC channels has recently been solved there is still little knowledge of the parts of the channel involved in channel gating. The research in this thesis has used mutagenesis and electrophysiological techniques to provide significant further insight into the structure and function of the ClC-1 common gate.

ClC-1 mutations known to cause the dominant form of the muscle hyperexcitability disorder myotonia, and which are therefore likely to affect the common gating process, cluster in the H, I, P, and Q helices, which are at the interface of the ClC-1 dimer, as well as the G helix, which is situated immediately behind the H and I helices. Introduction of mutations into the G, H, and I helices of ClC-1 causes changes in channel gating, in most cases affecting the common gating process. Mutations in the P and Q helices also affect channel gating, again primarily through affects on ClC-1 common gating, although mutations in P and Q generally have less affect on ClC-1 gating than those in G, H and I. This research has also looked at the interaction of zinc with the ClC-1 channel, showing that zinc is able to attenuate currents through ClC-1 by stabilising the closed state of the channel, rather than through mechanisms such as occlusion of the channel pore. Furthermore, the interaction of zinc with mutant channels exhibiting altered common gating suggests that zinc can stabilise the closed state of the channel common gate.

Declaration

This thesis contains no material which has been accepted for the award of any other degree or diploma in any university or other tertiary institution and, to the best of my knowledge and belief, contains no material previously published or written by another person, except where due reference has been made in the text.

I give consent to this copy of my thesis, when deposited in the University Library, being available for loan and photocopying

Signed: 25/11/05

Acknowledgments

This thesis is dedicated to all those who have touched my life…

For my supervisors, and other members of the lab, whose unwavering loyalty to deciphering the mysteries of science has supported me through the highs and lows of this research…

For my family and friends, whose love and friendship has supported me during my studies, and has been so responsible bringing me to this point in life, and making me the person that I am…

Chapter I: Literature Review

I-1 Introduction

Research over the past five years has greatly enhanced our knowledge of the structural basis of ion channel activity, and particularly those structural features responsible for controlling ion permeation in channels such as the KcsA potassium channel (Doyle et al., 1998). This review, however, concentrates primarily on the investigation of ion channel gating mechanisms, which for many channels, including the ClC family, still remain a great unknown.

I-2 ClC Chloride Channels

The ClC family of ion channels are chloride conducting channels which are found in species ranging from mammals, plants and yeasts to prokaryotes. The ClC channel family was first identified through the cloning of the ClC-0 channel from the electric ray *Torpedo marmorata* (Jentsch et al., 1990), where it is found in high concentrations within the electric organ. Since then numerous other ClC channels have been found in a range of both eukaryotic and prokaryotic species. There are currently 9 known mammalian ClC channels, ClC-1, ClC-2, ClC-3, ClC-4, ClC-5, ClC-6, ClC-7, ClC-Ka and ClC-Kb (see Jentsch et al., 2002). Although all these ClC channels show some degree of sequence similarity, there are significant contrasts between them in terms of their tissue expression patterns, their functions, and even their sub-cellular localisation. In fact, recent research has even thrown doubt on the assumption that all members of the ClC family function as ion channels (Accardi and Miller, 2004), showing that at least one bacterial ClC 'channel'

in fact functions as an exchange transporter. Although this recent finding shows that the description of ClC proteins as members of a 'chloride channel family' is actually incorrect, this description is in common usage, and is used below for the sake of brevity, as well as to maintain clarity and consistency with the published literature. At present no mammalian ClC family members have been shown to have exchange transporter activity, although this function remains a possibility for some of the less well-characterised ClC proteins.

Members of the ClC channel family have a variety of important physiological roles in plant, animal and bacterial species. The nine mammalian ClC channels have been investigated to varying degrees. Figure I-1 shows how closely related these nine channels are, based on sequence homology, as well as summarising the known expression patterns, functions and diseases associated with each channel type.

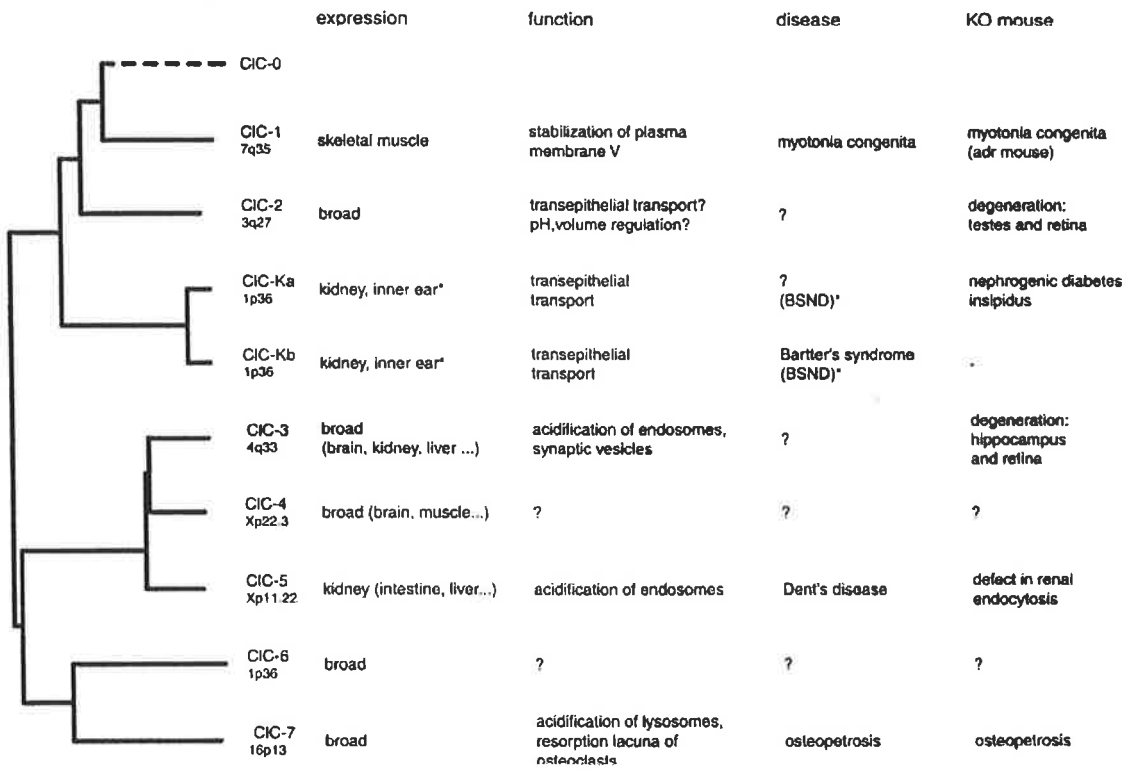

Figure I-1: The nine known mammalian ClC family members
Figure indicates the relationship between the nine mammalian ClC channels based on protein homology. Also shown for each channel is the human chromosome location, tissue expression pattern, function, the human disease(s) associated with each channel, and the phenotype of the knock-out (KO) mouse model of the corresponding channel.
Asterisk (*) indicates that mutations in the ClC-K β-subunit cause Barrter syndrome with sensorineural deafness (BSND) – see text for more details (from Jentsch et al., 2002).

Members of the first branch of mammalian ClC channels, that is ClC-1, ClC-2, ClC-Ka and ClC-Kb, are believed to be predominantly expressed in the plasma membrane, whilst channels from the other two branches, ClC-3, ClC-4, ClC-5, ClC-6 and ClC-7, are intracellularly expressed. As also shown in Figure I-1, to date defects in both the ClC-1 and ClC-K channels, as well as the intracellular ClC-5 and ClC-7 channels, have been linked to the occurrence of human disease states – again emphasising the importance of the ClC channels.

Of the four currently known plasma membrane expressed ClC channels – ClC-1, ClC-2, ClC-Ka and ClC-Kb – only the ClC-2 channel has a broad expression pattern. The precise function of this channel is as yet unknown, although is likely that it may play some role in transepithelial transport, and/or in pH or volume regulation of cell events. The ClC-Ka, ClC-Kb and ClC-1 channels show more localised expression than ClC-2, with the ClC-1 channel found in skeletal muscle, whilst the ClC-K channels are predominantly found in the kidney.

It is the ClC-1 channel that forms the primary focus of this thesis. As mentioned above, ClC-1 is primarily expressed in skeletal muscle (Steinmeyer et al., 1991b), where it contributes 70 – 80 % of resting membrane conductance (Bretag, 1987).

ClC-1, like other ClC channels, is believed to be a dimer (Fahlke et al., 1997b) (see I-3 below), with non-stationary noise analysis (Pusch et al., 1994) and single channel recordings (Saviane et al., 1999) showing that each pore has a conductance in the ~1 pS range. In this conductance range single channel recordings under physiological conditions are impossible, so the majority of research into the ClC-1 channel has been carried out on preparations utilising whole-cell currents (eg. two-electrode voltage clamp, whole cell patch clamp, inside-out patch clamp).

Electrophysiological examination of ClC-1 currents shows that ClC-1 mediates currents that are inwardly rectifying, and that are depolarisation activated (Steinmeyer et

al., 1991b). Gating of ClC-1 is affected by both intracellular and extracellular anions (Rychkov et al., 1998), as well as pH (Rychkov et al., 1996). Anion substitution experiments suggest that the ion permeation pathway contains two anion binding sites (Rychkov et al., 1996; Fahlke et al., 1997a; Rychkov et al., 1998; Rychkov et al., 2001).

The ClC-1 channel is responsible for the majority of the resting Cl^- conductance of skeletal muscle, stabilising the muscle membrane potential (Bretag, 1987). Consistent with this role, mutations in the ClC-1 channel have been found to be associated with the skeletal muscle hyperexcitability disorder myotonia (Koch et al., 1992).

The final two plasma membrane expressed channels, the ClC-K channels, are important for transepithelial transport in various parts of the kidney. Mutations in one of these channels, ClC-Kb, are associated with the occurrence of Bartter's syndrome, a severe salt-wasting disorder. Interestingly both ClC-K channels require the presence of an additional β-subunit, barttin, for proper expression (Estevez et al., 2001), the first example of a ClC β-subunit. Barttin is a relatively small protein, and has only two transmembrane domains. Co-expression of barttin with the ClC-K channels in heterologous expression systems leads to greatly enhanced ClC-K currents due to an increased expression of ClC-K channels at the cell surface (Estevez et al., 2001), suggesting that barttin may be important in regulation of ClC-K channel surface expression. Mutations in the barttin β-subunit are also related to the occurrence of Bartter's syndrome with sensorineural deafness, and with kidney disease (Birkenhäger et al., 2001).

Most of the intracellularly expressed ClC channels are broadly expressed throughout the body. The functions of the ClC-4 and ClC-6 channels remain to be elucidated, although it would seem likely that these channels play a role similar to that of ClC-3, ClC-5 and ClC-7, which are important in the acidification of intracellular organelles, such as endosomes and lysosomes. These channels allow the movement of the negatively charged chloride ion (Cl^-) as a counter-ion to the positively charged hydrogen

ion (H^+) – allowing the establishment of low pH in the intracellular organelles, without the simultaneous occurrence of large potential differences. Defects in ClC-5 have been linked to the occurrence of Dent's disease (Lloyd et al., 1996), a disorder in which proteinuria, hypercalciuria and hyperphosphaturia lead to secondary kidney stones, nephrocalcinosis and rickets (Wrong et al., 1994; Scheinman, 1998). ClC-7, whilst broadly expressed, appears to be of particular importance in the control of bone turnover, which is understandable given the importance of acidification in bone resorption by osteoclast cells. Mutations in this channel have been associated with the occurrence of osteopetrosis, a disorder in which thickening of bones occurs due to inhibited bone resorption, in knock-out mice, and in humans (Kornak et al., 2001).

I-3 Structure of ClC Channels

I-3-1 Early Model of ClC Transmembrane Topology

Initial hydropathy analysis of the ClC-0 channel showed the presence of 13 hydrophobic regions, labelled D1 through D13, that could conceivably form the transmembrane domains of the channel (Jentsch et al., 1990). A range of further biochemical investigations in ClC-0, ClC-1 and ClC-2, including site-directed mutagenesis (Gründer et al., 1992), glycosylation scanning and protease protection assays (Schmidt-Rose and Jentsch, 1997b), and cysteine modification studies (Fahlke et al., 1997c), further refined this model. These studies show that both the amino and carboxyl termini of ClC channels are intracellularly located (Gründer et al., 1992), and that D13 was not actually a transmembrane domain, but part of the intracellular carboxyl terminus of the channel. The D13 region is now recognised as one of two CBS domains present in the carboxyl tail of

all known mammalian ClC channels (Schmidt-Rose and Jentsch, 1997a). CBS domains, named after one of the proteins in which they are found – cystathionine-β-synthase – are present in a range of proteins (Bateman, 1997; Ponting, 1997), with a recent study suggesting that these regions form a binding site for adenosine derivatives (Scott et al., 2004). In addition, the D4 domain is relatively poorly conserved between ClC channel types, and evidence suggests that this region is located extracellularly (Schmidt-Rose and Jentsch, 1997b; Kurz et al., 1999). All of this evidence therefore led to the initial suggested ClC transmembrane topology, which has between 10-12 transmembrane domains (Figure I-2).

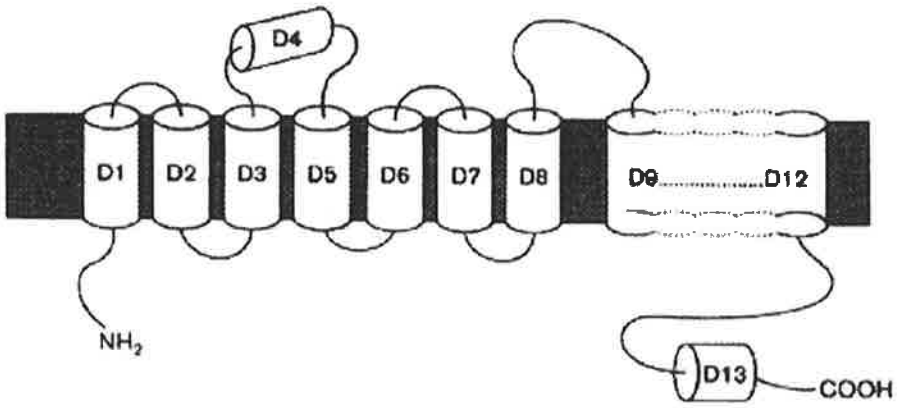

Figure I-2: Proposed transmembrane topology of ClC chloride channels
Hydrophobic domains are labelled D1 through D13 (from Jentsch, 1996; Schmidt-Rose and Jentsch, 1997b).

There were, however, still some problems with this proposed channel topology. The region of the channel in proximity to domains D3 to D5 was the subject of some controversy, with some studies providing evidence that D4 might in fact cross the cell membrane (Fahlke et al., 1997c). The transmembrane topology of the D9 to D12 region was also difficult to resolve. This region corresponds to a broad hydrophobic region in the ClC channels (Jentsch et al., 1990), and whilst it was shown that the beginning of D9 was extracellular (Kieferle et al., 1994; Middleton et al., 1994; Schmidt-Rose and Jentsch,

1997b), and the end of D12 intracellular (Middleton et al., 1996), the number of membrane crossings occurring between these was unable to be determined. These issues with the proposed ClC topology were not satisfactorily addressed until 2002, when the crystal structures of 2 prokaryotic ClC channels were solved (Dutzler et al., 2002). These structures show that the actual ClC channel topology is vastly different, not only to the previously predicted topology, but also to the topology of any other crystallised ion channel.

I-3-2 Dimeric, Double-Barrelled Structure

At the quaternary level of ClC channel structure there is much evidence that ClC channels exist as dimers. Sedimentation studies of ClC-0 (Middleton et al., 1994) and ClC-1 channels (Fahlke et al., 1997b) provide evidence that the naturally occurring form of these channels is dimeric. Electrophysiological studies investigating ClC-1 mutant/WT co-expression show current recordings that are best explained by the presence of ClC channels as a heteromultimer of two subunits (Fahlke et al., 1997b).

In addition to the evidence that ClC channels function as a dimer, there is also overwhelming evidence from electrophysiological studies that ClC channels are 'double barrelled', containing two independent conduction pathways, or pores. Analysis of single-channel currents from the ClC-0 channel reconstituted from the *Torpedo* electric organ shows currents consisting of long periods of zero current, interspersed with bursts of channel activity to one of two equally spaced conductance levels – either ~10 pS or ~20 pS (Miller, 1982; Hanke and Miller, 1983; Miller and White, 1984). Analysis of these currents led to the 'double barrel' model, which proposes that ClC-0 contains two identical pores, with the ~10 pS conductance level being the result of opening of a single pore, and the ~20 pS level from opening of both pores (Miller, 1982). The ClC-0, ClC-1 and ClC-2 channels have now all been studied at the single-channel level, with these three channels all showing

the presence these two equally spaced conductance levels (Ludewig et al., 1996; Middleton et al., 1996; Saviane et al., 1999; Weinreich and Jentsch, 2001). This in itself, however, does not prove the presence of two independent pores within a channel, and could be equally well explained by a channel having a single pore with multiple conductance states. In ClC-0 the two conductance levels observed in single channel recordings are extremely close to a ratio of 1:2 in current magnitude, which is unlikely to occur in a single pore with two subconductance states. Moreover, appearance of the two conductance levels follows a binomial distribution, as would be expected from independently gated pores (Miller, 1982; Hanke and Miller, 1983; Bauer et al., 1991; Middleton et al., 1994; Chen and Miller, 1996; Ludewig et al., 1997; Lin et al., 1999). It is also know that the disulfonic stilbene 4,4'-diisothiocyanatostilbene-2,2'-disulphonic acid (DIDS) initially causes a block of the largest conductance level, which is followed later by a block of the smaller level (Miller and White, 1984), again suggesting the presence of two pores which can be independently blocked, as opposed to a single pore. Further evidence comes from studies in which the single-channel properties of WT and mutant ClC-0 heteromers have been investigated. It is observed that mutant homomeric channels retain the two equally spaced conductance levels predicted by the double barrel model (Ludewig et al., 1996; Middleton et al., 1996). Co-expression of mutant/WT heteromers leads to single-channel recordings containing unequal conductance levels, which are of the same size as the conductance levels observed in the WT and mutant homomeric channels (Ludewig et al., 1996; Middleton et al., 1996). Finally, concatamers of ClC-0 with either ClC-1 or ClC-2 channels show the presence of a substate with conductance matching ClC-0, and another matching that of ClC-1 or ClC-2 (Weinreich and Jentsch, 2001). All of this evidence strongly suggests that ClC channels exist as dimers containing two independent conduction pathways. Given the ability to exchange channel pores, as observed with mutant/WT ClC-0 heteromers and ClC-0/ClC-1,

ClC-2 concatamers, these studies also suggest that the pores of ClC channels are contained within the individual subunits, and not formed by the interface of the two subunits.

Although evidence of the double-barrelled nature of ClC channels is strong, there was some opposition to this viewpoint. Based on concatameric ClC-1 constructs containing introduced cysteine residues Fahlke et al. (1998) suggested that equivalent residues within the two ClC subunits were located close together, and therefore likely to be located at the interface of the channel dimer. The assumption that these residues projected into the ClC-1 pore (Fahlke et al., 1998; Fahlke et al., 1997c) led to the conclusion that ClC channels, have a single pore formed at the interface of the two channel subunits. This argument obviously clashes strongly with the evidence supporting the double-barrelled model of ClC channels. The mutations used by Fahlke et al. (Fahlke et al., 1998), however, also affect the gating of the ClC-1 channel, and these affects on gating could also explain these results. Therefore almost all experimental evidence accumulated prior to 2001 either supported, or could be explained by, a model of ClC channels in which the channel is a dimer, with each subunit forming its own pore.

I-3-3 ClC Crystal Structures

In 2001 the controversy regarding the structure of ClC channels appeared to be close to over, with the first publication of a ClC crystal structure by Mindell et al. (2001) (Figure I-3). Although only a two-dimensional image at relatively low resolution (6.5 Å) this structure provided support for what had been previously deduced about ClC channel structures. As the figure shows, each individual ClC channel is symmetrical, confirming the dimeric nature of ClC channels predicted by previous sedimentation and electrophysiological studies (see I-3-2 above). In addition, off-axis regions of low electron density most likely reflects the presence of a kinked water-filled pore in each subunit (Mindell et al., 2001), supporting the already generally accepted double-barrelled model of

ClC (see I-3-2 above). The lack of a prominent region of low electron density at the axis of symmetry (Mindell et al., 2001) does not support the dimeric single-pored ClC model which had also been proposed (Fahlke et al., 1998).

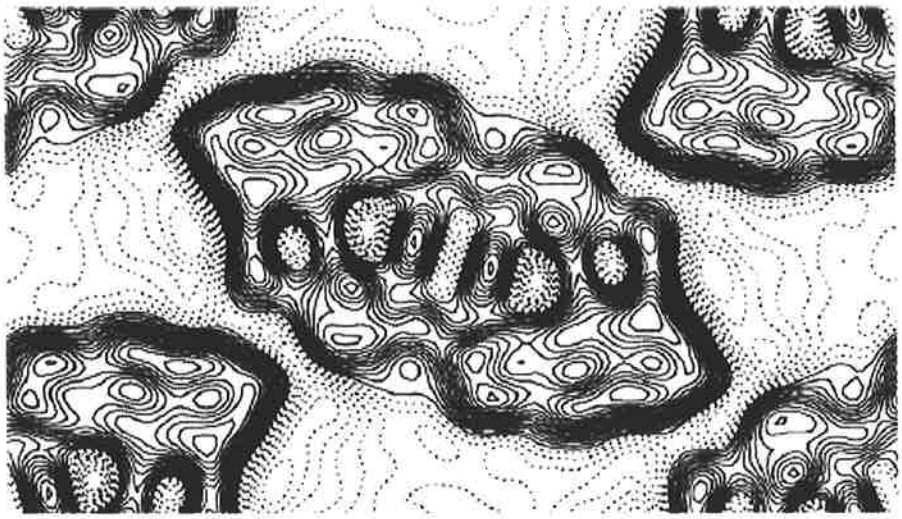

Figure I-3: Two-dimensional ClC crystal structure
Projection density map of EriC (*Escherichia coli* derived ClC channel) at 6.5 Å resolution (from Mindell et al., 2001).

Although providing much support for what had already been deduced about ClC channel structure, the crystallographic images obtained by Mindell et al. (Mindell et al., 2001) are only two-dimensional in nature. These structures are also of insufficient resolution to enable the identification of individual residues, or even helices, in the channel structure. It was, however, only a year later that Dutzler et al. (Dutzler et al., 2002) published the complete three-dimensional structure of ClC channels from *Salmonella enterica* serovar *typhimurium* and from *Escherichia coli*, at 3.0 and 3.5 Å resolution (Figure I-4). Again, as expected, this structure confirms the dimeric nature of the channel, with each channel displaying the two-fold symmetry of a dimer. These higher resolution structures also allow identification of the conduction pathway and selectivity filter within each dimer, again confirming the double-barrelled nature of the ClC channels (Dutzler et al., 2002). What was perhaps a more surprising finding from the high-resolution structure was the final identification of the ClC channel transmembrane topology (Figure I-5). As

this figure clearly shows, the actual topology of ClC channels is totally different, and far more complex, than the topology previously proposed (Figure I-2) (see I-3-1 above). The 13 domains previously identified by hydrophobicity scanning, with 10-12 transmembrane domains, are replaced by 18 α-helical regions (helices A-R). Each subunit also shows an internally repeating pattern, with the N-terminal half of the protein being structurally related to the C-terminal half. These similar repeated structures run antiparallel, such that related parts within each half-subunit have opposite orientations within the membrane (Figure I-6). This repeated pattern was not recognised previously from the amino-acid sequence of the channel protein. Looking at the three-dimensional structure of the channel (Figure I-4), it is seen that many of the ClC channel's 18 α-helices cross, or partly cross, the membrane. These α-helices are all of varying lengths, and are inserted into the membrane at various angles, rather than passing more perpendicularly through the membrane. This unusual structural arrangement of ClC channels, which is quite unlike that seen in other crystallised ion channel families, explains why previous structural and transmembrane topology predictions have been so inaccurate, although much of the information provided by these studies, and by electrophysiological studies, is supported and explained by the new ClC structure. It is, however, worth noting that this structure is derived from prokaryotic ClC channels, and as such is likely to show some differences to the structure of other ClC family members. The human ClC-1 channel, for example, contains nearly half of its sequence in intracellular structures formed by the N- and C-termini. None of this intracellular structure is visible from the prokaryotic channels so far crystallised, and it appears likely that the exact role(s) and structure of these intracellular channel regions will remain unknown until three-dimensional structures of these parts of the channel are obtained. Whatever the differences in structure between ClC family members it is still almost certain, due to the homology of ClC channels, that the basic

channel structure and the general positioning of the channel pores and conduction pathway will be consistent throughout all ClC channels.

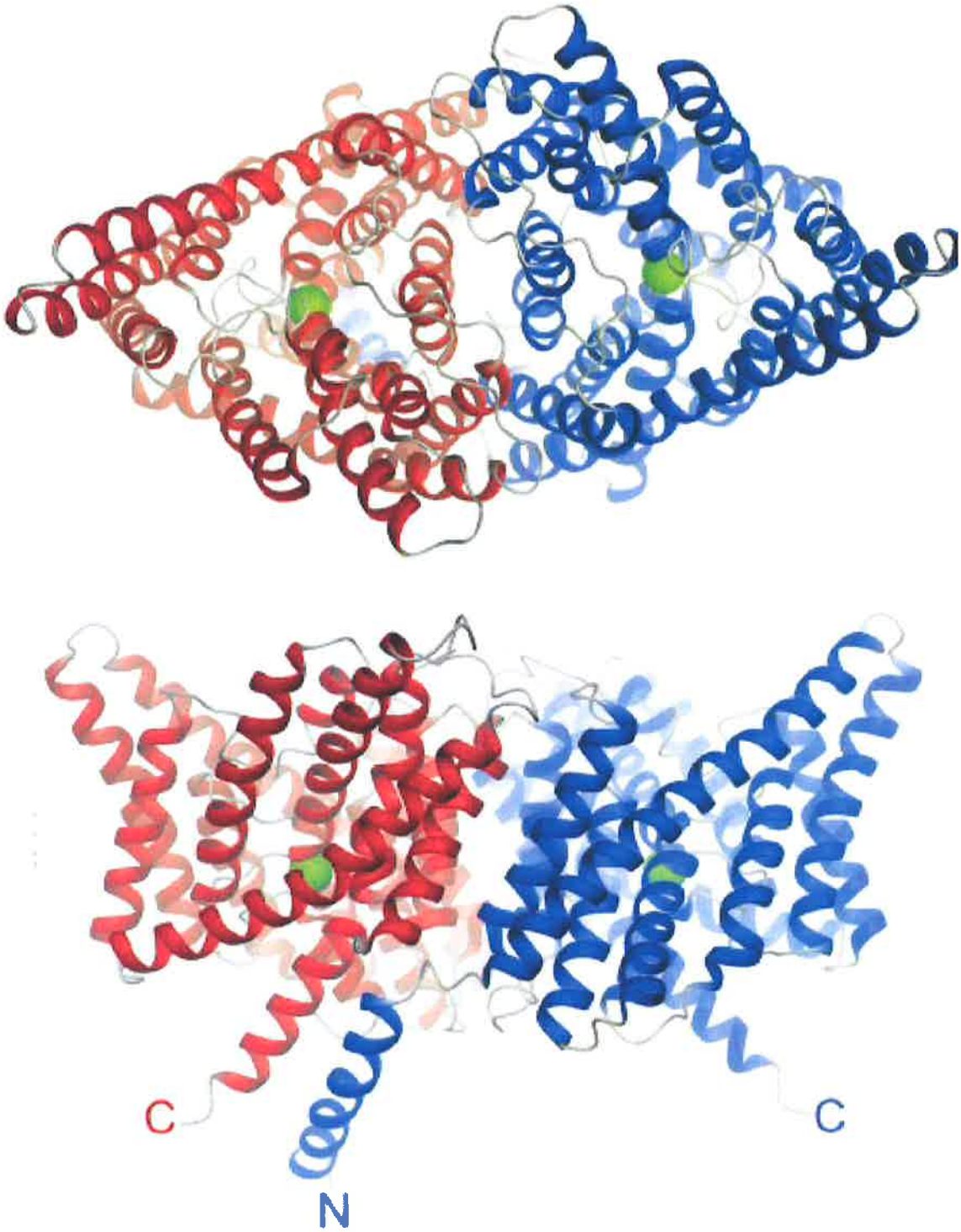

Figure I-4: Three-dimensional crystal structure of prokaryotic ClC channel
Ribbon representation of the structure of the S. typhimuruym derived ClC dimer, viewed from within the membrane with the extracellular side above (top), and from the extracellular side (bottom). The two subunits are coloured blue and red. Green spheres indicate the position of chloride ions within the structure (adapted from Dutzler et al., 2002).

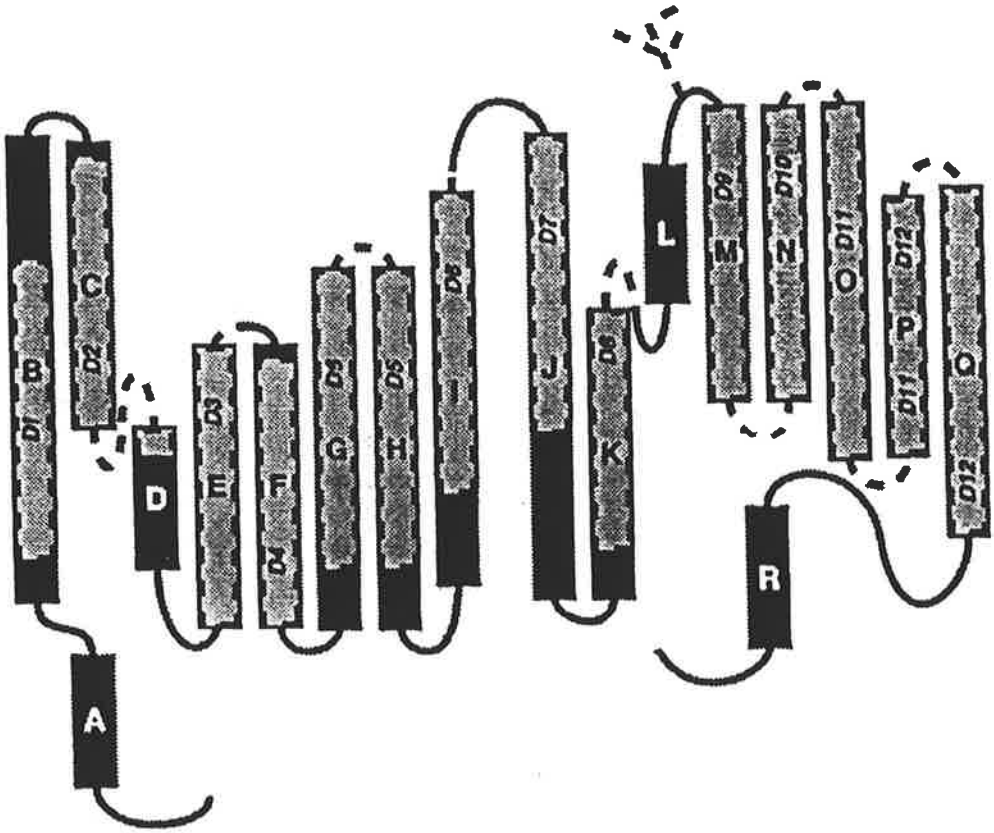

Figure I-5: ClC channel transmembrane topology
Transmembrane topology of ClC channels, based on the crystal structure of bacterial ClC channels produced by Dutzler et al., 2002. Shaded areas and dashed lines show the location of domains D1 to D12 in the previously proposed transmembrane topology (see Figure I-2) (from Jentsch et al., 2002).

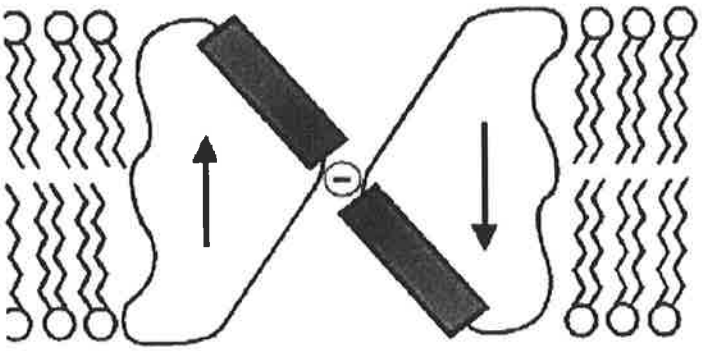

Figure I-6: Pore architecture of ClC channels
The pore architecture of each ClC monomer consists of similar halves, arranged with opposite orientations (as distinguished by arrows). This structure enables α-helix dipoles from opposite sides of the membrane to coordinate conduction of chloride ions through the channel (from Dutzler et al., 2002).

A more recent electrophysiological investigation of the ClC-ec1 channel from *Escherichia coli* (Accardi and Miller, 2004) has now shown the surprising result that this

channel is not in fact chloride channel, but a chloride exchange transporter. Although this finding does not throw doubt on the channel status of ClC-0, ClC-1 and ClC-2, it has implications for ClC-6 and ClC-7 which, prior to this, were also assumed to be chloride channels. This finding is particularly interesting as the ClC-ec1 structure has proved extremely useful in explaining observations made in the eukaryotic ClC channels – suggesting that very similar protein structures can form the basis of both channel and transporter activities.

I-4 Ion Channel Gating Mechanisms

Gating is the process whereby ion channels control the movement of ions through the conduction pathway, ensuring that ions are only allowed to pass through the channel under specific conditions. Such control of ion movement is vital to the proper functioning of ion channels, with processes such as action potential propagation relying on the precise regulation of the various ion movements involved. Ion channel gating can be controlled by various stimuli, including mechanical (eg. stretch and heat), electrical (potential difference) or chemical (eg. calcium or hormones) stimuli.

Although the stimuli resulting in channel gating are well known, the actual structural features that enable these stimuli to open and close ion channel conduction pathways are less well known. In more recent years methods such as x-ray crystallography have, however, given us some insight into the structural mechanisms of ion channel gating. These methods have shown that there is no single gating mechanism shared by all channel types, but rather a range of gating mechanisms that have evolved in different ion channel families. Currently known mechanisms of channel gating include 'ball and chain' inactivation gating (*Shaker* K+ channel), gating of potassium channels through helix tilting (caused by ligand binding, mechanical or electrical stimuli) and gating through helix

rotation (nicotinic acetylcholine receptor). These are almost certainly not the only mechanisms involved in channel gating, with gating mechanisms of many channels yet to be elucidated. Although the gating mechanisms of other ion channels have been postulated, this section of the review has concentrated on those channels for which detailed structural knowledge of gating mechanisms is available.

I-4-1 Ball and Chain Gating Mechanism

The 'ball and chain' mechanism was one of the first proposed mechanisms of ion channel gating. The mechanism was initially proposed to explain the inactivating process of sodium channels (Bezanilla and Armstrong, 1977), and later shown to occur in the *Shaker* potassium channel. In this process, channels are opened by membrane depolarisation, but stop conducting after a few milliseconds due to the actions of a separate inactivation gate. There is strong evidence that this inactivation gate is caused by a tethered ball and chain motif, formed from part of the channel's N-terminus, or from that of an associated subunit. After the channel is opened by a separate gating process, the tethered, cationic 'ball' peptide is able to insert and bind to the intracellular end of the channel pore, blocking ion conduction (Hoshi et al., 1990; Zagotta et al., 1990; Isacoff et al., 1991; MacKinnon et al., 1993; Lopez et al., 1994; Holmgren et al., 1996).

I-4-2 Helix Tilting Gating Mechanisms

Potassium channels have been a fruitful source of information on ion channel permeation and gating mechanisms since ion channels were first identified. The initial x-ray crystallographic structures of the bacterial KcsA channel (see Figure I-7, Doyle et al., 1998) provide vital information on the structure and permeation mechanisms of potassium channels, and the tetrameric cation channels in general, but less useful information on the

mechanism of gating in these channels. This is because the captured x-ray structure of KcsA only shows the channel in the closed state. In addition, the KcsA channel is a relatively simple ion channel, consisting primarily of the helices involved in channel pore formation, and lacking the gating domains, seen in more complex channels, whose role is to convert electrical or chemical stimuli into a mechanical response, opening the channel.

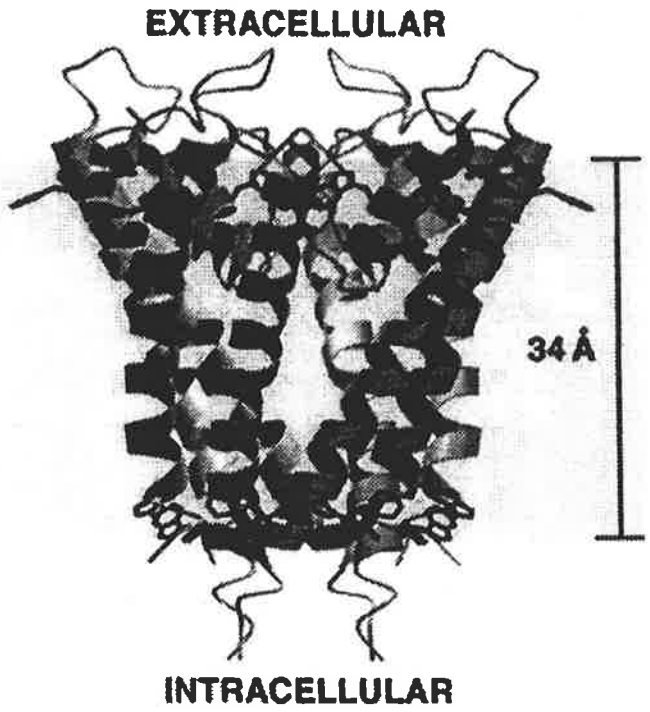

Figure I-7: Crystal structure of the KcsA potassium channel pore
Ribbon representation of the KcsA tetramer, showing the portion of channel embedded in the plasma membrane (from Doyle et al., 1998).

Since the initial crystallography of the KcsA channel however, further research and x-ray crystallography on a variety of related channels has provided much more information on the mechanisms underlying gating of members of tetrameric cation channel families. We now have good examples of how channels like these can be gated by electrical, chemical (ligand-binding) and mechanical stimuli. Again, however, it is unlikely that these known mechanisms of gating represent all of the gating mechanisms that are utilised by ion channels.

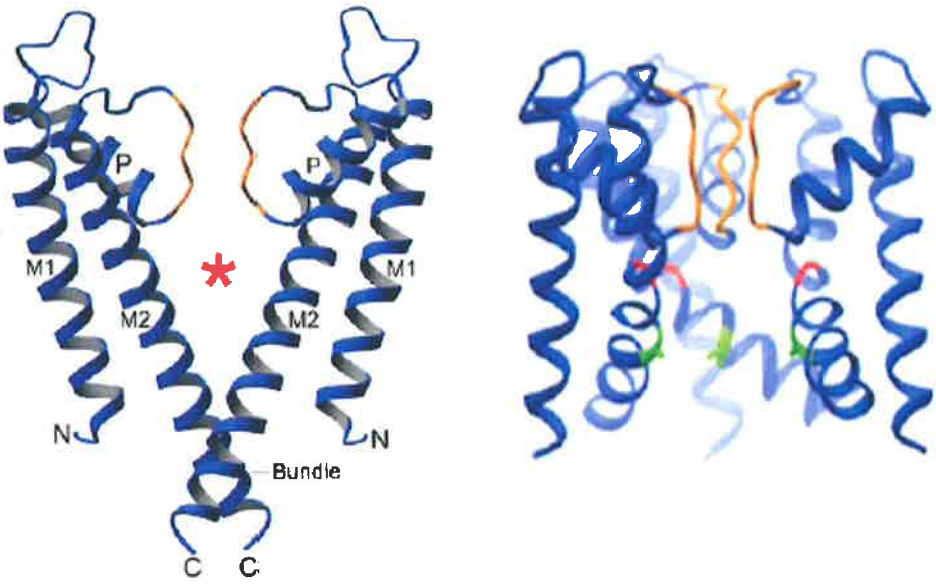

Figure I-8: Open and closed K+ channel states
(*Left*) Representation of two KcsA subunits in the closed channel (extracellular surface of channel at top). The figure illustrates the three α-helical segments - the outer helix (M1), pore helix (P) and inner helix (M2). The selectivity filter is shaded orange, and the central cavity of the channel is indicated by *.
(*Right*) Representation of three MthK subunits in the open channel state (extracellular surface of channel at top). The selectivity filter is shaded orange, the gating hinge glycine in red, and the amino acid at the narrowed point of the MthK intracellular pore in green (from Jiang et al., 2002b).

Recent x-ray crystallography of the MthK channel, a ligand gated potassium channel, has now provided images of the open-channel state of potassium channels (Jiang et al., 2002b). By comparing this with the KcsA channel structure (Doyle et al., 1998), it is possible to look at channel transitions which are likely to occur during the gating process (Figure I-8). The pore structure of potassium channels, and probably also of sodium and calcium channels, is formed by four subunits, each contributing two transmembrane helices and a 'pore loop' region (Doyle et al., 1998). The outer helix structure provides structural support for the pore, the pore loop region forms the selectivity filter of the channel, and the inner helices support the selectivity filter, as well as lining the inner vestibule of the channel. By comparing the open and closed channel states (Figure I-8) it is seen that potassium channel opening involves a tilting and hinging of the intracellular ends

of the inner and outer helices, such that the inner vestibule is widened. This widening allows potassium permeation to occur (Jiang et al., 2002b).

I-4-2-1 Ligand Induced Gating

The MthK channel from which the open-state potassium channel structure has been obtained (see I-4-2 above) is a calcium-gated potassium channel from *Methanobacterium thermoautotrophicum*. This channel consists of a pore region very similar to that seen in the KcsA channel (see I-4-2 above) (Doyle et al., 1998), which contains four subunits, each contributing an outer helix, inner helix and pore loop region. Unlike in the KcsA channel, however, there are also intracellular domains associated with this membrane region, which are responsible for regulating the potassium conductance of the MthK channel (RCK domains). These RCK domains are responsible for the gating of the MtHK channel in the presence of intracellular calcium. These domains form a 'gating ring' which is attached to the channel pore region on the intracellular side. The binding of intracellular calcium to sites on the RCK domains causes a conformational change in the structure of this gating ring. This is transferred to the channel pore region, causing tilting of the pore region inner and outer helices, as described in I-4-2 above, and resulting in opening of the channel conduction pathway (Figure I-9)(Jiang et al., 2002a). In the reverse process, disassociation of calcium from the RCK domains causes the conformation of the gating ring to revert, pulling the pore helices back to the closed channel state. Therefore, by linking the basic potassium channel structure seen in KcsA (Doyle et al., 1998) with the RCK domains, a ligand-gated potassium channel is produced – in the case of MthK, one in which gating is controlled by intracellular calcium.

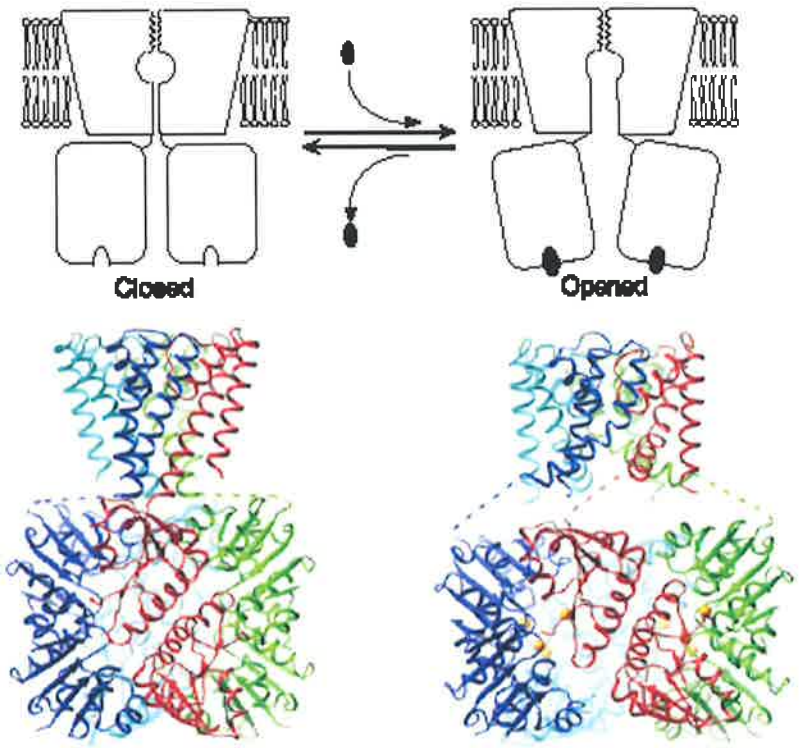

Figure I-9: MthK channel diagram showing pore and RCK regions
(*Top*) Diagrammatic representation of gating of ligand-gated ion channels. A ligand (black oval) binds to channel receptor domains, inducing opening of the channel.
(*Bottom*) Ribbon representations of proposed gating mechanisms of the MthK channel. Left model shows the crystal structure of the MthK channel in a closed conformation. Right model shows a hypothetical model of the MthK channel in an open conformation. Subunits and RCK domains are shown in different colours. Disordered linkers are shown as dashed lines, and calcium ions as yellow spheres (from Jiang et al., 2002a).

I-4-2-2 Electrically Induced Gating

The voltage-dependent cation channels (potassium, sodium and calcium) have very similar structures, consisting of a total of 24 hydrophobic segments. In voltage-gated potassium channels this structure is formed by the combination of four subunits, of which each contributes 6 transmembrane domains and an associated pore loop (Figure I-10). In the voltage-gated calcium and sodium channels there is only a single subunit, containing four homologous domains, each containing 6 transmembrane segments and a pore loop (Figure I-10). These 6 hydrophobic domains are referred to as domains S1 to S6.

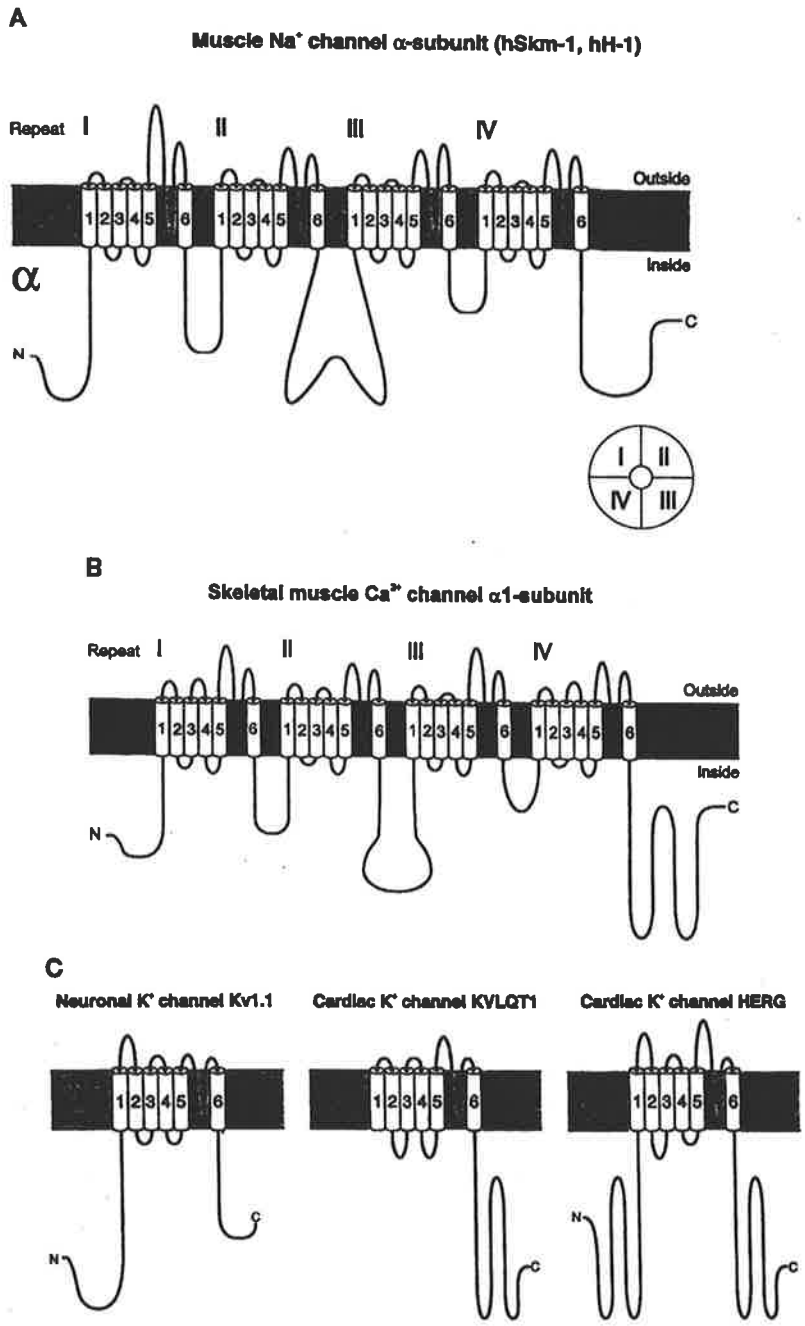

Figure I-10: Transmembrane topology of voltage-gated cation channels
Transmembrane topology of voltage-gated cation channels. (*A*) Skeletal (hSkm-1) and cardiac (hH-1) muscle sodium channel α-subunits, and (*B*), skeletal muscle calcium channel α1-subunits, consist of four repeats (I to IV) of six transmembrane domains (1 to 6), which assemble around a central pore, as shown in bottom right of *A*. (*C*) Neuronal (Kv1.1) and cardiac (KVLQT1, HERG) potassium channels consist of four identical subunits, each with six membrane spanning domains (1 to 6) (adapted from Lehmann-Horn and Rüdel, 1997).

Previous research has shown that the S5-S6 regions, including the pore loop region, form the pore and selectivity filter of these channels. These regions are equivalent to the two domains and pore regions seen in the simpler KcsA potassium channel (see I-4-2 above) (Doyle et al., 1998). The S1-S4 domains are unique to the voltage-gated channels, and form the voltage-sensing machinery. Of particular importance is the S4 region, which contains a number of charged amino acids known to be responsible for the majority of the gating charge required for voltage sensing (Aggarwal and MacKinnon, 1996; Seoh et al., 1996).

The original model of voltage-sensing in the voltage-dependent cation channels assumed that either translational or rotational movement of the charged S4 helices occurred in response to changes in transmembrane potential difference, and was responsible for the gating movements required to open or close the channel pore (Figure I-11) (Bezanilla, 2002; Gandhi and Isacoff, 2002; Horn, 2002). More recent structural evidence, however, has presented a new model of voltage-sensing, and of how this is linked to gating of these channels.

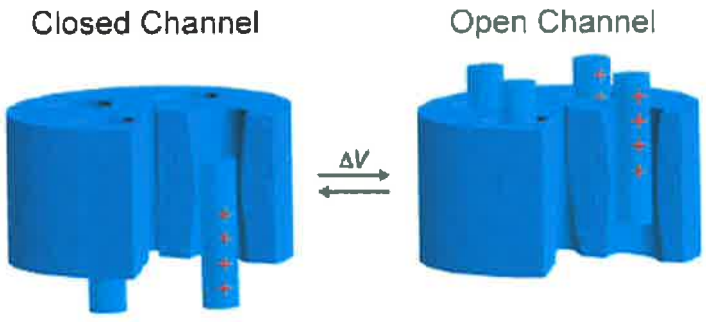

Figure I-11: Conventional model of voltage sensing
In this conventional gating model gating charges (represented by red plus signs) are carried across the membrane by translational and/or rotational movements of α-helical domains within 'gating pores' (adapted from Jiang et al., 2003a). The extracellular side of the channel is to the top of the figure.

Recent research by MacKinnon's group has now obtained crystal structures of a member of the voltage-gated cation channel family – that of the KvAP voltage-gated potassium channel from *Aeropyrum pernix* – which is likely to be representative of the structure of all of the voltage-gated cation channels (Jiang et al., 2003a). As expected, the pore and selectivity filter regions of the channel, formed by the S5-S6 region, are almost structurally identical to that of the simpler KcsA channel. The S1-S4 voltage sensing regions, however, form a previously unseen structure (Figure I-12). This involves helices S1 and S2 forming another layer of structural helices surrounding the S5-S6 pore region. Rather than forming a single transmembrane helix the S4 domain, in conjunction with S3, forms a helix-turn-helix structure which has been referred to as a 'voltage-sensor' paddle, as shown in Figure I-12. This hydrophobic paddle structure is linked to the rest of the channel in a flexible manner, such that it can move more freely across the membrane in response to changes in membrane potential. Therefore, this new model of channel voltage sensing has the gating charges carried from the intracellular side of the membrane to the extracellular side on flexible 'paddle' structures (Figure I-13), rather than through transmembrane helix movement (Figure I-11).

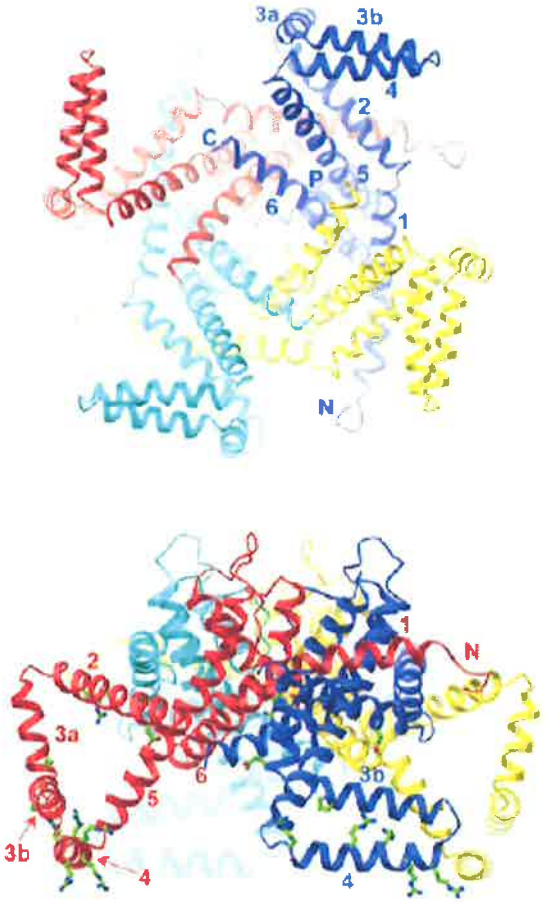

Figure I-12: KvAP channel structure
Ribbon representation of the KvAP tetramer viewed from the intracellular side of the membrane (*Top*), and from the side, with the extracellular solution below (*Bottom*). Each subunit is represented in a different colour. Helical regions are labelled from S1 to S6, with P marking the pore helix, and N and C marking the termini (from Jiang et al., 2003a).

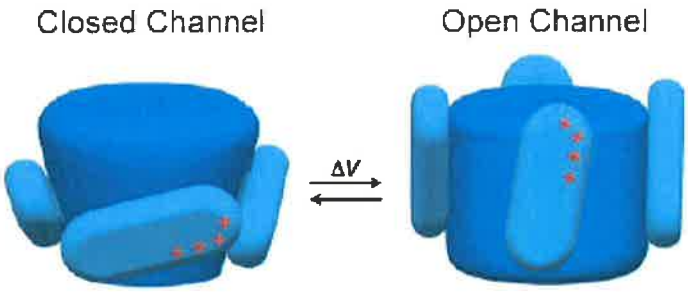

Figure I-13: New model of voltage sensing
In the new model gating charges (represented by red plus signs) are carried through the membrane by movements of flexible voltage-sensing paddles on the exterior of the channel (adapted from Jiang et al., 2003a). The extracellular side of the channel is to the top of the figure.

The structural movement of the pore during voltage-dependent gating is believed to be very similar to that occurring during ligand-dependent gating of potassium channels (see I-4-2-1 above). The structure obtained from the KvAP channel suggests that a change in membrane potential results in movement of the flexible voltage-sensing paddles across the cell membrane alongside the channel (Jiang et al., 2003b). This movement, translated through the S4-S5 linker region, causes tilting of the S5 and S6 pore helices (outer and inner pore helices), resulting in opening or closing of the channel conduction pathway (Figure I-14).

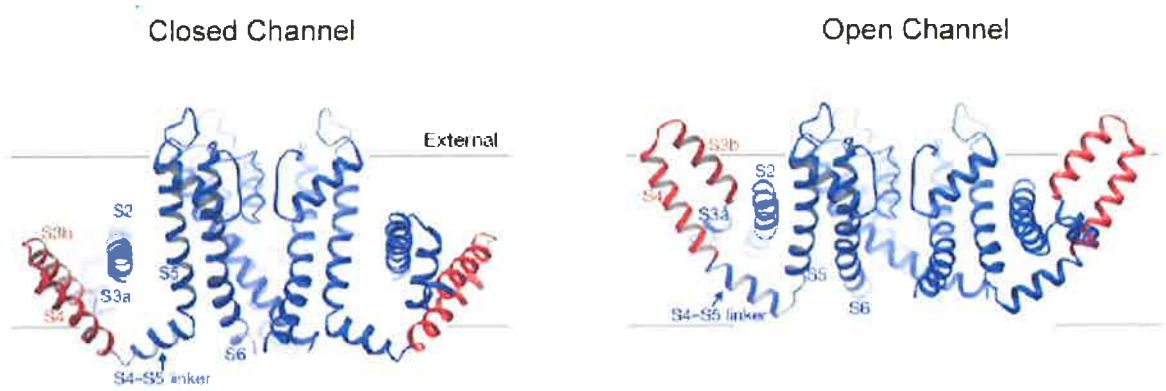

Figure I-14: Open and closed KvAP conformations
Proposed channel conformation and paddle position in closed (*Left*) and open (*Right*) KvAP channel. Voltage-sensing paddles are coloured red, channel pore structure in blue. Pore conformation of the closed channel is based on the closed KcsA crystal structure (see Figure I-7), whilst conformation of the open channel is based on the KvAP crystal structure (adapted from Jiang et al., 2003b).

It is worth noting, however, this newly proposed mechanism of voltage-gating in potassium channels has not been met without controversy, with many ion channel researchers expressing puzzlement at how the crystal structure relates to previous experimental evidence (Miller, 2003). Future research in this field will almost certainly be able to tell us how the new crystal structure fits with previous evidence, or whether in fact the structure is in some way flawed.

A third mechanism of voltage-dependent gating has recently been proposed in which voltage dependence arises from movement of the transmembrane electric field

around the gating charges, rather than the movement of the gating charges through the electric field. In this model very small changes in channel structure cause the movement of a highly focused electric field around the channel gating charges, resulting in gating of the channel (Figure I-15) (Starace and Bezanilla, 2004).

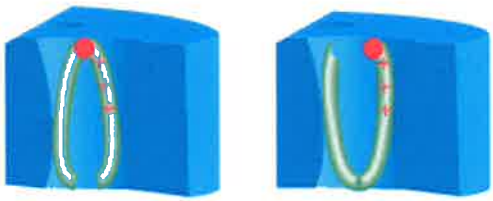

Figure I-15: Focused electric field model of gating
In this model of gating (represented in a single subunit) small changes in channel structure result in exposure of the channel gating charges (red plus signs) to either the extracellular (above channel) or intracellular (below channel) fluid, and movement of a tightly focused electric field across the gating charges. This model is based on a mutation in the outermost S4 amino acid (red circle). The model on the left is of the channel in the closed state, and on the right in the open state (figure adapted from Blaustein and Miller, 2004).

Each of the three gating models described above provides a very different view of the voltage-dependent gating process. Further research will be required in order to ascertain which of these models best describes the intricacies of voltage-dependent ion channel gating.

The similarity observed in the gating mechanisms of ligand- and voltage-gated channels is not unexpected, given the strong conservation of the pore region between these different channel types. In fact, the S1-S4 voltage-sensing apparatus could be thought of merely as an alternate 'RCK' domain (as described in I-4-2-1 above), which 'plugs-in' to the basic potassium channel pore structure, providing channel sensitivity to voltage, rather than ligands such as calcium, as occurs with the MthK channel (see I-4-2-1 above).

I-4-2-3 Mechanically Induced

Mechanosensitive channels are another group of ion channels, in which gating occurs as a response to mechanical stimulation, such as changes in membrane tension. Such channels are involved in critical processes, including transducing touch and hearing, and in osmoregulation. The MscL channel is a large conductance mechanosensitive channel, which opens in response to a change in membrane tension (Sukharev et al., 1997; Wood, 1999; Hamill and Martinac, 2001). The channel consists of multiple subunits, each containing two transmembrane domains, which form inner and outer pore helices, similar to those seen in KcsA (Rees et al., 2000). Unlike KcsA, however, the MscL channel is a pentamer, made up from 5, rather than 4, subunits (Chang et al., 1998; Rees et al., 2000). There are also differences in the orientations of the outer helices, although inner helices of both KcsA and MscL are in similar relative positions. The MscL channel contains no pore-loop region similar to that forming the KcsA selectivity filter, and contains an additional intracellular α-helical domain at the carboxyl terminus of the channel.

The structure of the MscL channel has been obtained using x-ray crystallography (Chang et al., 1998), and MscL gating has been investigated through the use of paramagnetic resonance spectroscopy (Perozo et al., 2002). These results show that under conditions of increased membrane tension the MscL channel pore opens due to a dramatic tilting of both transmembrane domains (to around 45° to membrane normal). Along with some helix rotation this creates a large water-filled pore ($\geq$ 25 Å), lined by helix 1 (see Figure I-16). A potential intermediate gating state has also been identified (see Figure I-16), in which the channel is still closed, but some minor movements in transmembrane domains have already occurred.

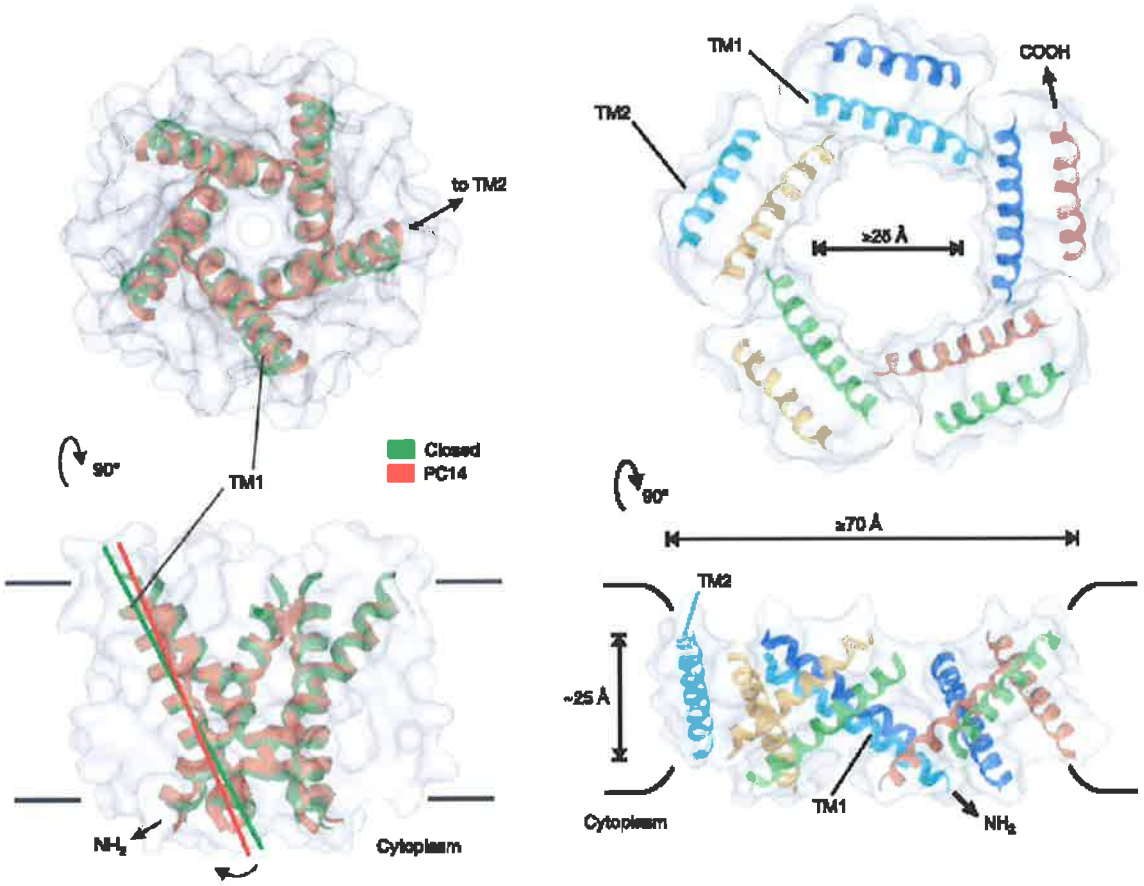

Figure I-16: Gating of MscL
(*Left*) Ribbon representation of TM1 α-helix of the pentameric MscL channel in the closed (red) and intermediate closed (green) states, as viewed from the extracellular side (Top), and from within the membrane (Bottom). Molecular surface represents the structure of the remaining MscL transmembrane segments. (*Right*) Ribbon representation of the TM1 and TM2 α-helices of the pentameric MscL channel in the open state, as viewed from the extracellular side (Top), and from within the membrane (Bottom). Helices from the same subunit have the same colour. Molecular surface represents the structure of the remaining MscL transmembrane segments (from Perozo et al., 2002).

Therefore, although the MscL channel structure does show some similarities to that of the cation channels previously described, the actual gating movements are much more dramatic. These movements require significant tilting and rotation of the entire transmembrane domains (Perozo et al., 2002), rather than minor tilting of the intracellular hinged domain regions, as seen with the potassium channels (Jiang et al., 2002b). In addition, the mechanism which is responsible for transducing changes in membrane tension to MscL channel opening appears to be intrinsic to the basic channel structure,

without requiring additional channel regions, such as the RCK or voltage-sensing domains of MthK and KvAP (see I-4-2-1 and I-4-2-2 above).

I-4-3 Helix Rotation Mechanism

The nicotinic acetylcholine receptor (nAChR) is a cation (primarily sodium and potassium) selective channel, predominantly found at the nerve muscle synapse, where it is responsible for depolarising the muscle membrane in response to the release of the neurotransmitter acetylcholine (ACh) from the presynaptic neuron. The nAChR forms a pentameric channel (see Figure I-17), consisting of two ACh binding α subunits, and three other homologous subunits, β, γ and δ (Lester, 1992; Karlin, 1993; Galzi and Changeux, 1994; Dani and Mayar, 1995; Corringer et al., 2000; Hille, 2001a; Karlin, 2002). Along with the anion-permeable glycine and GABA receptors the cation-permeable nAChR is a member of the ligand-gated ion channel superfamily, showing that cation and anion channels do not necessarily require unique permeation and gating mechanisms. This is confirmed by studies showing that point mutations can be used to change the nAChR from cation- to anion-selective (Galzi et al., 1992; Corringer et al., 1999), and glycine receptors from anion- to cation-selective (Keramidas et al., 2000; Keramidas et al., 2002).

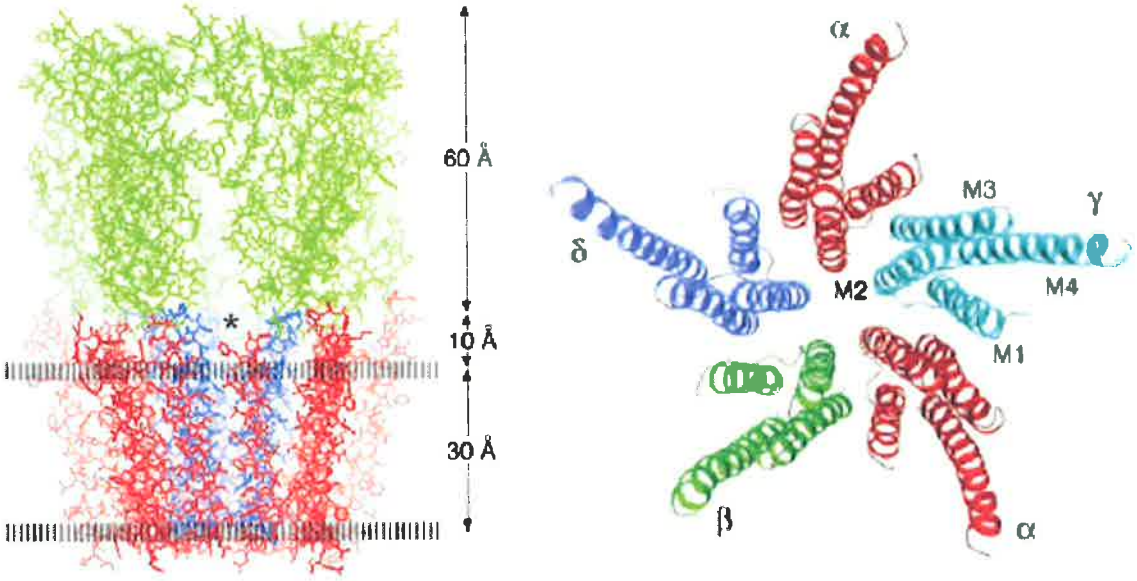

Figure I-17: Crystal structure of the nACh receptor
(*Left*) Ball-and-stick representation of nACh receptor viewed from within the membrane, showing the pore structure, with pore-facing α-helices coloured blue, lipid-facing helices coloured red, and the ligand-binding domain β-sheet structure coloured green.
(*Right*) Ribbon representation of nACh receptor pore helices, viewed from the extracellular side, showing the pentameric structure of the channel. α subunits are coloured red, β green, γ cyan, and δ blue (from Miyazawa et al., 2003).

X-ray crystal structures of the nAChR in the ACh bound and unbound (open and closed) states show that gating of the nAChR involves rotation of pore-lining helices formed by the receptor α-subunits (Miyazawa et al., 2003). The nAChR pore is lined by the M2 helices of each of the 5 subunits. In the closed channel state a slight kinking of these helices, in conjunction with the presence of large hydrophobic residues, creates a constriction of the pore in the region at the middle of the membrane. At this point he radius of the pore is too small to allow sodium or potassium ion to pass through. Binding of ACh to the extracellular domain of the α-subunits causes a rotation in these domains of around 15°. This rotational movement in the extracellular domain is transmitted to the M2 helices, causing destabilisation of the pore constriction (see Figure I-18), and resulting in the M2 α-helices taking up an alternate conformation in which the channel pore is widened sufficiently for ion permeation to occur (Miyazawa et al., 2003).

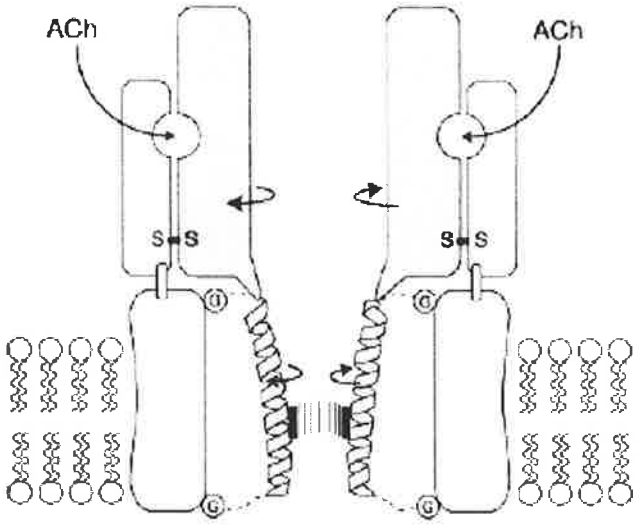

Figure I-18: Model of gating in the nAChR
Proposed gating model of the nAChR, showing relevant moving parts of the receptor shaded. ACh binding to the extracellular ligand-binding domain (indicated above) causes a rotational movement of the ligand-binding α subunits (upper arrows), which is transmitted to the pore-lining α-helices (lower arrows). These helices then assume an alternate conformation in which the channel is permeable to ions. Disulphide bonds (S-S) form a pivot in the ligand-binding domain, whilst flexible glycine loops (G) allow the pore-lining α-helices to move freely during gating (from Miyazawa et al., 2003).

I-5 ClC Channel Gating

Gating of ClC channels has been studied most extensively in the ClC-0 channel from the marine ray *Torpedo*, where ClC-0 channels are abundant in the electroplax (the electric organ). Single channel analysis of the ClC-0 channel shows the presence of two equally spaced subconductance states of the channel, which led to the initial suggestion of a double-barrelled channel (see I-3 above for detailed discussion). Examination of single channel recordings from ClC-0 also led to the identification of two different and independent gating processes – a 'fast' gating process, which opens and closes each of the individual channel protopores independently of the other, and a slower, 'common' gating process, which is able to open and close both channel pores simultaneously (Miller, 1982). These two gating processes are depicted in Figure I-19.

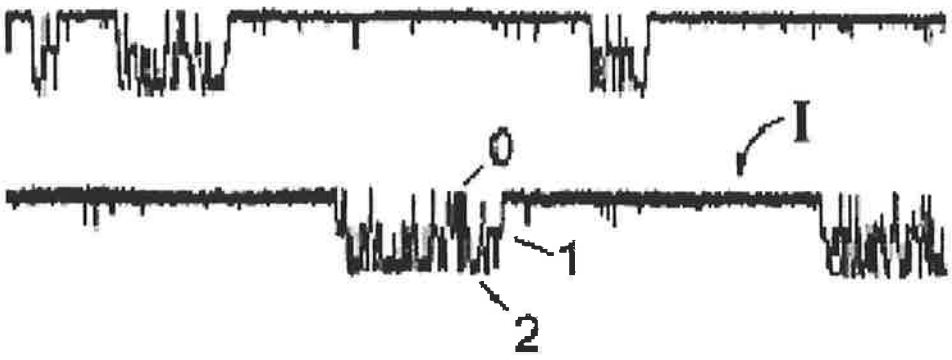

Figure I-19: A recording illustrating the two gating processes of ClC-0
Channel recording from ClC-0, illustrating the presence of the fast and common gating processes. Channel openings are observed as a downward deflection in the current trace from baseline. At the point indicated by '0' both of the ClC-0 fast gates are closed, at the conductance level marked by '1' one fast gate is open, and at the level indicated by '2' both of the ClC-0 fast gates are in the open state. The marker 'I' indicates a long-lived inactivation event, in which the ClC-0 common gate is closed (from Chen and Miller, 1996).

In the ClC-0 channel these two gating processes show opposite voltage dependence; the fast gates are opened by depolarisation, whilst the common gate is opened, over a much longer time scale, by hyperpolarisation (Miller, 1982).

The ClC-1 channel, like ClC-0, is gated by two different gating processes. Until recently evidence for this was only available from whole-cell recordings, due to the small single-channel conductance of ClC-1 (Pusch et al., 1994). Single channel recordings have now, however, also been obtained for the ClC-1 channel, confirming the presence of these two gating processes (Saviane et al., 1999). The gates in ClC-1 appear to act in the same way to those in ClC-0, with a 'fast' gating process closing each protopore independently, and the slower, 'common', gating process closing both simultaneously. In ClC-1, however, both of these processes show similar voltage dependence, with both gates opening at depolarised potentials (Saviane et al., 1999). Additionally, the difference between the kinetics of the two gating processes is less visible in ClC-1 than in ClC-0, although these do separate more at more positive potentials (Accardi and Pusch, 2000).

I-5-1 ClC Fast Gating

As mentioned above, the ClC fast gating process acts independently on each of the ClC channel protopores. In both ClC-0 and ClC-1 the fast gating process is voltage-dependent, causing channel opening in response to depolarisation (Miller, 1982; Saviane et al., 1999). Of particular interest is the way in which this voltage-dependence is conferred on the channel. It was initially discovered that the fast gating process of ClC-0 is strongly dependent on the extracellular concentration of the permeating anion, chloride (Pusch et al., 1995a). This has led to models of ClC-0 fast gating in which movement of chloride in the membrane electric field – which could be either an actual movement of ions, or a rearrangement of the electric field – provides the gating charge required for fast gate opening and closing (Pusch et al., 1995a; Chen and Miller, 1996). Therefore in this gating model the voltage-dependence of the ClC-0 fast gating process arises from interactions with the permeating anion, rather than through an intrinsic voltage-sensing mechanism, as is seen in the voltage-dependent cation channels (see I-4-2-2 above).

Electrophysiological investigation of the ClC-1 channel has shown that the open probability of this channel is also sensitive to extracellular chloride (Rychkov et al., 1996), which suggests that a similar chloride dependent gating mechanism may occur in ClC-1 (Rychkov et al., 1996; Accardi and Pusch, 2000; Rychkov et al., 2001) as that described for ClC-0 fast gating (Pusch et al., 1995a; Chen and Miller, 1996). Although these findings were initially complicated by an inability to separate the two ClC-1 gating processes in whole cell recordings, more recent techniques have overcome this barrier, and show that the fast gate of ClC-1 can be identified with the ClC-0 fast gating process (Saviane et al., 1999; Accardi and Pusch, 2000). In ClC-1, as in ClC-0, this process can be described by a model in which voltage-dependence is brought about through interactions with the permeating chloride ion (Accardi and Pusch, 2000). This fast gating mechanism may therefore be common within the ClC family of ion channels.

With the publication recently of the ClC crystal structure (Dutzler et al., 2002) (see Figure I-4) there has been some success in elucidating the mechanisms underlying the ClC fast gating process. In the prokaryotic ClC crystal structure it was observed that a conserved glutamate residue, E148, obstructs the chloride conduction pathway, suggesting that this residue might in fact be responsible for gating of the channel (Dutzler et al., 2002). More recent X-ray crystallography studies, combined with electrophysiology, show that this does in fact appear to be the case (Dutzler et al., 2003). When the equivalent conserved residue in the ClC-0 channel, E166, is mutated to Ala, Gln or Val, fast gating of the channel is effectively abolished. Crystal structures of the bacterial ClC channel with the equivalent mutations at E148 show structures in which the E148 residue side chain no longer blocks the conduction pathway, and is instead replaced with a region of high anion density. These results strongly suggest that this conserved glutamate residue forms the basis of the ClC fast gating process. In the fast gate closed state the glutamate side chain mimics a chloride ion, blocking the conduction pathway, whilst in the open state the side chain is swivelled out of the conduction pathway, and replaced by a chloride ion (Dutzler et al., 2003).

It is interesting to note that this proposed mechanism of ClC gating is quite unlike the gating mechanisms currently described in other channel types (discussed in I-4 above). All of these processes tend to rely, to a greater or lesser extent on large 'global' changes in protein structure, such as α-helix rotations or translations. In contrast, it appears that ClC fast gating occurs through a very localised change in protein structure – the swivelling of a single amino acid side chain. Possible reasons for the different 'scales' of gating have been discussed by Dutzler et al. (Dutzler et al., 2003), who suggest that the more 'global' gating movements seen, for example, in potassium channel gating (see I-4-2 above), allow gating to be regulated by more complex external factors, such as ligand binding domains. In

contrast to this the 'local' gating movements suggested for ClC fast gating allow regulation of gating only by very local physio-chemical properties.

The proposed mechanism underlying the ClC fast gating process can explain the observation that fast gating is an independent process, acting separately on each channel protopore (Miller, 1982). The proposed fast gating mechanism involves the single glutamate residue at position 148 (in the bacterial channel structure), with each channel protopore containing its own 'glutamate gate'. It is unlikely, therefore, that the very localised movements of the glutamate sidechain in one pore will affect the conformation of the other pore, allowing the fast glutamate gates to act independently of each other (Dutzler et al., 2003). The 'glutamate gate' mechanism can also explain the regulation of ClC fast gating by chloride ions. With the glutamate side-chain acting, in essence, as a surrogate anion which replaces the permeating chloride ion and blocks channel conduction, it could easily interact with internal and external chloride ions, as has been previously described for the ClC fast gate (Pusch et al., 1995a; Chen and Miller, 1996; Rychkov et al., 1996; Accardi and Pusch, 2000; Rychkov et al., 2001). Under the correct conditions of membrane potential and concentration chloride ions would enter the intracellular side of the channel, and electrostatic interactions with the glutamate side-chain would cause the pore to open, allowing chloride ions to occupy the site previously taken by the glutamate residue, and permeate the channel. A change in membrane potential or ion concentration which results in the glutamate gating site being less occupied by permeating ions would then allow the residue to swivel back into place, closing the channel. This process is considerably more simple than the complex gating processes described for other types of ion channels (see I-4 above), and further research will be required to show whether the ClC fast gating process is in fact this simple, or whether there are other more complex protein interactions involved.

I-5-2 ClC Common Gating

The ClC 'common', or 'slow', gating process, is a ClC gating process, separate from fast gating, which acts to open and close both channel protopores simultaneously. In ClC-0 this process shows the opposite voltage-dependence to that of the fast gating process, being opened by hyperpolarisation, and occurs over a very long time scale (10 to 100 seconds) (Miller, 1982). Similarly to the fast gating process, ClC-0 common gating is influenced by extracellular anions (Chen and Miller, 1996; Pusch et al., 1999). The ClC-1 common gate shows some striking differences to that seen in ClC-0. In ClC-1 this process is much faster, occurring over a time scale of hundreds of milliseconds, rather than seconds (Saviane et al., 1999; Accardi and Pusch, 2000). Also, the ClC-1 common gating process shows a similar voltage-dependence to that of the ClC fast gate, and opposite to that of the ClC-0 common gate, being opened by depolarisation (Saviane et al., 1999; Accardi and Pusch, 2000). Single channel recordings of ClC-1 do however show that this process still acts on both channel protopores simultaneously (Saviane et al., 1999), supporting the identification of this process with the ClC-0 common gate. In addition, several ClC-1 mutations have resulted in a conversion of ClC-1 currents from depolarisation- to hyperpolarisation-activated (Fahlke et al., 1995; Wollnik et al., 1997; Zhang et al., 2000), suggesting that the difference in voltage dependence of the ClC-0 and ClC-1 common gates is not a major inconsistency.

Despite these recent advances in understanding ClC structure and function the mechanisms underlying ClC common gating and the relationship between the fast and common gating processes are yet to be determined. The fact that common gating acts on both channel subunits simultaneously, rather than on individual protopores, suggests that unlike the ClC fast gating process (see I-5-1 above) common gating is likely to involve much more 'global' changes in channel structure and conformation. This is supported by evidence that mutations in only one of the dimer subunits are able to influence the common

gating process (Ludewig et al., 1996). Additionally, temperature dependence studies on the ClC-0 channel show that the common gate is extremely temperature dependent, with a Q_{10} in the range of 40 (Pusch et al., 1997). This high temperature dependence suggests that the common gating process involves complex structural rearrangement of the channel, again supporting the idea that common gating involves large global changes in channel conformation, rather than the local changes associated with fast gating, which has a fairly low temperature dependence, with a Q_{10} of 2.2 (Pusch et al., 1997). Common gating in the ClC-1 channel does not show the same temperature sensitivity as that of ClC-0, with a Q_{10} of only around 4 (Bennetts et al., 2001), suggesting that there may be differences between common gating in the ClC-0 and ClC-1 channels. Although the structural mechanisms underlying common gating are yet to be determined, it has been suggested on the basis of the high temperature dependence of ClC-0 common gating that this process may relate to subunit/subunit interactions within the channel dimer (Pusch et al., 1997). Whilst it is likely that the ClC common gating process involves global changes in protein conformation, there are presently no clues as to whether such gating movements are similar to those identified for other channels (see I-4 above), or, given the lack of similarity between ClC channels and other known ion channel families, whether a completely novel form of gating is involved.

I-5-3 Other ClC Gating Processes

Although the fast and common gating processes described above are the major ClC gating processes, there has been the occasional suggestion that other ClC gating processes exist. Of particular interest is the observation that in single channel ClC-0 recordings there are very rare events observed in which only a single protopore is closed for a long period of time (in the range of seconds) (Ludewig et al., 1997). Gating of this form does not fit with any of our present models of ClC gating. The closure of a single protopore suggests

fast gating, but a time scale of seconds is too slow for ClC-0 fast gating, whilst common gating acts over a longer time scale, and involves closure of both protopores. It is possible that this gating may reflect a rare substate of either the ClC-0 fast or common gating processes. Alternatively these events may represent a rare, and so far undetermined, third gating process.

Also interesting is the observation that there are point mutations in the ClC-1 channel able to dramatically alter the voltage-dependence and time course of the common gating process, such that it appears much more similar to the common gate of ClC-0 (Fahlke et al., 1995; Wollnik et al., 1997; Zhang et al., 2000). A similar hyperpolarisation-activated gating process can be induced in WT ClC-1 under conditions of low intracellular pH (Rychkov et al., 1996). Although this is likely to merely reflect an alteration in the ClC-1 common gating process (see I-5-2 above), it is also possible that this is not the case, and that the hyperpolarisation-activated gate seen in ClC-1 is another gating process, only revealed under low pH conditions, or in the presence of certain point mutations.

Therefore it may be that the fast and common ClC gating processes described above represent not the only ClC gating processes, but merely those which are the most visible, and most thoroughly studied. Further research will be necessary to reveal whether further ClC gating processes exist, and if so, what their possible roles are in ClC channels.

I-6 ClC-1 Mutations and Myotonia

Unlike most mammalian cells, the resting conductance of skeletal muscle is dominated by a chloride conductance, which accounts for ~80% of resting conductance (Bretag, 1987). This resting chloride conductance acts to stabilise the muscle membrane potential, preventing the occurrence of muscle hyperexcitability which can lead to spurious, repetitive action potential firing – a condition resulting in the muscle stiffness

disorder myotonia. Evidence for this was first produced nearly 40 years ago, when a reduced chloride conductance was shown in muscle biopsies from myotonic goats (Lipicky and Bryant, 1966), and from human patients (Lipicky et al., 1971). Following the cloning of the primary skeletal muscle chloride channel (Steinmeyer et al., 1991b), ClC-1 became an excellent candidate for the protein mutated in myotonia. This was confirmed with the identification of ClC-1 mutations in the *adr* myotonic mouse model (Steinmeyer et al., 1991a), and then in human myotonia (Koch et al., 1992).

Myotonia congenita occurs in both autosomal recessive (Becker type) and dominant forms (Thomsen type). Graded pharmacological inhibition has shown that myotonic symptoms occur only when total muscle chloride conductance is reduced to 25% of normal, or less (Kwiecinski et al., 1988). ClC-1 mutations which affect only one subunit generally cause a decrease in muscle chloride channel function of 50% or less when forming heteromers with a WT subunit, resulting in the recessive form of myotonia (Saviane et al., 1999). These types of mutations include severe truncating mutations (Meyer-Kleine et al., 1995), mutations which reverse the ClC-1 voltage dependence (Fahlke et al., 1995; Wollnik et al., 1997; Zhang et al., 2000), and mutations which reduce the single channel conductance (Wollnik et al., 1997).

The dominant form of myotonia is usually caused by mutations that shift the voltage dependence of ClC-1 gating to more depolarised potentials (Pusch et al., 1995b; Kubisch et al., 1998), thereby reducing the macroscopic chloride conductance at resting membrane potentials. These mutations are observed to have a dominant negative effect on the channel, such that the presence of a single mutant subunit is enough to result in altered gating within a WT/mutant heteromer (Pusch et al., 1995b; Beck et al., 1996; Wollnik et al., 1997; Kubisch et al., 1998). Experimental results suggest that these mutations are able to have this effect through altering the ClC-1 common gating process, thereby exerting an influence over gating of even normal WT subunits (Saviane et al., 1999). This contrasts

with recessive mutations, where the common gating process is unaffected (Saviane et al., 1999). Therefore it appears likely that mutations resulting in the dominant form of myotonia can give us information regarding the ClC-1 common gating process. This concept has formed the basis of some of the research presented here, and is discussed in more detail later in this thesis (see Chapter III: Involvement of Helices at the Dimer Interface in ClC-1 Common Gating).

I-7 ClC-1 Pharmacology and Block

Ion channel pharmacology has often provided significant information about the function of ion channels, with drugs that interact with the pore of voltage-gated cation channels providing significant information on channel gating and permeation (Hille, 2001b). Although there are no highly specific blockers of ClC-1, or of ClC channels in general, there are a number of chemicals which are less specific blockers of these channels. The primary pharmacological interaction that the current research has investigated has been that of the divalent cations – particularly zinc (Zn^{2+}) - with the ClC-1 channel. Other ClC blockers include the disulphonic stilbenes, such as 4,4'diisothiocyanostilbene-2,2'disulphonic acid (DIDS), and the monocarboxylic aromatic acids, such as anthracene-9-carboxylic acid (A9C) and p-chloro-phenoxy-propionic acid (CPP). These chemicals are discussed briefly below.

I-7-1 4,4'diisothiocyanostilbene-2,2'disulphonic acid (DIDS)

Whilst the effects of DIDS on the ClC-1 channel are yet to be characterised, DIDS has been shown to be a potent blocker of ClC-0, where it affects the channel through irreversible blockage of the individual channel protopores (Miller and White, 1984; Jentsch

et al., 1990; Goldberg and Miller, 1991). The ClC-3, -4 and –K channels have also been reported to show blockage by DIDS (Uchida et al., 1993; Adachi et al., 1994; Kawasaki et al., 1994; Duan et al., 1997; Dick et al., 1998; Duan et al., 1999; Kawasaki et al., 1999), whilst there is controversy regarding the sensitivity of the ClC-2 (Thiemann et al., 1992 Clark et al., 1998; Enz et al., 1999) and ClC-5 (Steinmeyer et al., 1995; Sakamoto et al., 1996; Lindenthal et al., 1997) channels to DIDS.

I-7-2 9-Anthracene Carboxylic Acid (A9C)

A9C and other related polycyclic monocarboxylic aromatic acids have been shown to induce myotonic symptoms in mammalian muscle by causing a decrease in the chloride conductance of the muscle (Bryant and Morales-Aguilera, 1971; Palade and Barchi, 1977). This chemically induced myotonia resembles inherited myotonia congenita in a number of ways (Rudel and Lehmann-Horn, 1985). It has been shown that A9C acts through blockage of the ClC-1 channel (Steinmeyer et al., 1991b; Fahlke et al., 1995; Astill et al., 1996; Lorenz et al., 1996; Rychkov et al., 1997). Blockage of ClC-1 by A9C is voltage and pH dependent (Rychkov et al., 1997, see Pusch et al., 2002). Due to the slow time course of A9C block and recovery (see Pusch et al., 2002) the mechanism of block is difficult to study. There is also contention about the side of the channel at which A9C block occurs, with different experimental systems suggesting that block occurs only from the intracellular (see Pusch et al., 2002) or extracellular (Rychkov et al., 1997) sides of the channel. This argument regarding the sidedness of A9C action is yet to be fully explained. Recent mutagenesis studies, based on the ClC crystal structure, suggest that the A9C binding site is located in a hydrophobic pocket on the intracellular side of the channel (Estévez et al., 2003), which is consistent with results showing that A9C blocks from the intracellular, but not extracellular sides (see Pusch et al., 2002). This does not however explain the results suggesting that A9C blocks from the extracellular, and not intracellular

sides (Rychkov et al., 1997; Aromataris unpublished observations). Diffusion of the hydrophobic A9C through the cell membrane in whole cell experiments can explain an action of extracellularly applied A9C when binding intracellularly, but not the absence of action observed when applied intracellularly (Aromataris unpublished observations). Most likely this inconsistency in the observed sidedness of A9C action arises due to differences between the channels and experimental systems used. The experiments of Aromataris showing an extracellular sidedness of A9C action have been conducted on rat ClC-1 channels expressed in Sf9 insect cells, using whole-cell patch clamp techniques (Aromataris unpublished observations), whilst those showing intracellular action have utilised human ClC-1 in oocytes and HEK293 cells, applying the inside-out patch clamp configuration (Pusch et al., 2002).

Other polycyclic monocarboxylic aromatic acids, including diphenylamine-2-carboxylic acid (DPC), 5-nitro-2-(3-phenylpropylamino)benzoic acid (NPPB) and 2-(3-trifluoromethylanilino)-nicotinic acid (niflumic acid), have also been found to block various members of the ClC family (Jentsch et al., 1990; Thiemann et al., 1992; Adachi et al., 1994; Astill et al., 1996; Sakamoto et al., 1996; Buyse et al., 1997; Furukawa et al., 1998; von Weikersthal et al., 1999).

I-7-3 p-Chloro-phenoxy-propionic Acid (CPP)

Similarly to the polycyclic monocarboxylic aromatic acids the clofibric acid derivatives, such as CPP, have been seen to cause myotonic symptoms in mammals (Langer and Levy, 1968; Dromgoole et al., 1975; Eberstein et al., 1978; Kwiecinski, 1978). This was later confirmed to be due to a decrease in chloride conductance across the muscle membrane (Conte-Camerino et al., 1984; Bettoni et al., 1987; Kwiecinski et al., 1988; De Luca et al., 1992). It was also found that this action was stereo-specific, with the S-(-) enantiomer reducing chloride conductance much more effectively than the R-(+)

enantiomer (Bettoni et al., 1987; Conte Camerino et al., 1988b), which at low concentrations actually caused some increase in chloride conductance (Conte Camerino et al., 1988a; De Luca et al., 1992).

Investigation of the affects of CPP on ClC-1 currents has shown that, as might be expected, CPP is able to inhibit the channel in a stereo-specific manner. It appears that these chemicals exert their effect by causing a shift in the $V_{½}$ of channel gating to more positive potentials, such that the open probability of the channel at physiological potentials is greatly reduced (Aromataris et al., 1999; Pusch et al., 2000). It also appears that this shift is predominantly due to a reduction in the open probability of the fast channel gates, rather than the common gate (Accardi et al., 2001; Aromataris et al., 2001). Detailed examination of this block in both ClC-0 (Pusch et al., 2001) and ClC-1 (Accardi et al., 2001) has led to the conclusion that CPP and related chemicals act by binding in a voltage-dependent manner to the individual closed gates, thereby affecting their gating.

I-7-4 Divalent Cations

Divalent cations, such as zinc (Zn^{2+}), have been shown to inhibit the resting conductance of skeletal muscle (Hutter and Warner, 1967; Stanfield, 1970; Bretag et al., 1984). Most of this conductance is due to the presence of the ClC-1 channel (Steinmeyer et al., 1991b), and more recent research has shown that $Zn^{2+}$and other divalent cations are able to directly inhibit currents through ClC-1 (Kurz et al., 1997; Rychkov et al., 1997; Kurz et al., 1999). Zinc causes a slow block of ClC-1 currents, occurring over a time course of tens of minutes, which is not reversible on Zn^{2+} wash-out (Kurz et al., 1997). Zinc does not appear to change the reversal potential or the open probability of the ClC-1 channel, suggesting that it is not causing a change in the ion selectivity of the channel, nor is it interacting with the voltage-dependence of channel gating (Kurz et al., 1997).

Investigation of ClC-0 has shown that this channel is also inhibited by Zn^{2+} (Chen, 1998). In ClC-0 this inhibition has been shown to occur through Zn^{2+} causing a facilitation of the common gating process, such that the rate of channel inactivation by the common gate is increased (Chen, 1998). This mechanism of action is further supported by research utilising the C212 ClC-0 mutant, in which a loss of the common gating process is associated with a large reduction in Zn^{2+} sensitivity of the channel (Lin et al., 1999). The structural mechanism underlying the facilitation of common gating by Zn^{2+} is still unknown.

It is yet to be determined whether Zn^{2+} and other divalent cations also inhibit ClC-1 currents through an interaction with the common gating process. The sensitivities of ClC-0 and ClC-1 to Zn^{2+} are quite different, with ClC-0 having an IC_{50} for Zn^{2+} around a hundred times lower than that seen for ClC-1. In addition, Zn^{2+} inhibition of ClC-0 is reversible, whilst in ClC-1 it is irreversible. These differences suggest that the Zn^{2+}-mediated inhibition of ClC-1 currents may occur in a different manner to the facilitation of common gating observed in the ClC-0 channel. The mechanism of Zn^{2+} inhibition in the ClC-1 channel therefore remains to be explained, but once understood may well enlighten our knowledge of the processes involved in ClC-1 gating.

Aims

It is clear that the ClC family of chloride channels is structurally significantly different to other well-characterised ion channels, such as the voltage-gated cation channel families. Whilst significant advances have been made in understanding ClC channels, both at a structural and functional level, there is still much to be determined. In particular, the nature of the common gate of the ClC channels remains to be elucidated. The research described in this thesis has aimed to further our understanding of the ClC-1 channel, and in particular the processes involved in the gating of these channels.

The aims of this research have been:

- To investigate the relationship between structure and function of the ClC-1 chloride channel, utilising knowledge of naturally occurring mutations to identify possible structures involved in ClC-1 gating.

- To investigate the role of these identified structures in ClC-1 channel gating through the use of site-directed mutagenesis.

- To investigate the mechanism of ClC-1 channel Zn^{2+} block, in order to gain further information on whether zinc block occurs through direct blockage of the conduction pathway, or through interactions with ClC-1 gating.

Chapter II: General Methods

II-1 Molecular Biology

Two-step PCR-based site-directed mutagenesis (Ho et al., 1989) was used to introduce point mutations into hClC-1 cDNA (Steinmeyer et al., 1994). This technique introduces specific point-mutations into a DNA plasmid utilising four synthetic oligonucleotide primers and two PCR reactions. The synthetic primers used are schematically represented in Figure II-1. As this figure shows this technique requires two mutagenic and two outside primers. The outside primers are identical in sequence to a portion of the coding strand upstream of the mutation site (primer A), and to a portion of the non-coding strand downstream of the mutation site (primer D). The location of these primers is chosen such that they encompass two unique restriction sites on the plasmid; one upstream and one downstream of the mutation site (Figure II-1). The two mutagenic primers are identical to the coding (primer C) and non-coding (primer B) strands, except at the mutation site, where they contain the nucleotide substitutions required to insert the desired amino acid mutation into the DNA sequence. A number of factors taken into consideration in the design of the primers are described in II-2 below.

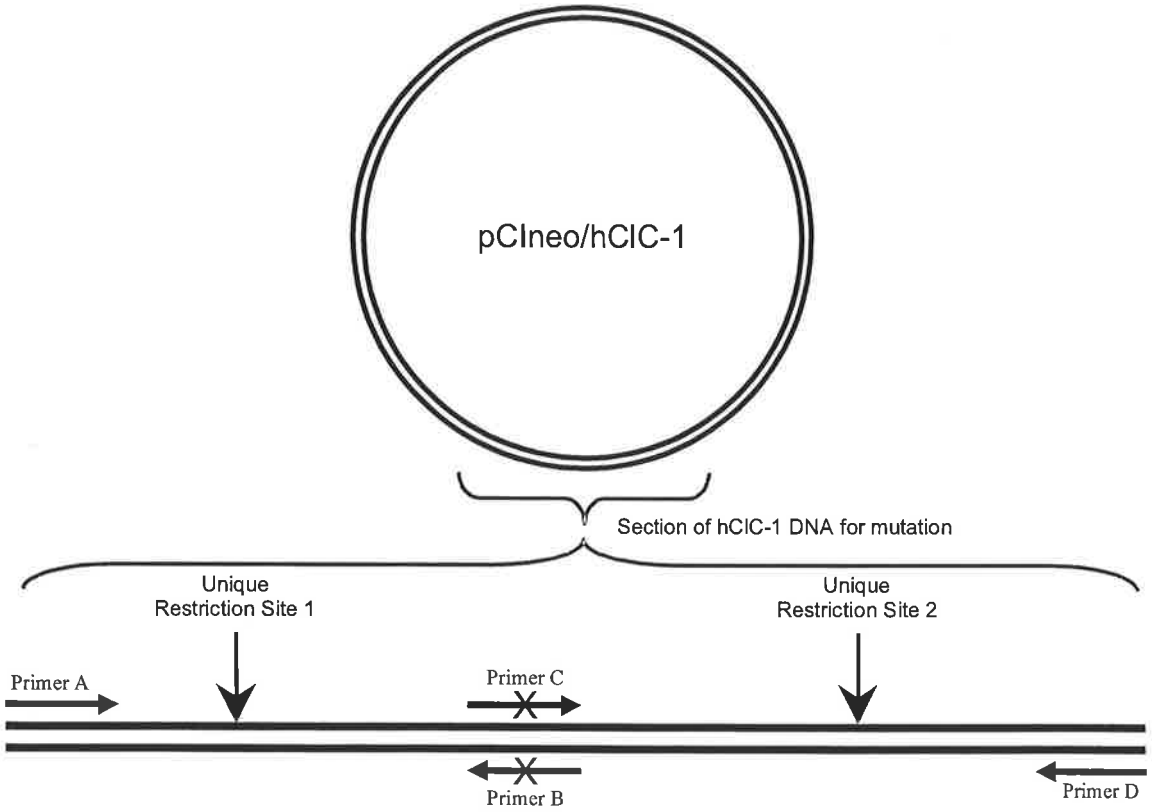

Figure II-1: Site directed mutagenesis of hClC-1
A schematic diagram of the pCIneo/hClC-1 vector, showing an enlarged view the hCLC-1 DNA segment in immediate proximity to the site of the desired point mutations (the site at which the 'mutagenic' primers B and C bind). 'X' indicates the site of mutations within primers B and C. Also shown are the relative positions of the 'outside' primers, A and D, and of the unique restriction sites required on either side of the mutation site.

The first PCR step in the mutagenesis process involved two separate PCR reactions. One of these reactions utilised the primer pair A and B, and the other the primer pair C and D, as schematically represented in Figure II-2. The products of these PCR reactions were two amplified sequences, one upstream of the mutation site and one downstream of the mutation site, each containing a short overlapping sequence at the mutation site. All PCR steps in the mutagenesis procedure utilised Pwo DNA polymerase (Roche Applied Science, Mannheim, Germany) for hi-fidelity amplification, and to reduce the number of polymerase introduced mutations.

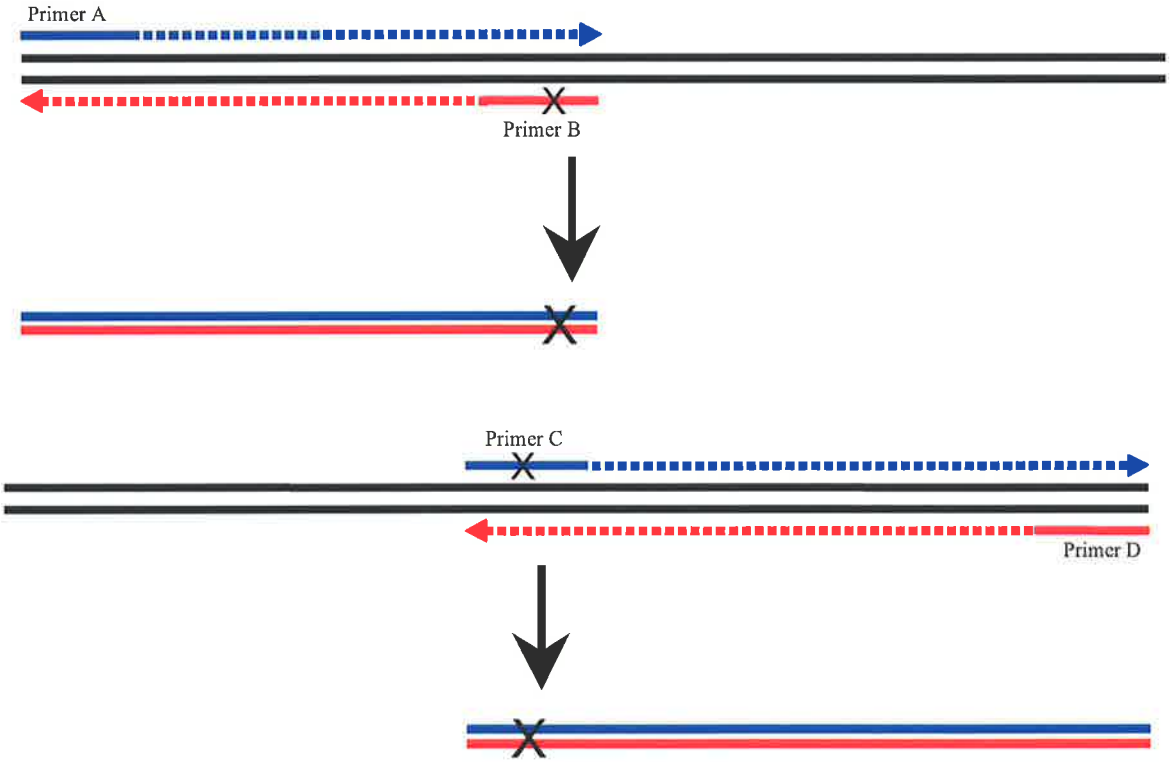

Figure II-2: The first PCR step
Schematic representation of the first PCR step, during which primer pairs A,B and C,D were utilised to produce DNA segments either side of the mutation site, each containing the desired point mutation and a slight DNA overlap. The mutation site in primers B and C, and in the DNA product, is marked with 'X'.

A typical first PCR step would therefore consist of two separate reactions:

Reaction 1		*Reaction 2*	
dNTPs* (25 mM each) (dATP, dGTP, dTTP, dCTP)	0.7 µL	dNTPs* (25 mM each) (dATP, dGTP, dTTP, dCTP)	0.7 µL
Pwo polymerase† (5U/µL)	0.5 µL	Pwo polymerase† (5U/µL)	0.5 µL
10× Pwo buffer†	5.0 µL	10× Pwo buffer†	5.0 µL
pCIneo/WT hClC-1# (template) (50 µg/µL)	1.0 µL	pCIneo/WT hClC-1# (template) (50 µg/µL)	1.0 µL
Primer A‡ (10 µM)	2.0 µL	Primer C‡ (10 µM)	2.0 µL
Primer B‡ (10 µM)	2.0 µL	Primer D‡ (10 µM)	2.0 µL
milli-Q (MQ) H_2O	38.8 µL	MQ H_2O	38.8 µL
Total Volume	*50.0 µL*	*Total Volume*	*50.0 µL*

*New England Biolabs, Beverley, MA, USA
†Roche Applied Science, Mannheim, Germany
‡Sigma Genosys, Australia
#Steinmeyer et al., 1994

The typical PCR cycle utilised for this first PCR step was:

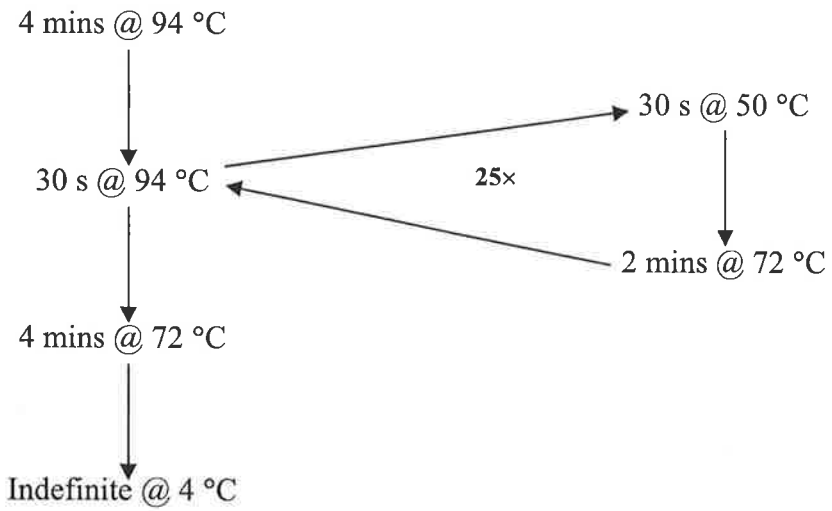

(Cycle times and temperatures were adjusted to optimise conditions based on factors such as the primer pair utilised, and the length of the expected PCR product.)

Following the first PCR step, the PCR products were run on a 1% agarose gel, and the length of PCR products was checked against a DNA ladder. The PCR products were then cut out of the gel, and extracted (QIAquick Gel Extraction Kit, QIAGEN Pty Ltd, Victoria, Australia).

The second PCR step involved the recombination of these two PCR products such that the entire sequence between the outside primers, A and D, was amplified (Figure II-3). The PCR products from step 1 (see Figure II-2) were used as templates, along with the two outside primers, to produce a sequence between the outside primers, containing the introduced mutation.

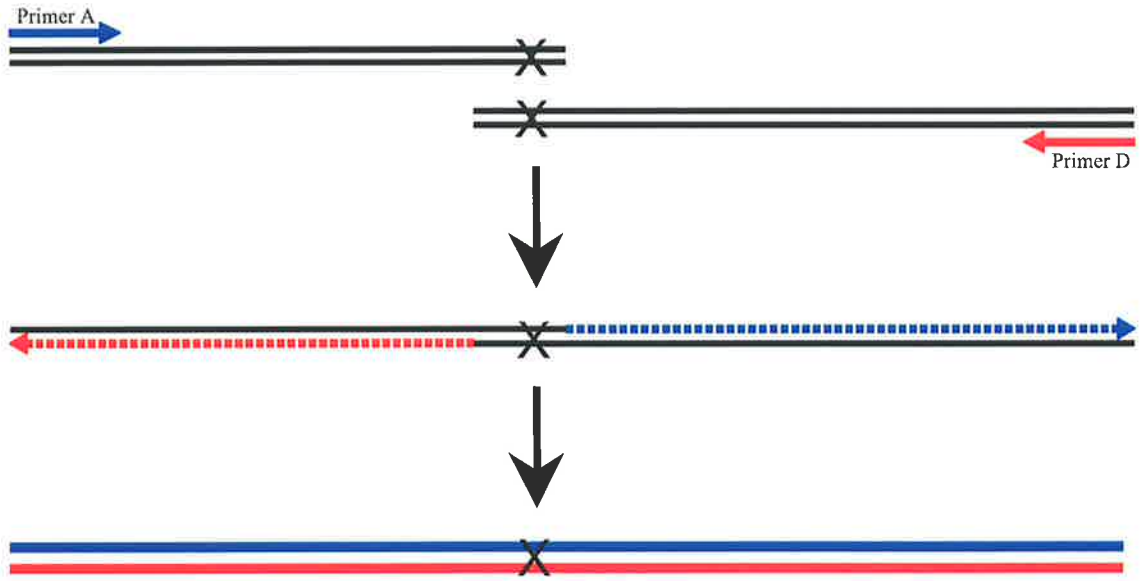

Figure II-3: The second PCR reaction
A schematic representation of the second PCR reaction, during which primers A and D, and the products from the initial PCR reaction (see Figure II-2), were utilised to produce a DNA segment containing the desired point mutation. The position of the point mutation within the segments is marked with 'X'.

A typical second PCR step would therefore consist of a single reaction:

dNTPs* (25 mM each) (dATP, dGTP, dCTP, dTTP)	0.7 µL
Pwo polymerase† (5U/µL)	0.5 µL
10× Pwo buffer†	5.0 µL
Purified PCR 1 Reaction 1 product	2.0 µL
Purified PCR 1 Reaction 2 product	2.0 µL
Primer A‡ (10 µM)	2.0 µL
Primer D‡ (10 µM)	2.0 µL
MQ H_2O	35.8 µL
Total Volume	*50.0 µL*

*New England Biolabs, Beverley, MA, USA
†Roche Applied Science, Mannheim, Germany
‡Sigma Genosys, Australia

The second PCR cycle was generally very similar to the first PCR cycle:

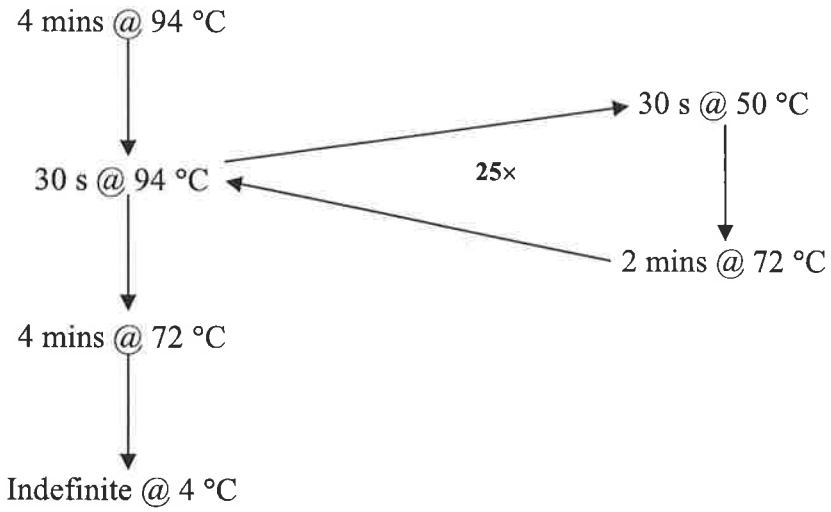

(Cycle times and temperatures were again adjusted to optimise conditions based on factors such as the primer pair utilised, and the length of the expected PCR product.)

Following the second PCR step the products were again run on a 1% agarose gel, and the length of PCR products was checked against a DNA ladder. The PCR products were then cut out of the gel, and extracted (QIAquick Gel Extraction Kit, QIAGEN Pty Ltd, Victoria, Australia).

Because of the location chosen for the two outside primers (Primers A and D), the final PCR product contained two unique restriction enzyme recognition sites (see Figure II-1), one either side of the mutation site. The final step in the site-directed mutagenesis procedure involved cutting both the original plasmid (without the point mutation) and the final PCR product (which contained the mutation) with these restriction enzymes. These reactions were carried out as follows:

PCR Product Reaction		*Vector Reaction*	
PCR reaction 2 product	dried down	pCIneo/WT hClC-1[†] (50 μg/μL)	8.0 μL
10× enzyme buffer[*]	2.0 μL	10× enzyme buffer[*]	2.0 μL
Restriction Enzyme 1[*] (10U[‡])	1.0 μL	Restriction Enzyme 1[*] (10U[‡])	1.0 μL
Restriction Enzyme 2[*] (10U[‡])	1.0 μL	Restriction Enzyme 2[*] (10U[‡])	1.0 μL
MQ H_2O	16.0 μL	MQ H_2O	8.0 μL
Total Volume	*20.0 μL*	*Total Volume*	*20.0 μL*

*New England Biolabs, Beverley, MA, USA
†Steinmeyer et al., 1994
‡ (Where the concentration of Restriction Enzyme was not 10U/μL the volume was adjusted so that 10U of enzyme was used, and the total reaction volume maintained at 20μL.)

These reactions were adjusted in order to maintain each enzyme at 10U, and the final volume at 20μL. Where the two restriction enzymes were not able to utilise the same enzyme buffer the reaction was run firstly with one enzyme, the product then separated and extracted on a 1% agarose gel, and then a second reaction was run with the second enzyme. Digestion reactions were generally run at 37 °C for at least 3 hrs, except where specific enzymes required different reaction times and / or temperatures.

Following the digestion reaction the vector reaction was alkaline phosphatase treated at 37 °C for at least 1 hr, to reduce the possibility of self-ligation occurring.

Vector digest (described above)	20.0 μL
Alkaline Phosphatase[*]	3.0 μL
Total Volume	*23.0 μL*

*New England Biolabs, Beverley, MA, USA

Both the vector and PCR product digests were then run on a 1% agarose gel, and the length of each DNA restriction fragment was checked against a DNA ladder. The products were then cut out of the gel, and extracted (QIAquick Gel Extraction Kit, QIAGEN Pty Ltd, Victoria, Australia).

After alkaline phosphatase treatment the final PCR product was ligated into the host plasmid, producing a plasmid identical to the original template (see Figure II-1), but containing the desired mutation.

Ligation Reaction		*Control Ligation*	
Product from PCR digestion	dried down		
Vector digest	1.0 µL	Vector digest	1.0 µL
10× T4 ligase buffer*	1.0 µL	10× T4 ligase buffer*	1.0 µL
T4 ligase*	1.0 µL	T4 ligase*	1.0 µL
MQ H_2O	7.0 µL	MQ H_2O	7.0 µL
Total Volume	*10.0 µL*	*Total Volume*	*10.0 µL*

*New England Biolabs, Beverley, MA, USA
These reactions were incubated at 37 °C for 4 hrs.

The ligation and control products were then transformed into XL-1 Blue chemically competent bacteria (Stratagene, US), following the directions provided by the manufacturer, and plated onto LB agar plates containing 100 µg/mL Ampicillin (the pCIneo/WT hClC-1 vector contained an Ampicillin resistance gene).

These plates were incubated at 37 °C overnight, and then stored at 4 °C. Where colonies grew on the ligation plate, but not the control plate, colonies were picked, grown up in LB medium overnight, and then plasmid DNA extracted via mini-prep protocol. This DNA was then sequenced:

Sequencing mix (BigDye Terminator)*	6.0 µL
Sequencing primer† (1 µM)	3.0 µL
Mini-prep DNA	2.0 µL
MQ H_2O	9.0 µL
Total Volume	*20.0 µL*

*Applied Biosystems, CA, USA
†Sigma Genosys, Australia

The cycle settings used for the sequencing reaction followed the standard protocol suggested by the manufacturer. For this reaction the sequencing primer was chosen so as to entirely sequence the area of the plasmid between the two unique restriction sites in order to confirm the introduction of the desired mutation into the ClC-1 DNA. Where this was

not possible in one sequencing reaction, due to the length of DNA between the restriction sites, several sequencing reactions were carried out utilising different primers to ensure that the whole length contained no undesired mutations. Following confirmation of the mutation, the mini-prep DNA was again grown up in bacteria, and a midi-prep (QIAGEN Plasmid Midi Kit, QIAGEN Pty Ltd, Victoria, Australia) performed to obtain plasmid DNA suitable for transfection into HEK-293 cells for patch-clamping (see II-3 below).

II-2 Design of PCR Primers

PCR primers utilised in the site-directed metagenesis procedure (described in II-1 above) were designed as follows:

Mutagenic primers were designed to overlap the site of the desired mutation. Primers were of exact complementary base sequence to the template DNA, except for the nucleotides which required alteration in order to introduce the desired mutation. The number of nucleotide changes required to introduce each mutation was minimised where possible. Mutagenic primers were designed to contain at least several matching bases either side of the mismatched bases.

Outside primers were exactly complementary to the template DNA strand, and were designed to:

a) bind to positions either side of the mutation site

b) allow incorporation of unique restriction sites into the PCR product, and

c) produce PCR products of unique lengths, enabling distinct products to be identified and extracted using gel electrophoresis (see II-1 above).

Both types of primers were designed to match the following specifications as closely as possible:

a) 18-22 bases in length

b) have an AT:GC ratio of close to 50%

c) have a melting temperature of around 55 °C

d) have several G or C nucleotides at each end of primer (to assist in binding of the primer to the template DNA strand)

Where necessary the binding location of primers was altered to reduce the possibility of primer dimerisation and hairpin formation.

II-3 Cell Culture

Human embryonic kidney (HEK293) cells were grown in Dulbecco's modified Eagle's medium (Invitrogen Australia, Melbourne, Australia), containing 10% (v/v) fetal bovine serum (Trace, Melbourne, Australia), supplemented with L-glutamine (2 mM; Sigma, St. Louis, MO), and maintained at 37°C in 5% CO_2. Cell cultures were transfected with 700 ng of either WT or mutant pCIneo/hClC-1 cDNA using LipofectAMINE PLUS reagent (Invitrogen, CA, USA), following the standard protocol described by the manufacturer, in 25 mm culture wells. Cells were co-transfected with 70 ng of green fluorescent protein plasmid cDNA (pEGFP-N1; Clontech, Palo Alto, CA), to allow identification of transfected cells during patch-clamp experiments. Cells were replated for patch-clamping at least 3 h after transfection, and electrophysiological measurements were commenced approximately 24 h after transfection.

II-4 Electrophysiology

Patch-clamping experiments were performed on transfected HEK293 cells in the whole-cell configuration using a List EPC 7 (List, Darmstadt, Germany) patch-clamp amplifier and associated standard equipment, at room temperature (24 ± 1 °C). Standard bath solution contained: 140 mM NaCl, 4 mM KCl, 2 mM $CaCl_2$, 1mM $MgCl_2$, 5 mM HEPES, adjusted to pH 7.4 with NaOH. Standard pipette solution contained: 75 mM Cs glutamate, 40 mM CsCl, 10 mM EGTA, 10 mM HEPES, adjusted to pH 7.2 with KOH. Patch pipettes of 1 – 3 MΩ were pulled from borosilicate glass. Series resistance did not exceed 5 MΩ, and was 70 – 85% compensated. Currents obtained were filtered at 3 kHz, and collected and analysed using pClamp software (Axon Instruments, Foster City, CA, U.S.A.). Potentials listed are pipette potentials expressed as intracellular potentials relative to outside zero. Data presented in figures and tables have been corrected for liquid junctions potentials, estimated using JPCalc (Barry, 1994), except where otherwise indicated.

Chapter III: Involvement of Helices at the Dimer Interface in ClC-1 Common Gating

III-1 Introduction

The physiological role of ClC-1 is to stabilise the resting membrane potential of skeletal muscle (Bretag, 1987). Mutations of this channel can reduce whole cell Cl^- conductance, resulting in myotonia, a muscle stiffness disorder characterised by repetitive action potential firing, and prolonged muscle contraction (see eg Pusch, 2002). Such myotonias can be inherited in both recessive and dominant forms. This varied inheritance pattern appears to result from differential effects of various mutations on the channel dimer (Kubisch et al., 1998; Saviane et al., 1999). In heterozygous individuals, assuming that both alleles are expressed and the product inserted into the membrane, 75% of the dimeric channels will contain either one or two copies of the normal subunit. Mutations causing recessive myotonia most likely affect properties of the pore in one subunit, such as fast gating or conductance, leaving the other pore unaffected in WT/mutant heterodimers (Wollnik et al., 1997; Kubisch et al., 1998; Saviane et al., 1999; Weinreich and Jentsch, 2001). This would result in a residual whole cell Cl^- conductance of 50% or more, which is considered to be sufficient to avoid myotonic symptoms (Furman and Barchi, 1978). On the other hand, mutations causing dominant myotonia must affect both ClC-1 subunits to reduce the whole cell Cl^- conductance in a heterozygous person to less than 50% in order to produce myotonic symptoms (Kwiecinski et al., 1988). The necessary interaction between the product of the mutated gene and that of the subunit transcribed from the WT gene is probably occurring through effects on the ClC-1 common gate, which is shared by both pores. A number of naturally occurring dominant negative ClC-1 mutations have been

shown to alter the voltage dependence of the common gate (Saviane et al., 1999; Aromataris et al., 2001).

While the naturally occurring mutations in the ClC-1 channel which produce myotonia are scattered throughout the channel primary sequence, including the carboxyl tail, there is a cluster of dominant mutations at the interface of the channel monomers (Figure III-1), particularly in the H and I helices, although there are also some in the P and Q helices. Additionally, the mutations C212S and C213S in ClC-0, and C277S in ClC-1, which are in the G helix, affect the common gate (Lin et al., 1999; Accardi et al., 2001). This suggests that the G, H, I, P and Q helices are important for the ClC common gating process. We have now investigated the effects of a further eleven point-mutations within these helices on gating properties of the ClC-1 channel, and have shown that the majority of these mutant channels exhibit alterations in channel gating, particularly in the common gating process.

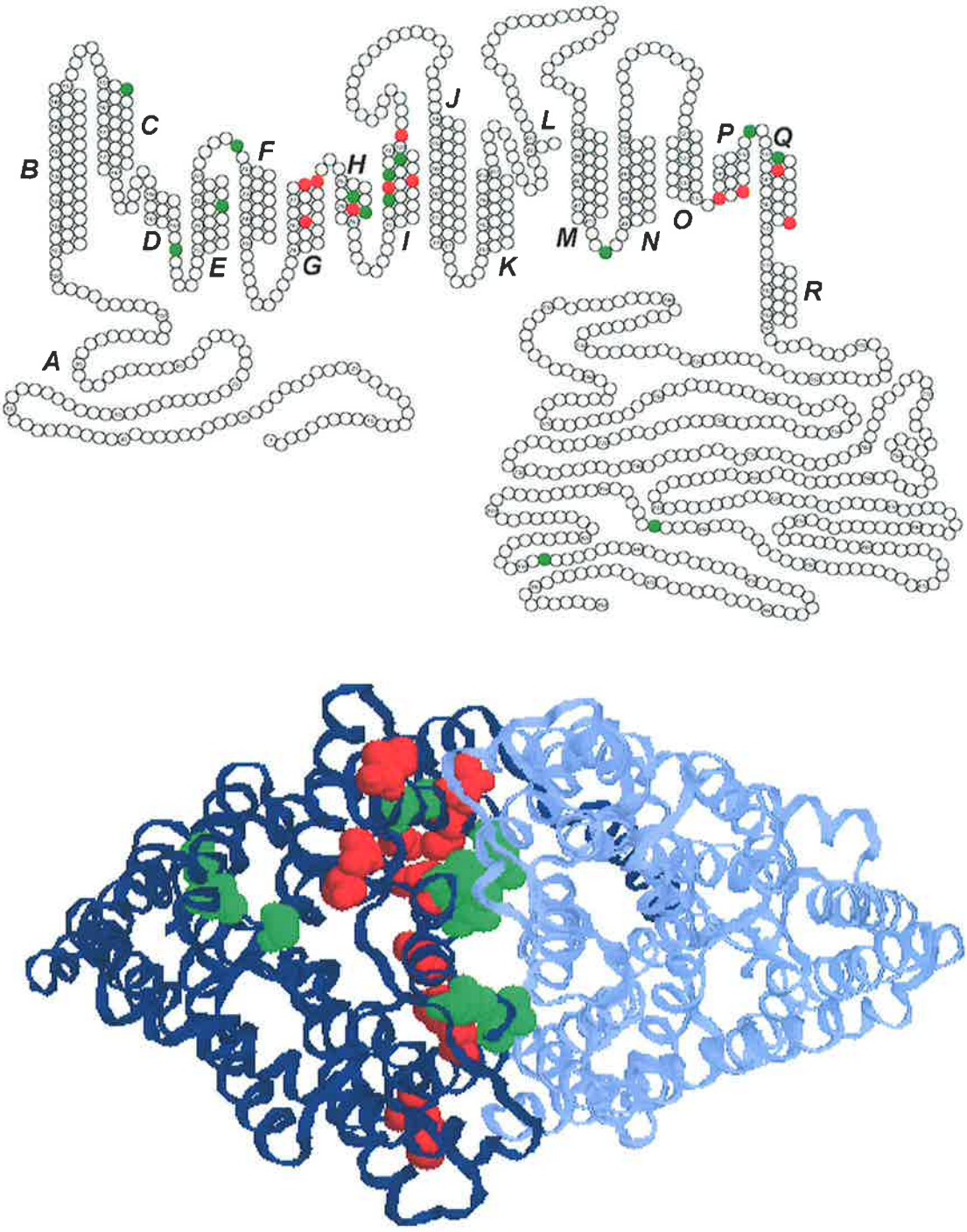

Figure III-1: Structure and topology of the ClC channel
(*Top*) Transmembrane topology of the ClC-1 channel, based on ClC structure determined by Dutzler et al., 2002, showing the transmembrane alpha-helical regions of the channel. (*Bottom*) Crystal structure of the ClC dimer (adapted from Dutzler et al., 2002). In both figures the positions of naturally occurring mutations causing dominant myotonia are indicated in green, whilst the positions of the mutations investigated in the present study are indicated in red.

III-2 Materials and Methods

III-2-1 Mutations

Eleven point mutations in the G, H, I, P and Q helices of the hClC-1 channel were studied in the present work. These mutations were: T268M, C277S, and C278S in helix G; S289A in helix H; T310M, S312A and V321S in helix I; T539A and S541A in the P helix; and M559T and S572V in helix Q. T268M was the only mutation investigated that has been previously reported as myotonic (Brugnoni et al., 1999). The C277S and C278S mutations are equivalent to the C212S and C213S mutations in ClC-0, which have been implicated in the common gating process of that channel. The remaining mutations were selected randomly to cover the G, H, I, P and Q helices, but with particular interest in residues in close proximity to known myotonic mutations. In these cases hydrophobic residues were switched for hydrophilic residues of about the same relative size, and vice versa.

III-2-2 Site-Directed Mutagenesis

Two-step PCR-based site-directed mutagenesis (Ho et al., 1989) was used to introduce point mutations into hClC-1 cDNA (Steinmeyer et al., 1994). This technique has been described above (see Chapter II: General Methods).

III-2-3 Cell Culture and Transfection

Human embryonic kidney (HEK293) cells were cultured and transfected as previously described (see Chapter II: General Methods).

III-2-4 Electrophysiology

Patch clamping experiments were performed as described previously (see Chapter II: General Methods).

III-2-5 Data Analysis

The time course of the ClC-1 current relaxations was fitted with an equation of the form:

$$I(t) = A_1 \exp(-t/\tau_1) + A_2 \exp(-t/\tau_2) + C \qquad \text{(III-1)}$$

where A_1 and A_2 represent the amplitude of the fast and slow exponential components, τ_1 and τ_2 are their time constants, C represents the amplitude of the steady state component and t is time.

Overall apparent open probability (P_o) for WT and mutant channels was calculated from normalised peak tail currents for voltage steps to –100 mV following test pulses ranging from +120 to –140 mV. Data points were fitted with a Boltzmann distribution with an offset to obtain P_o curves:

$$P_o(V) = P_{min} + \frac{1 - P_{min}}{1 + \exp((V_{1/2} - V)/k)} \qquad \text{(III-2)}$$

where P_{min} is an offset, or a minimum P_o at very negative potentials, V is the membrane potential, $V_{1/2}$ is the half-maximal activation potential, and k is the slope factor. Such a distribution assumes a maximal P_o of 1.

Open probability of the common gate was determined from protocols similar to those used to determine overall P_o, but with the addition of a brief (400 μs) activation pulse to 180 mV between the test pulse and the –100 mV tail pulse, to fully open the channel fast gates (Accardi and Pusch, 2000). Data points were fitted with Boltzmann distributions, as per Equation III-2.

Open probability of the fast gate was determined from the amplitudes of the fast deactivating component (Equation III-1) of ClC-1 currents in response to voltage steps ranging between –140 and –40 mV (as described previously by Aromataris et al., 2001), or by dividing overall P_o by the P_o of the common gate (as described in Accardi and Pusch, 2000). Both methods gave similar results.

The opening rate (α) and closing rate (β) of the common gate at a particular voltage were calculated according to:

$$\alpha = P_o^c / \tau_2 \qquad \text{(III-3a)}$$

$$\beta = (1 - P_o^c)/\tau_2 \qquad \text{(III-3b)}$$

where τ_2 is the time constant of the slower gating relaxations (Equation III-1) and P_o^c is the open probability of the common gate.

III-3 Results

All of the ClC-1 point-mutants investigated (T268M, C277S, C278S, S289A, T310M, S312A, V321S, T539A, S541A, M559T and S572V) produced currents deactivating at negative potentials with a double exponential time course (Figure III-2).

Some of the mutant channels investigated in this study (T268M, S289A, T310M, V321S and T539A) required prepulses to +120 mV, for up to 1600 ms, for full activation of the common gate. For better assessment of the changes produced by the mutations we therefore used a similar protocol for all channels, including WT and C277S channels. Comparison of the P_o curves of the C277S mutant (which has been shown to lock the ClC-1 common gate open; Accardi et al., 2001), obtained using protocols with either 200 or 800 ms long prepulses, shows that they are almost identical (Figure III-3*A, B*) and therefore it is unlikely that the longer protocols used in the present study have introduced

significant errors in determination of the $V_{1/2}$ or minimum P_o due to Cl^- accumulation or depletion. Results were also similar for the WT channel, however with longer voltage protocols the overall P_o curves were somewhat shifted to the right, and minimum P_o of the common gate was lowered from 0.41 to 0.36 (Figure III-3*C, D*), suggesting the presence of a small slower component in ClC-1 gating, in addition to the fast and slow gating processes usually investigated (cf Rychkov et al., 1996).

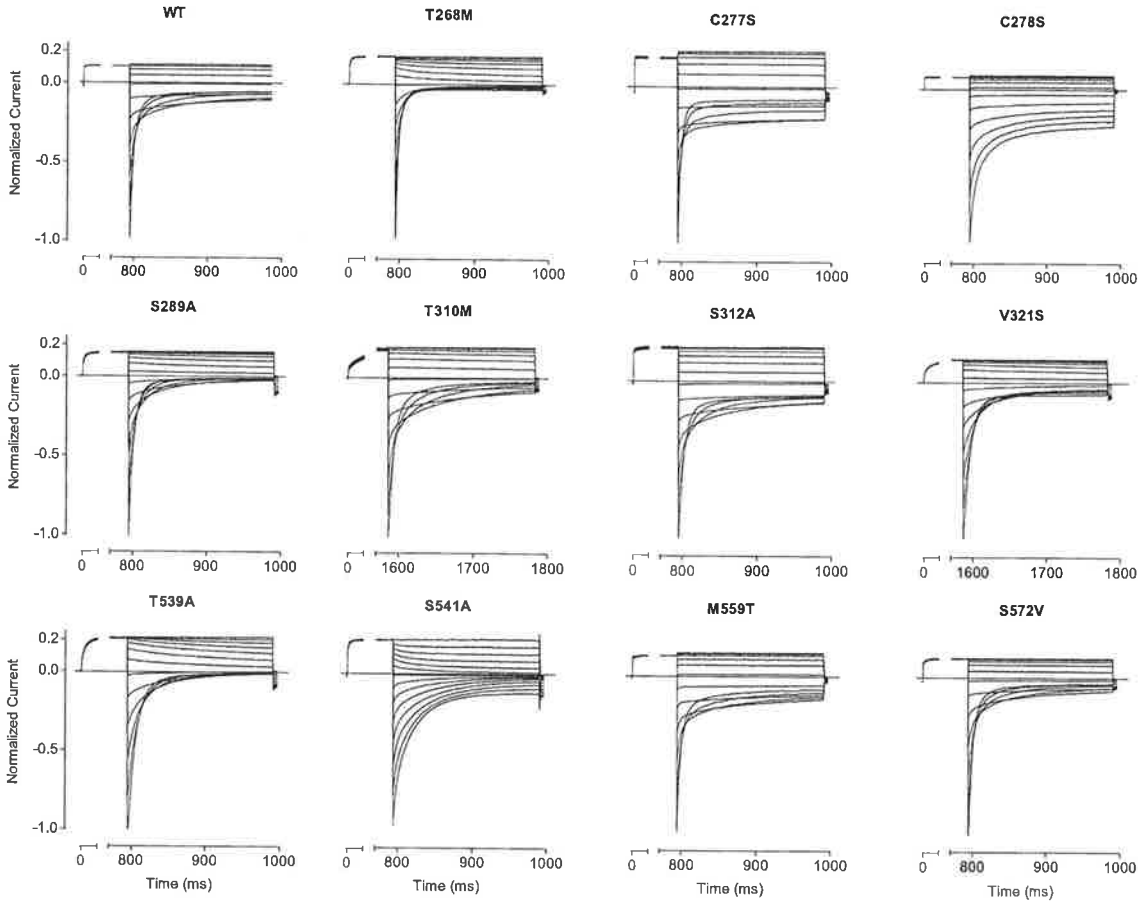

Figure III-2: Whole-cell currents in HEK 293 cells expressing wild-type (WT) and mutant ClC-1 channels
Currents were activated by the following voltage protocol: holding potential was –30 mV; a prepulse to either +40 (WT, C277S, and C278S) or +120 mV (all other mutations) was followed by steps ranged from –140 to +120 mV in 20 mV increments. Currents in each panel are normalised to the maximum peak current observed at –140 mV.

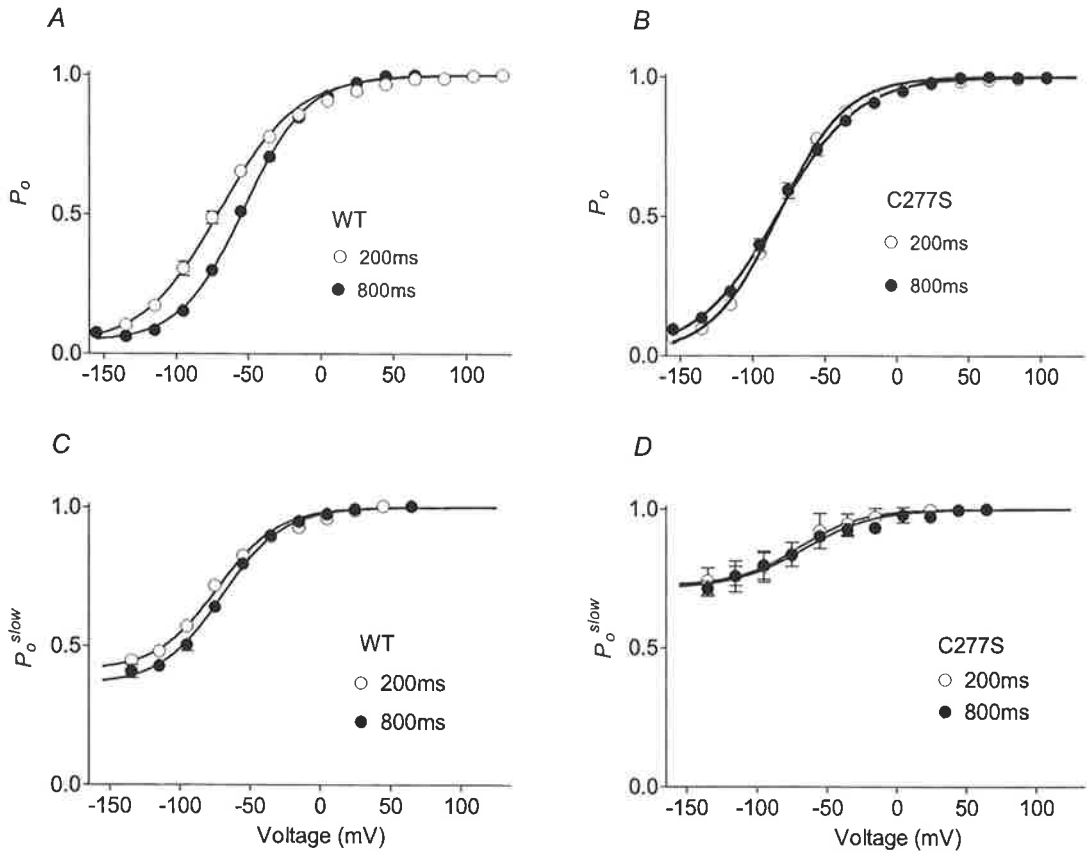

Figure III-3: Effect of prepulse duration on P_o of WT and C277S ClC-1 channels
Overall P_o (*A, B*) and P_o of the common gate (*C, D*) of WT (*A, C*) and C277S (*B, D*) ClC-1 channels. Data points are obtained as described in III-2-5: Data Analysis, and fitted with a Boltzmann distribution with an offset. (Equation III-2; n = 4–10).

The time constants of the exponential components of the currents of nine mutant channels out of eleven were all within 2.5-fold of those of the WT channel (Figure III-4), while S312A and M559T showed currents virtually identical to that of WT ClC-1 (not shown). Visible changes of the kinetics of current deactivation were predominantly due to significant changes in the relative amplitudes of those exponential and steady state components that reflect changes in the P_o of the fast and common gates (Aromataris et al., 2001).

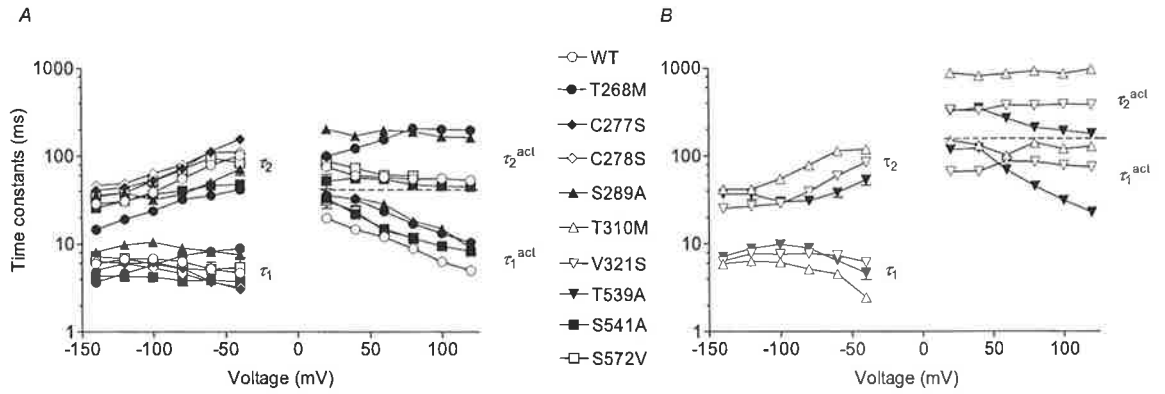

Figure III-4: Time constants of current relaxations of ClC-1 WT and mutant channels
Time constants at negative potentials are extracted from deactivating currents, as shown in Figure III-2, and correspond to the relaxation of the fast (τ_1) and common (τ_2) gate. Time constants at positive potentials (τ_1^{act}, τ_2^{act}) are extracted from activating currents, as shown in Figure III-7, and correspond to relaxation of the common gate (n=3–12). The dotted line separates the time constants τ_1^{act} and τ_2^{act}. Voltages shown are not corrected for liquid junction potentials.

Investigation of the voltage dependence of the P_o of the seven channels with mutations in the G, H and I domains showed that some mutations shifted $V_{1/2}$ to more positive potentials (T268M, S289A, T310M and V321S), whilst others shifted $V_{1/2}$ to more negative potentials (C277S and C278S), and the mutation S312A had no effect on $V_{1/2}$ (Figure III-5, Table III-1). Separation of the P_o of the fast and the common gates by either of the methods described previously (Accardi and Pusch, 2000; Aromataris et al., 2001) revealed that only two of the mutations investigated (T268M and C278S) affected the P_o of the fast gate (Figure III-6, Table III-1), while five mutations (T268M, C277S, S289A, T310M, V321S) changed the P_o of the common gate (Figure III-6, Table III-1). The majority of mutations shifted the $V_{1/2}$ towards more positive potentials and reduced the minimum P_o. Mutations C278S and C277S, however, did not shift the $V_{1/2}$, but increased the minimum P_o of the fast and common gates respectively.

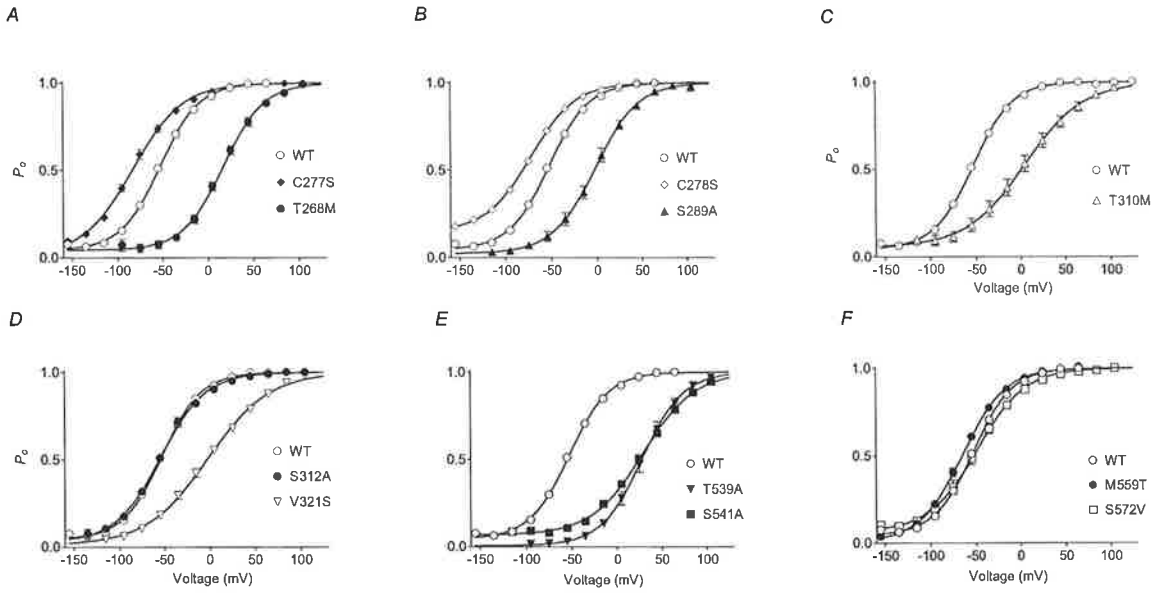

Figure III-5: Open probability of WT and mutant ClC-1 channels as a function of membrane potential
Data points are extracted from tail currents as described in III-2-5: Data Analysis, and fitted with a Boltzmann distribution with an offset (Equation III-2; n= 4 –12).

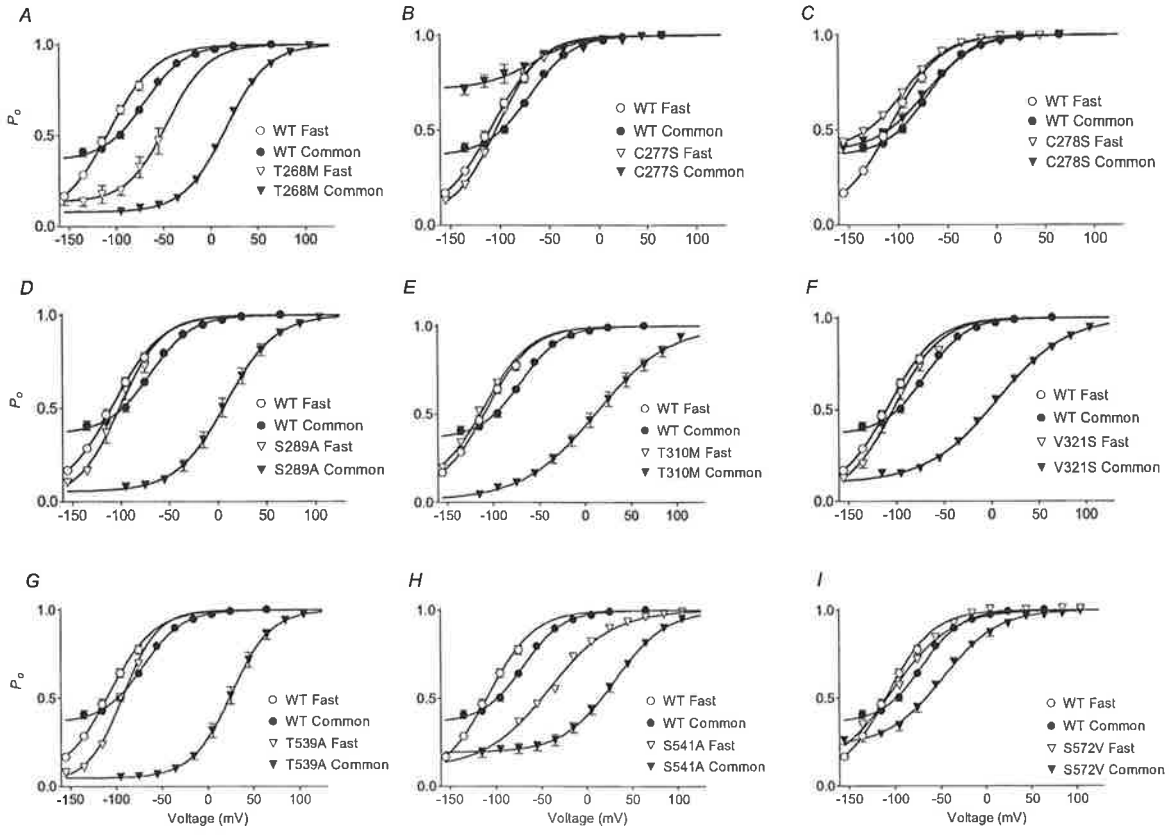

Figure III-6: Open probability of the fast and common gate of WT and mutant ClC-1 channels as a function of membrane potential
Data points are obtained as described in III-2-5: Data Analysis, and fitted with a Boltzmann distribution with an offset. (Equation III-2; n = 4–10).

Table III-1: Gating parameters for WT and mutant ClC-1 channels

Mutant	Overall P_o		Fast P_o		Common P_o	
	$V_{½}$ (mV)	P_{min}	$V_{½}$ (mV)	P_{min}	$V_{½}$ (mV)	P_{min}
WT	-52.7±1.0	0.04±0.01	-107.3±1.7	0.05±0.02	-68.5±1.2	0.36±0.01
T268M	+17.2±1.0	0.04±0.01	-45.7±2.4	0.13±0.02	+16.4±0.6	0.09±0.09
C277S	-82.5±1.5	0.02±0.02	-101.8±1.8	0.05±0.03	-66.2±4.9	0.72±0.02
C278S	-72.2±0.4	0.15±0.01	-94.4±0.6	0.40±0.01	-72.3±1.0	0.39±0.01
V286A	Shifts by +61					
S289A	-1.7±1.0	0.02±0.01	-100.8±2.9	0.02±0.04	+8.2±1.0	0.05±0.01
I290M	Shifts by +75		Shifts by +74		Shifts by +87	
F307S	Shifts by +74		Shifts by +14		Shifts by +63	
T310M	+5.2±1.3	0.05±0.01	-109.1±4.3	0.09±0.05	+11.0±1.5	0.01±0.01
S312A	-54.2±1.2	0.03±0.01	-111.4±3.6	0.03±0.05	-53.5±2.0	0.33±0.02
A313T	Shifts by +113		Shifts by +9		Shifts by +99	
V321S	-2.1±1.4	0.01±0.01	-102.2±3.6	0.02±0.04	+5.9±1.5	0.10±0.01
T539A	+28.1±0.4	0.01±0.01	-92.0±2.7	0.03±0.04	+25.9±0.2	0.05±0.01
S541A	+29.0±0.9	0.07±0.01	-41.7±4.1	0.10±0.05	+29.8±0.5	0.19±0.01
M559T	-64.9±0.6	0.01±0.01	-121±4.0	0.02±0.06	-60.8±1.0	0.20±0.01
S572V	-48.6±1.0	0.07±0.01	-102.7±4.9	0.08±0.06	-47.3±1.5	0.23±0.01

Parameters of Boltzmann fits ($V_{½}$ and P_{min}) for the P_o of WT and mutant ClC-1 channels and the P_o of their fast and common gates (n = 3 – 10). Also shown are the changes in $V_{½}$ caused by dominant negative mutations previously investigated by others: V286A (Kubisch et al., 1998), I290M (Pusch et al., 1995b; Accardi and Pusch, 2000), F307S and A313T (Aromataris et al., 2001)

Mutations in the P and Q domains also showed altered voltage dependence of gating, with three out of the four mutations investigated (T539A, S541A and S572V) shifting $V_{1/2}$ of the P_o of the common gate to more positive potentials, while S541A also showed a shift in fast gating (Figure III-6, Table III-1).

In order to understand these changes in gating it is necessary to calculate the opening and closing rates of the ClC-1 gating processes. Two exponential components of ClC-1 current relaxations reflect the fast and common gating processes and can be consistently extracted from deactivating macroscopic currents at negative potentials

(Saviane et al., 1999). At more positive potentials gating relaxations become exponentially faster, to such an extent that the time constant of the fast gate cannot be extracted from the currents at +80 mV, as it falls below 100 μs (Accardi and Pusch, 2000). Time constants of the common gate relaxation remain in the range of milliseconds for potentials of up to +200 mV and, theoretically, can be obtained from the time course of ClC-1 activation at positive potentials. We recorded activating ClC-1 currents in response to positive voltage steps, following a prepulse to -120 mV (Figure III-7). Analysis of the current kinetics revealed that WT ClC-1 activated with a double exponential time course, with time constants in the range of 5–20 ms and 50–100 ms (Figure III-4). The mutation C277S, which removed most of the common gating, also drastically diminished current activation at positive potentials, to the point where activating components could not be reliably extracted. In contrast, mutations T268M, S289A, T310M, V321S and T539A, which shifted $V_{1/2}$ of the common gating to more positive potentials and reduced minimum P_o, also demonstrated increased current activation at positive potentials (Figure III-7). Activating currents for all of these mutants could be fitted with two exponential components. In the T310M, V321S and T539A mutants these components were significantly slower than those of the WT, T268M and S289A channels (Figure III-4). In the WT channel and most of the mutants the time constant of the major exponential component, which was the faster component that accounted for 70-90 % of the current amplitude, and presumably represents the common gating process, showed clear voltage dependence similar to that reported by Accardi and Pusch, 2000. In T310M and V321S mutants the major component was the slower one, and unconstrained double exponential fit produced time constants that were virtually voltage independent. Open probability of both these mutants, however, is clearly voltage dependent in this voltage range. Therefore it is likely that the voltage pulses that were employed to activate the currents were not long enough (1600 ms) for accurate extraction of the slow time constants. Adequately long

pulses to such high voltages, however, usually resulted in the electrical breakdown of the cell membrane and could not be routinely used.

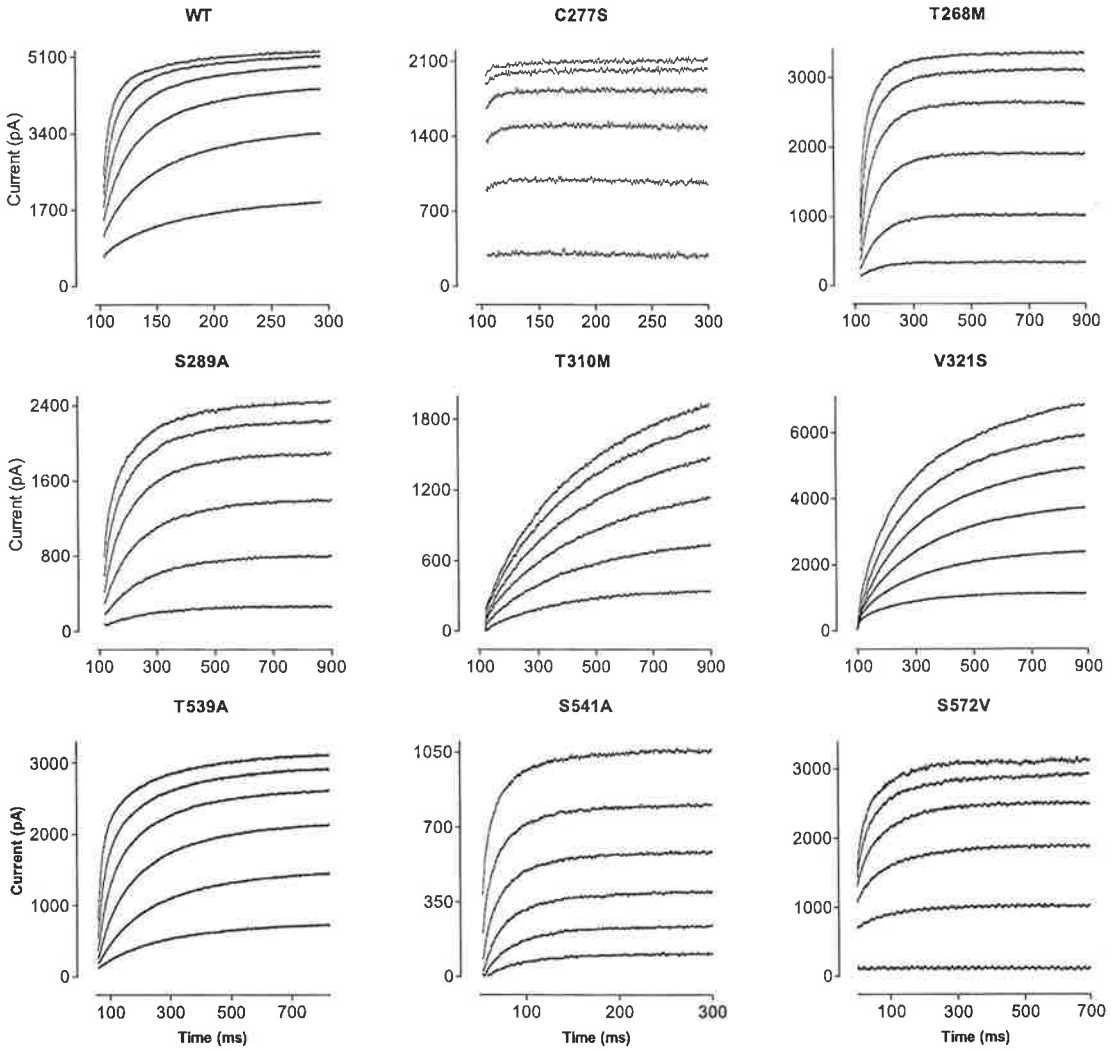

Figure III-7: Kinetics of activation of WT and mutant ClC-1 channels
Currents were recorded in response to voltage steps ranging from +20 mV to +120 mV, in 20 mV increments, following a prepulse to –120 mV (not shown).

At voltages where time constants could be extracted from activating or deactivating currents, and with the P_o known, it was possible to calculate opening and closing rates of the common gate of the WT and mutant channels, using Equations III-3a and III-3b. Calculations showed that mutation C277S reduced the closing rate of the common gate without affecting its opening rate. In contrast, T310M reduced the opening rate, without

affecting the closing rate of the common gate. Other mutations affected both opening and closing rates to different extents (Figure III-8).

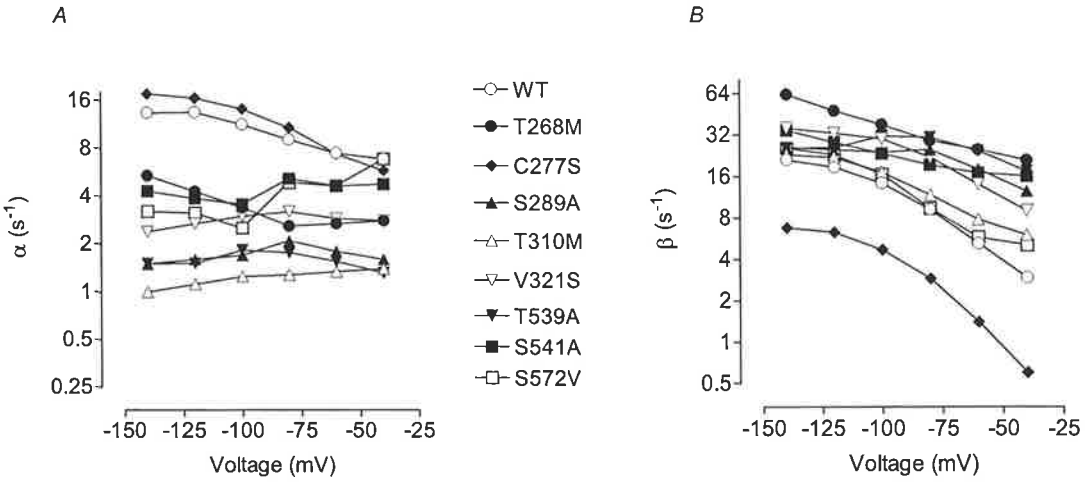

Figure III-8: Rate constants for WT and mutant ClC-1 channel common gating at negative potentials
Opening (*A*) and closing (*B*) rate constants were calculated from open probabilities shown in Figure III-6 and time constants shown in Figure III-4, as described in III-2-5: Data Analysis (n=3–10).

III-4 Conclusions

Results from single-channel recordings and extensive mutagenesis studies have long suggested that ClC-0 and ClC-1 channels have a double-barrelled structure with two parallel, independent, pores (Middleton et al., 1994; Ludewig et al., 1996; Middleton et al., 1996; Saviane et al., 1999). It has been proposed that each pore of these channels is gated by an independent, so-called 'fast' gating process, whilst another process, the 'slow' or 'common' gating process, opens and closes both pores simultaneously. High-resolution crystal structures of two bacterial proteins homologous to ClC-1 have now provided a definite confirmation of the double-barrelled structure of ClC channels. The molecular mechanisms of gating in both ClC-1 and ClC-0 channels, however, remain poorly understood. In particular it is yet to be determined whether the common gate is a distinct molecular structure that closes both protopores simultaneously, or if the common gating process arises from an interaction between the two fast gates that locks them

simultaneously into a closed conformation. In any case, the common gating process must involve interaction between the two channel subunits, and, judging by its high temperature dependence (Pusch et al., 1997; Bennetts et al., 2001), is accompanied by substantial structural rearrangements.

Allosteric interactions between the two subunits of ClC channels are likely to occur through the regions where they are joined. According to the crystal structure (Dutzler et al., 2002) the orientation of the two subunits is such that the H and I helices of one monomer are in close proximity to the P and Q helices of the other. Consequently the dimer interface comprises four helices on each side. Unlike the bacterial ClC channels, ClC-0 and ClC-1 have extensive cytoplasmic N- and C-terminal regions, and the interaction of these may also contribute to the common gating process (Fong et al., 1998). Of the H and I helix mutations investigated in this study, three out of four (S289A, T310M and V321S) altered the common gating mechanism, without changing fast gating. Two other known mutations in these helices, F307S and A313T, also affect only the common gating process (Aromataris et al., 2001; Table III-1). All of these mutations produced similar changes in the common gating process; $V_{1/2}$ shifted to more positive potentials, and minimum P_o was reduced to values close to zero. In addition, the current in these mutant channels activated much more slowly at positive potentials.

Mutations in the P and Q helices had similar affects to those in the H and I domains. Three out four mutations investigated, two in the P helix (T539A and S541A) and one in the Q helix (S572V), caused shifts in $V_{1/2}$ to more positive potentials, and decreased minimum P_o of the common gate. Although the effect of the mutation M572V was not so dramatic, and mutation M559T showed the phenotype of the WT channel, at least one dominant myotonic mutation is currently known in the Q helix, I556N (Kubisch et al., 1998; Saviane et al., 1999). According to the ClC crystal structure, helix G has no direct contacts with the other subunit, as it lies behind the H and I helices (Dutzler et al.,

2002). Nevertheless, a number of mutations in this helix are known to have significant effects on the common gate. For example, mutation C277S removes most of the common gating process of ClC-1 (Accardi et al., 2001; present work). Surprisingly, mutation of the adjacent cysteine residue to serine, C278S, didn't affect the common gate, but significantly reduced fast gating, increasing minimum P_o of the fast gate from ~0.05 to ~0.4. Other mutations in the G and H helices, T268M and I290M (Saviane et al., 1999), shifted P_o of both gates to more depolarising potentials to a similar extent. In the P helix one of the mutants investigated, S541A, also shifted the fast gating process, in addition to its affect on the common gate, causing a shift in the $V_{1/2}$ of fast gating to more positive potentials. No known mutations in the I helix, or in the Q helix, affect fast gating.

Whole-cell current relaxations of the ClC-1 channel recorded during voltage steps to more negative potentials have been shown by direct single channel measurements to represent closure of the fast and common gates (Saviane et al., 1999). In the most comprehensive investigation to date of the kinetics of ClC-1 over a wide range of voltages Accardi and Pusch, 2000 showed that at negative potentials the time constants of the fast and common gating relaxations are virtually voltage independent, whilst at more positive potentials the time constants become exponentially smaller, to the point where activation of the fast gate is too fast to be extracted from the activating currents. In their study a single exponential was able to describe activation of the common gate. In the present work, however, two exponential components were required to fit activation of the WT channel, and most mutant channels, recorded during voltage steps to more positive potentials. The time constant of the first component corresponded well with the time constant of the common gate activation previously reported by Accardi and Pusch, 2000. The nature of the second component became apparent in the C277S mutant; while removing most of the slow exponential component from the current relaxation at negative potentials, this mutation also removed most of both exponential components at positive potentials. Hence,

it is likely that both of these two exponential components correspond to activation of the ClC-1 common gate, suggesting that at least a three-state kinetic model is required to describe the ClC-1 common gating process.

Open probabilities of both the fast and common gates of WT ClC-1 are voltage dependent, however at negative potentials they saturate at non-zero minimum values (Table III-1; Accardi and Pusch, 2000; Aromataris et al., 2001). Voltage dependence of the P_o of any channel arises from the voltage dependencies of its opening (α) and closing rates (β):

$$P_o(V) = \alpha(V)/(\alpha(V)+\beta(V)) \qquad \text{(III-4)}$$

Voltage dependence of α and β is described by the following equations:

$$\alpha(V) = \alpha(0) \exp (z_\alpha FV/RT) \qquad \text{(III-5a)}$$

$$\beta(V) = \beta(0) \exp (z_\beta FV/RT) \qquad \text{(III-5b)}$$

where $\alpha(0)$ and $\beta(0)$ are rates in the absence of voltage, and z is the gating charge of the corresponding gating transition. According to these equations a minimum P_o greater than zero is only possible if z_α and z_β become equal at some point, so that both rates vary with voltage in parallel. Calculations indicate that the opening and closing rates of the common gate of WT and mutant channels have the same voltage dependence at potentials negative to –80 mV, whilst at positive potentials the opening and closing rates have opposite voltage dependence. Such a pattern explains not only the non-zero minimum P_o, but also why the time constants of both fast and common gates of ClC-1 are virtually voltage independent at negative potentials, and become exponentially smaller at positive potentials (Accardi and Pusch, 2000). This case is similar to that seen for the fast gate of ClC-0 (Chen and Miller, 1996; Pusch et al., 2001).

To explain voltage dependence of the opening rate of the ClC-0 fast gate Chen and Miller, 1996 proposed the following model, with one unliganded (*C*) and two Cl^--liganded (C^{Cl}) closed states:

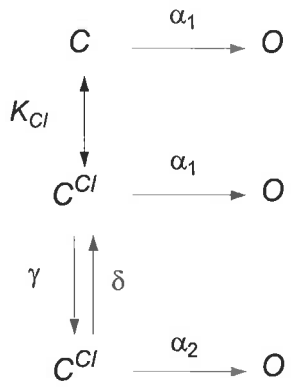

Most of the channel's voltage dependence is postulated to come from the transitions between the two Cl^--liganded closed states; with $\alpha_2 >> \gamma$, δ and α_1 at all accessible voltages. At negative potentials the rate-limiting step is the hyperpolarisation-favoured opening process, with an opening rate α_1:

$$\alpha_1(V) = \alpha_1(0) \exp(z_{\alpha 1}FV/RT) \qquad \text{(III-6)}$$

whilst at positive potentials Cl^- movement is the rate-limiting step, and the opening rate is determined by γ:

$$\gamma(V) = \gamma(0) \exp(z_{\gamma}FV/RT) \qquad \text{(III-7)}$$

The observed overall opening rate is therefore the sum of α_1, and γ weighted by a factor determined by $[Cl^-]_o$ and the Cl^- dissociation constant, K_{Cl}:

$$\alpha(V) = \alpha_1(V) + \gamma(V)([Cl^-]_o/K_{Cl})/(1+[Cl^-]_o/K_{Cl}) \qquad \text{(III-8)}$$

This model describes well the experimental data on voltage and Cl^- dependence of ClC-0, and predicts that at high positive potentials activation of the fast gate of ClC-0 should follow a single exponential time course.

Voltage and Cl^- dependence of both the fast and the common gates of ClC-1 are similar to that of the fast gate of ClC-0 (Chen and Miller, 1996; Accardi and Pusch, 2000;

Aromataris et al., 2001). In ClC-1, however, current activation between +20 and +120 mV follows a double exponential time course, suggesting a more complex mechanism for the common gating process of ClC-1 than that shown in Scheme 1: either α_2 is not so much bigger than the other rate constants, or there is another closed state of the common gate. In the absence of single channel recordings, however, which would allow comprehensive modelling of the ClC-1 common gating process, the model suggested by Chen and Miller (Scheme 1) can still be used for qualitative understanding of the changes in the common gating process caused by the mutations investigated in the present study.

For simplicity we therefore fitted ClC-1 activating currents with a single exponential, and used the corresponding time constants, together with the slow time constants of the deactivating currents, to calculate opening and closing rates for voltages between −140 and +100 mV. The results were fitted with equations III-5b and III-8, assuming that $([Cl^-]_o/K_{Cl})/(1+[Cl^-]_o/K_{Cl})$ is a voltage-independent constant at a constant $[Cl^-]_o$, and can therefore be incorporated into $\gamma(0)$. The apparent gating charge $z_{\alpha 1}$ was set to -0.3 and z_γ to 0.5, which is comparable with that seen for the fast gate of ClC-0 (Chen and Miller, 1996), and is consistent with the results of Accardi et al., 2001). It is clear that mutations T268M, and T539A shifted both opening rates of the common gate, α_1 and γ, along the Y-axis (Figure III-9). The observed shift of these opening rates could be attributed entirely to changes in the pre-exponential factors $\alpha_1(0)$ and $\gamma(0)$. In general, these factors depend on temperature and on the activation energy of the corresponding transitions in the absence of an electric field. In our case $\gamma(0)$ was also dependent on $[Cl^-]_o$ and K_{Cl}. It is unlikely, however, that K_{Cl} was altered, as not only $\gamma(0)$, but also $\alpha_1(0)$ was changed simultaneously by these mutations. Therefore it is probable that, compared to WT ClC-1, the energy of the unliganded closed state (Scheme 1) is lower in these mutants, such that the activation energies of the opening transitions at either negative or positive

potentials are increased. Consequently channel closing becomes energetically more favourable. A decrease in the opening rate explains both the shift of $V_{1/2}$ to more depolarised potentials, and the decreased minimum P_o of the common gate of these mutant channels, as well as the slower channel activation kinetics seen at positive potentials. Mutations T268M and T310M shifted $V_{1/2}$ of the common gate to approximately the same extent, however the kinetics of their activation at positive potentials are significantly different. This difference is explained by the fact that mutation T268M not only decreases the common gate opening rate, as T310M does, but also increases the closing rate. Although the increase in closing rate brings the same changes in the P_o as decrease of the opening rate, it makes the kinetics faster, not slower (Equation III-3b).

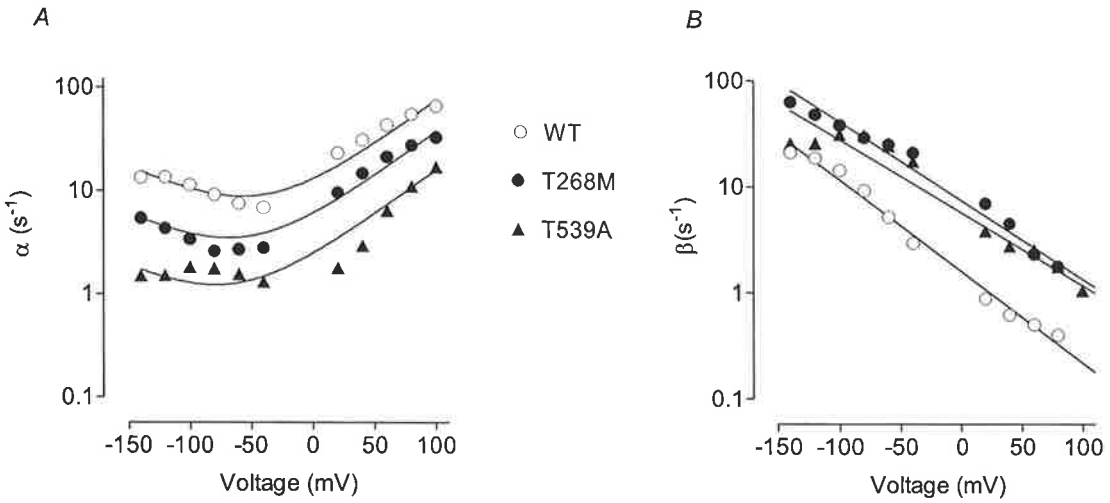

Figure III-9: Voltage dependence of opening and closing rate constants of the common gating process for WT, T268M, and T539A ClC-1 channel
Data points for opening (*A*) and closing (*B*) rate constants at negative potentials are as in Figure III-8; data points at positive potentials are obtained as described in III-4: Conclusions. Opening rates are fitted with a two-exponential distribution (Equation III-8 combined with Equations III-6 and III-7) with the gating charges set to –0.3 and 0.5 for $\alpha_1(V)$ and $\gamma(V)$ respectively. The parameters of the fit were: $\alpha_1(0)$ (2.8; 0.97; and 0.41) and $\gamma(0)$ (10.3; 5.1; and 1.5) for WT, T268M, and T539A respectively. Closing rates were fitted with a single-exponential distribution (Equation III-5b).

An example of a mutation that showed only changes in the closing rate of the common gate is C277S. This mutation significantly decreased the closing rate of the common gate, with minimal effect on the opening rate which suggests that the energy of

the closed state of this mutant is not different from that of the WT, but that the energy of the open state is lowered, such that the activation energy of the backward transition is greatly increased, and hence channel closing becomes energetically less favourable. An explanation for the increase of the minimum P_o of the common gate in C277S is thus provided.

In conclusion, this study has shown that the majority of mutations investigated at the interface between two monomers of ClC-1 are able to alter P_o and the kinetics of the common gate compared with WT channels. All of the effects on common gating caused by these mutations can be explained in terms of changes in either the common gate opening rate, the closing rate, or both, resulting from changes in the activation energies of the opening or closing transitions of the ClC-1 common gate. These results strongly support the hypothesis that the helices at the ClC-1 dimer interface are involved in the common gating process of ClC-1, however, these are unlikely to be the only regions of the channel involved in the common gating process. Mutations in a number of other helices are able to cause hyperpolarisation-induced activation of the ClC-1 channel, for example, S132C (helix A, Wu et al., 2002), D136G (helix A, Fahlke et al., 1995), K231A (helix F, Fahlke et al., 1997c) and G499R(helix N, Zhang et al., 2000), suggesting that these mutations either remove, or drastically alter, the ClC-1 common gating process. There are also a number of naturally occurring mutations within the carboxyl terminus of the ClC-1 channel, or within other regions of the channel, which cause dominant myotonia, suggesting that these mutations may also affect ClC-1 common gating, for example G200R (DE linker), A218T (helix E), G230E (EF linker), P480L (MN linker) and R894X, P932L (C terminus) (see Pusch et al., 2002). This suggests that although the ClC-1 dimer interface is important in ClC-1 common gating, that movements in other regions of the channel are also involved – the precise mechanism of this complex and interesting phenomenon is yet to be established.

Chapter IV: Temperature Dependence of the ClC-1 Common Gate Mutant T539A

IV-1 Introduction

Recent structure-function analysis of ClC-1 dominant myotonic mutations, combined with mutagenesis (Duffield et al., 2003; see Chapter III: Involvement of Helices at the Dimer Interface in ClC-1 Common Gating), and a structure-function analysis of mutations in the renal ClC-5 channel (Wu et al., 2003), show the importance of the region at the ClC dimer interface in the common gating process. Our previous research has shown that changes in common gating observed in a number of ClC-1 mutants in the interface region of the channel resulted from changes in the opening rate, the closing rate, or both rates, of the common gate (Duffield et al., 2003; see Chapter III: Involvement of Helices at the Dimer Interface in ClC-1 Common Gating). This research suggests that such changes are most likely due to changes in the energy of the open and/or closed common gate states of the mutant channels, leading to alterations in the transition rates between these states. The current research has therefore investigated the temperature dependence of one of those common gating mutants, T539A, and shows that the changes in common gating observed in this channel are indeed related to alterations in the energies of the open and closed common gate states.

IV-2 Methods

IV-2-1 Mutations

This research has analysed the temperature dependence of the ClC-1 mutant T539A. Kinetics and gating of this mutant have been described in our previous research (Duffield et al., 2003; see Chapter III: Involvement of Helices at the Dimer Interface in ClC-1 Common Gating).

IV-2-2 Site-Directed Mutagenesis

Two-step PCR-based site-directed mutagenesis (Ho et al., 1989) was used to introduce point mutations into hClC-1 cDNA (Steinmeyer et al., 1994). This technique has been described previously (see Chapter II: General Methods).

IV-2-3 Cell Culture and Transfection

Human embryonic kidney (HEK293) cells were cultured and transfected as previously described (see Chapter II: General Methods).

IV-2-4 Electrophysiology

Patch-clamping experiments were performed as described previously (see Chapter II: General Methods).

The temperature of the bath was varied in the range of 15 – 30 °C using a Peltier-based device with negative feedback, and measured approximately 1 – 5 mm from the clamped cell using a thermistor in the bath solution.

IV-2-5 Data Analysis

To analyse the temperature dependence of gating in the T539A mutant the protocols described in Chapter III: Involvement of Helices at the Dimer Interface in ClC-1 Common Gating, were used to determine the time constants of the fast and slow exponential components of ClC-1 channel gating, the channel apparent open probability (P_o), the fast and common gate open probabilities, and the opening and closing rates of the ClC-1 common gate, over the temperature range 15 – 30 °C. These variable were calculated from a number of cells, at different temperatures, and then pooled for analysis.

The temperature dependence of ClC-1 gating rate constants was analysed according to the Arrhenius equation:

$$\ln(\text{rate}) = \ln A - E_a/RT \qquad \text{(IV-4)}$$

where 'rate' is 'rate' is the opening or closing rate of the gating process (see Equations III-3a and III-3b, Chapter III) at the absolute temperature T, R is the gas constant, and A is a constant factor. This equation was also used to analyse the temperature dependence of ClC-1 gating time constants. The Arrhenius activation energy (E_a) was obtained from the slope of the Arrhenius plot (ln (rate) *versus* $1/T$), to allow calculation of the enthalpic component of the transition state ($\Delta H^{\ddagger}$):

$$\Delta H^{\ddagger} = E_a - RT \qquad \text{(IV-5)}$$

Q_{10} values were calculated according to:

$$Q_{10} = \text{rate}(T + 10\ \text{K})/\text{rate}(T), \text{ for } T = 293\ \text{K} \qquad \text{(IV-6)}$$

The Gibb's free energy of the transition state ($\Delta G^{\ddagger}$), and entropic component of the transition state ($\Delta S^{\ddagger}$) were determined using the equations:

$$\Delta G^{\ddagger} = -RTln(\text{rate}) + RTln(bT/h) \quad \text{(IV-7)}$$

$$\Delta S^{\ddagger} = (\Delta H^{\ddagger} - \Delta G^{\ddagger})/T \quad \text{(IV-8)}$$

Where b is Boltzmann's constant and h is Planck's constant.

For comparison with the T539A mutant channel a set of WT ClC-1 data obtained from the experiments of Brett Bennetts was analysed as described above.

IV-3 Results

The mutation T539A, which has previously been characterised (Duffield et al., 2003; see Chapter III: Involvement of Helices at the Dimer Interface in ClC-1 Common Gating), is located in the ClC-1 'P' helix. This mutation, as with several others at the dimer interface, shifts the voltage-dependence of the ClC-1 common gate, without affecting the fast gating process.

IV-3-1 Temperature Dependence of Common Gating Time Constants

In the T539A mutant both fast and slow gating relaxations became exponentially faster with increasing temperature (Figure IV-1, Figure IV-2). The T539A common gate had a mean activation enthalpy ($\Delta H^{\ddagger}$) of 89 ± 29 kJ mol^{-1}, and a corresponding Q_{10} of 3.5, at –140 mV. This was comparable with the common gate of the WT channel, which showed a mean activation enthalpy ($\Delta H^{\ddagger}$) of 83 ± 10 kJ mol^{-1}, and a corresponding Q_{10} of 3.2, at –140 mV. The activation enthalpies and Q_{10} values for the common gate were essentially voltage independent over the range –140 to –80 mV for both WT and T539A channels.

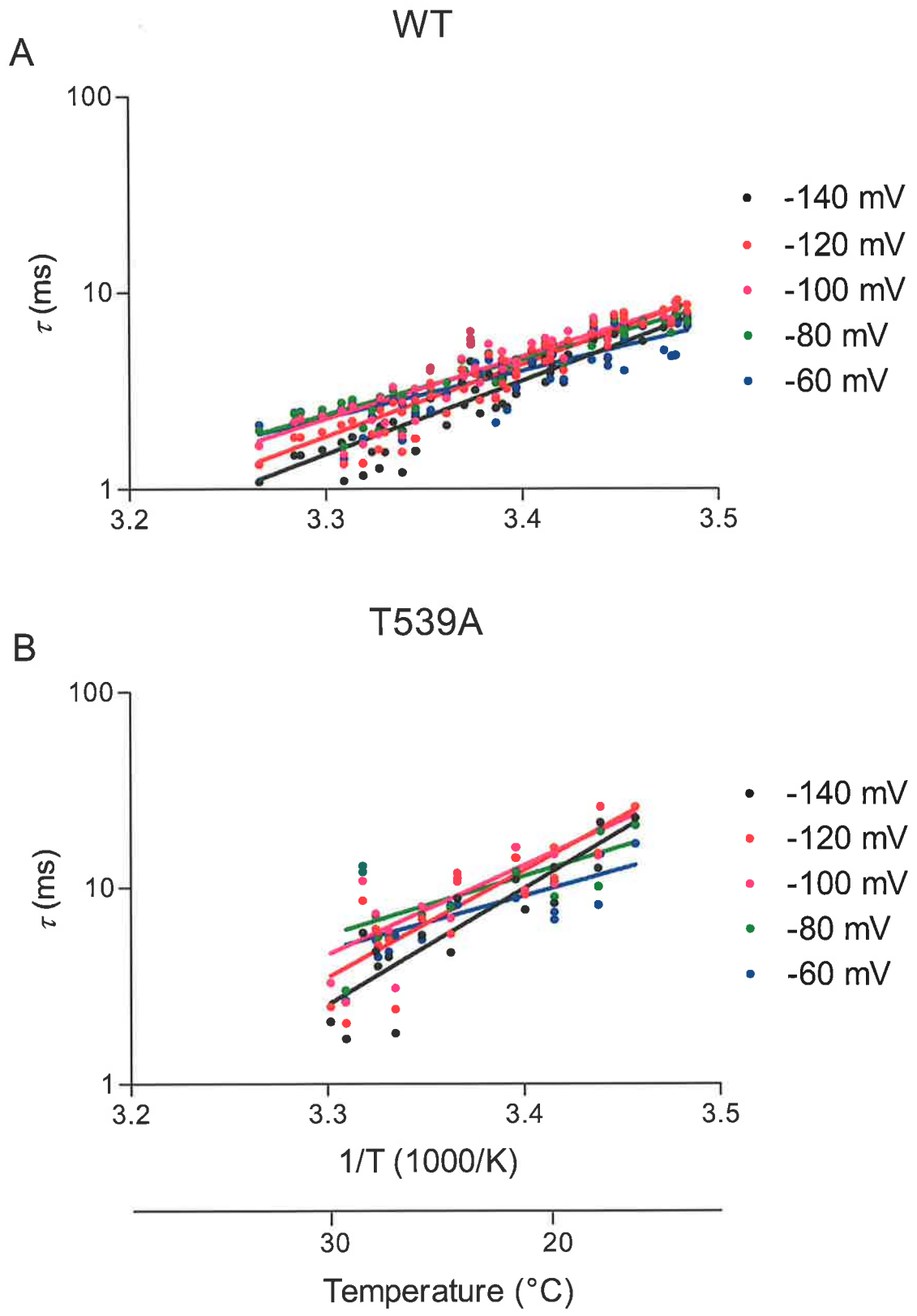

Figure IV-1: Temperature dependence of the ClC-1 fast gating time constant
Arrhenius plots of the ClC-1 fast gating time constant at voltages ranging from –60 to –140 mV, for both the WT (*A*) and T539A mutant (*B*) ClC-1 channels. Voltages shown are not corrected for liquid junction potentials.

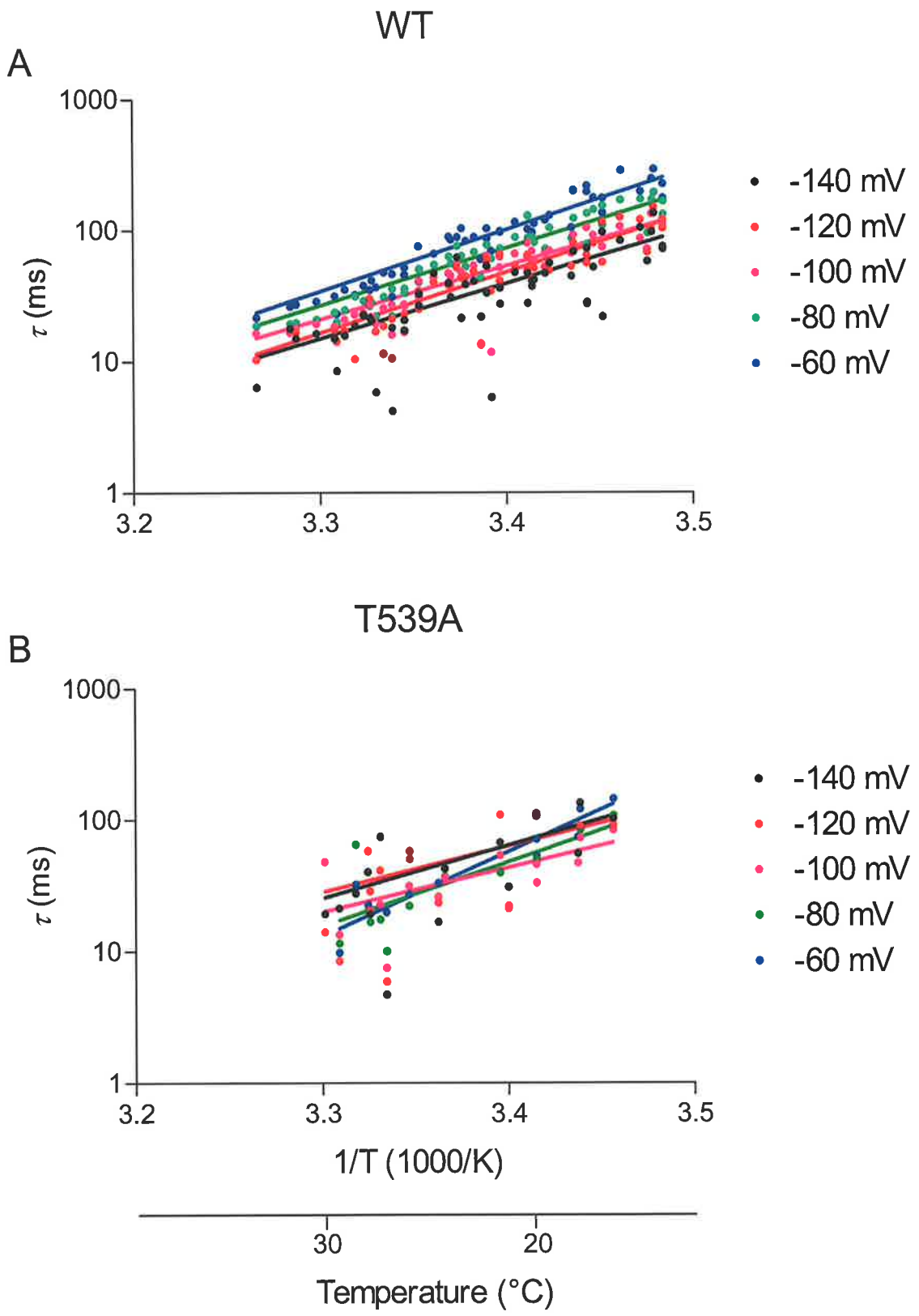

Figure IV-2: Temperature dependence of the ClC-1 common gating time constant
Arrhenius plots of the ClC-1 common gating time constant at voltages ranging from –60 to –140 mV, for both the WT (*A*) and T539A mutant (*B*) ClC-1 channels. Voltages shown are not corrected for liquid junction potentials.

IV-3-2 Temperature Dependence of Gating Open Probabilities

As has been previously described (Bennetts et al., 2001) the open probability of the WT ClC-1 channel is temperature dependent. In this study a shift in $V_{½}$ of 23.3 ± 1.8 mV towards more positive potentials per 10 °C increase in temperature (Figure IV-3) was observed. The minimal P_o of the WT channel did not appear to be temperature sensitive (Figure IV-4). Unlike the WT channel, the T539A channel showed no significant temperature dependence of either $V_{½}$ (Figure IV-3) or minimal P_o (Figure IV-4) over the temperature range investigated.

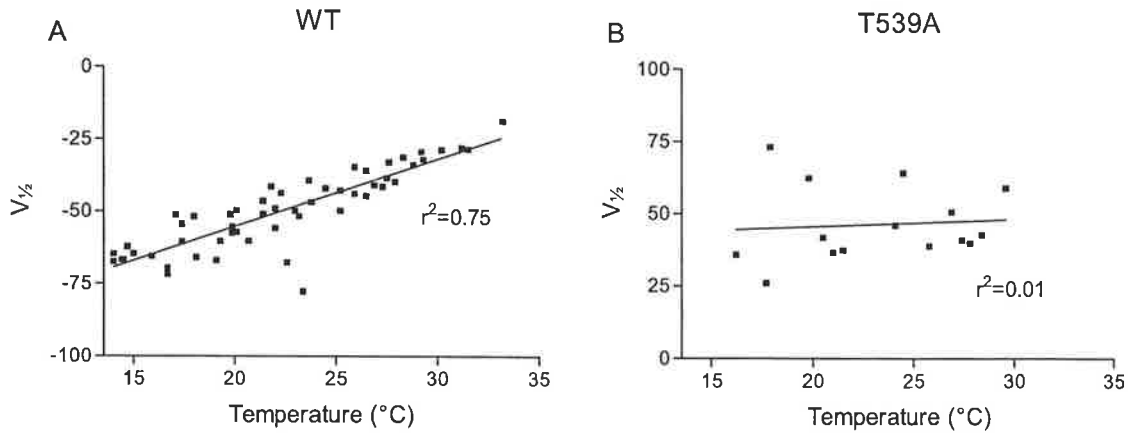

Figure IV-3: Effect of temperature on ClC-1 channel $V_{½}$
Temperature dependence of the half-maximal activation potential ($V_{½}$) for (*A*) WT and (*B*) T539A ClC-1 channels. The continuous lines are fitted in the form $V_{½}=mT+b$, where T is temperature, b is the $V_{½}$ at 0 °C, and m is the slope. $V_{½}$ values plotted are not corrected for liquid junction potentials.

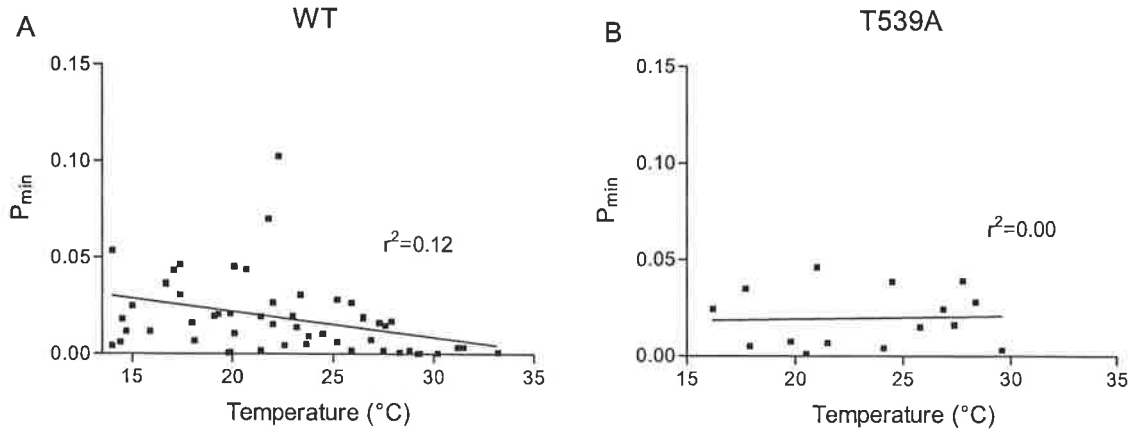

Figure IV-4: Temperature dependence of P_{min} for WT and T539A ClC-1 channels
Effect of temperature on the minimal open probability of the (*A*) WT and (*B*) T539A ClC-1 channels. The continuous lines are fitted in the form $P_{min} = mT + b$, where T is temperature, b is the P_{min} at 0 °C, and m is the slope.

Using the techniques described in IV-2-5: Data Analysis, the open probability of the common gating process was extracted from the channel open probability. It was observed that the common gate of the WT channel again showed temperature dependence, with a shift in $V_{½}$ towards more positive potentials of 16.5 ± 1.6 mV per 10 °C increase in temperature (Figure IV-5), and a decrease in minimal P_o, of 17.1 ± 2.0 % per 10 °C increase in temperature (Figure IV-6), while the T539A common gate open probability was again seen to show no temperature dependence, either in $V_{½}$ (Figure IV-5) or P_{min} (Figure IV-6).

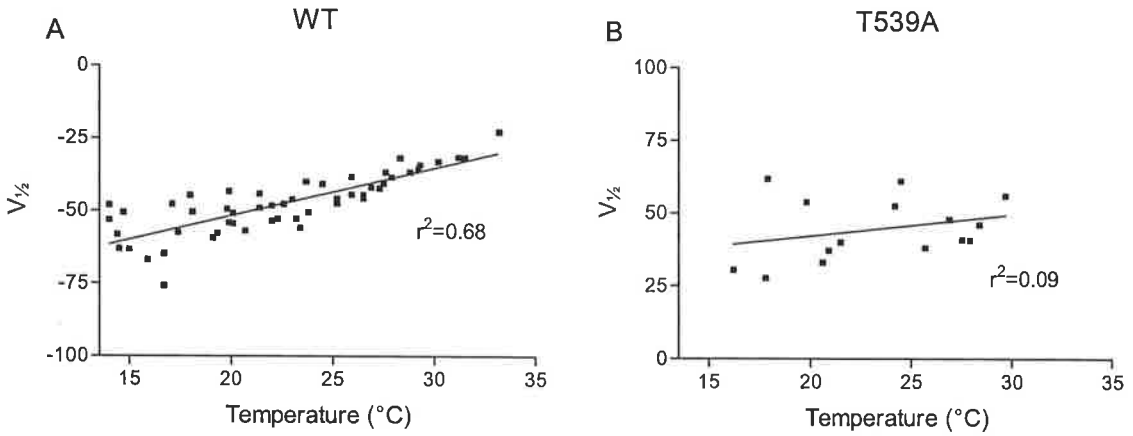

Figure IV-5: Temperature dependence of the ClC-1 common gate
V½ of the common gate is shown as a function of temperature for (A) WT and (B) T539A ClC-1 channels. The continuous lines are fitted in the form V½=mT+b, where T is temperature, b is the V½ at 0 °C, and m is the slope.

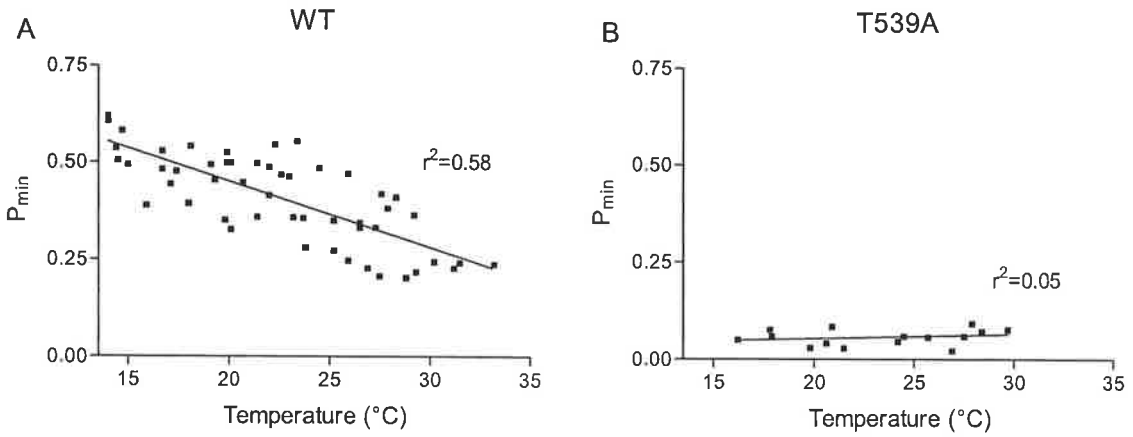

Figure IV-6: Effect of temperature on the ClC-1 common gate P_{min}
The temperature dependence of the minimal common gate open probability (P_{min}) is shown for (*A*) WT and (*B*) T539A ClC-1 channels. The continuous lines are fitted in the form $P_{min}=mT+b$, where T is temperature, b is the P_{min} at 0 °C, and m is the slope.

IV-3-3 Temperature Dependence of Gating Process Opening and Closing Rates

To further investigate the temperature dependence of ClC-1 common gating we have used the data described above to extract the opening and closing rates of the common gate for the WT and T539A channels, as described in Chapter II: General Methods.

The WT channel common gate opening and closing rates displayed some temperature dependence, with an increasing rate seen at higher temperatures. The common gate opening rate at –140 mV had a mean activation enthalpy ($\Delta H^{\ddagger}$) of 52.3 ± 9.5 kJ mol^{-1}, and Q_{10} of 2.1 (Figure IV-7). The common gate closing rate at this potential had a mean activation enthalpy ($\Delta H^{\ddagger}$) of 107.6 ± 8.8 kJ mol^{-1}, and Q_{10} of 4.4 (Figure IV-7). The temperature dependencies of the common gate opening and closing rates did not vary over the voltage range investigated.

The opening and closing rates of the T539A common gate were also temperature dependent. The opening rate showed a mean activation enthalpy ($\Delta H^{\ddagger}$) of 91.2 ± 31.9 kJ mol^{-1}, and Q_{10} of 3.6 at –140 mV (Figure IV-8), whilst the closing rate had a mean activation enthalpy ($\Delta H^{\ddagger}$) of 84.3 ± 34.6 kJ mol^{-1}, and Q_{10} of 3.24 (Figure IV-8). As with the WT channel, the temperature dependencies of both opening and closing rates did not change significantly over the voltage range investigated.

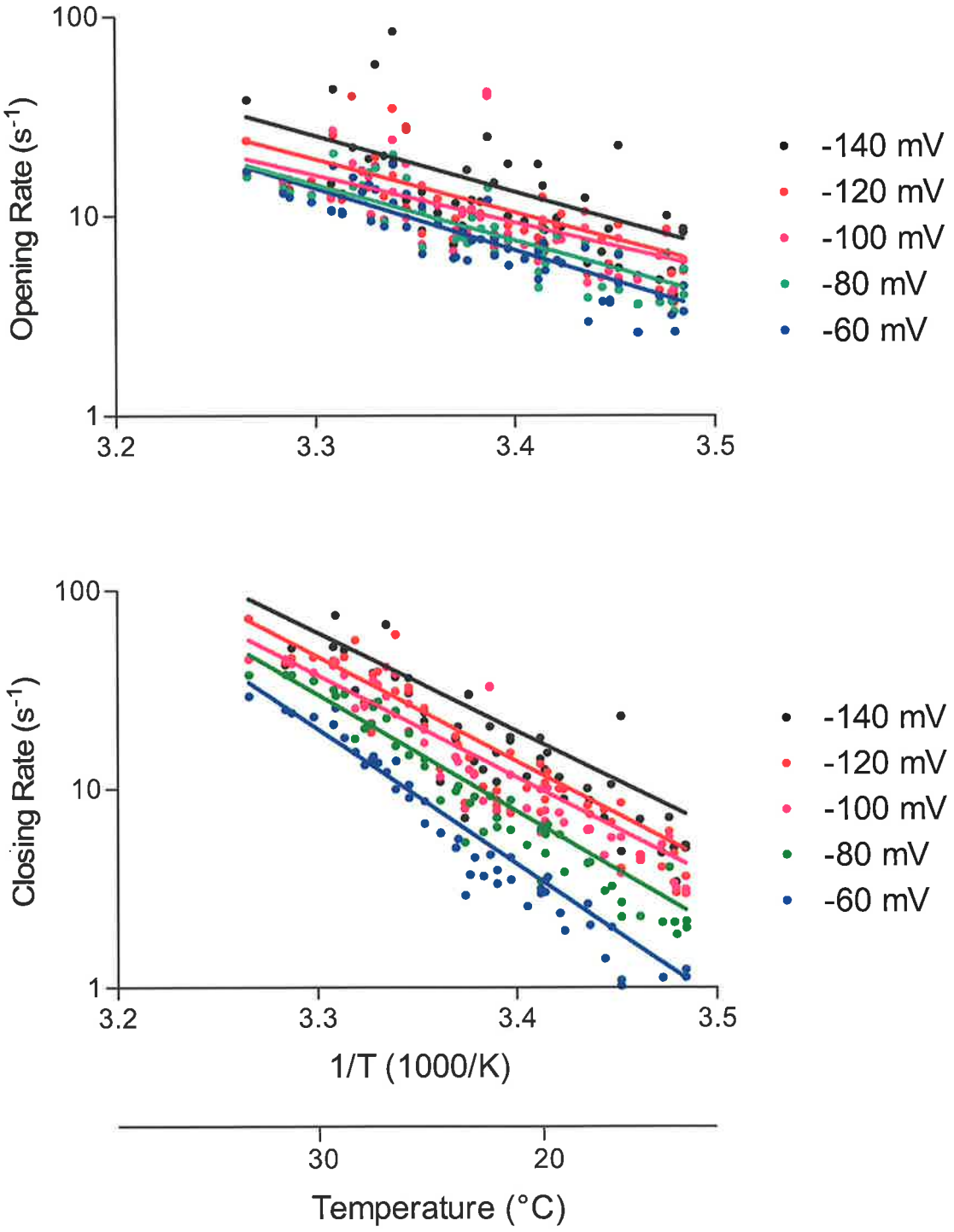

Figure IV-7: Temperature dependence of opening and closing rates of WT ClC-1 common gating
Arrhenius plots for the (*top*) opening and (*bottom*) closing rates of the WT ClC-1 common gate at voltages between –60 and –140 mV.

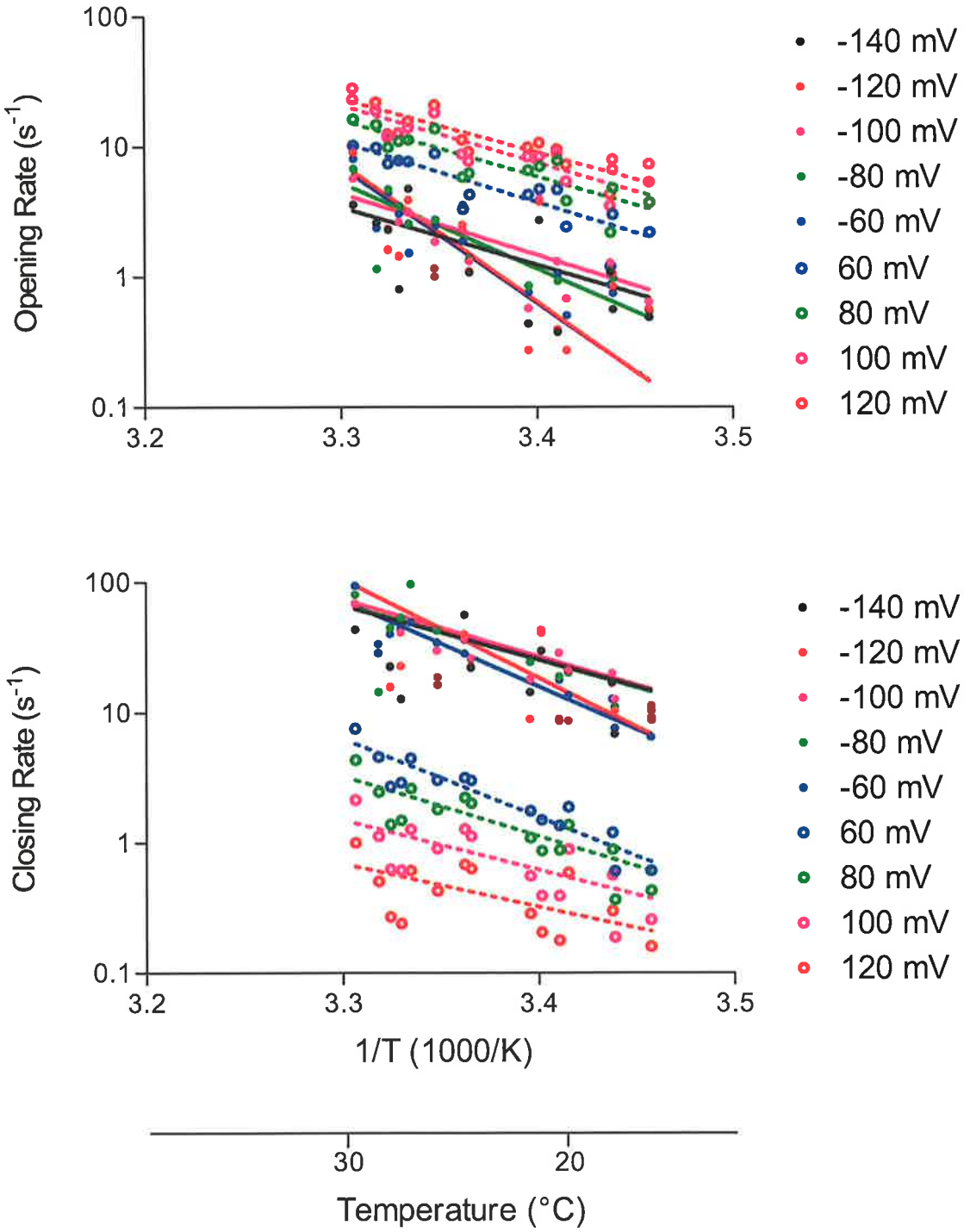

Figure IV-8: Temperature dependence of T539A ClC-1 common gate opening and closing rates

Arrhenius plots for the (*top*) opening and (*bottom*) closing rates of the T539A ClC-1 common gate at voltages between –60 and –140 mV.

IV-3-4 Energy of the Transition State Associated with ClC-1 Common Gating

Using the techniques described in IV-2: Methods, the Gibb's free energy associated with the opening and closing transition state of the ClC-1 common gate were calculated, along with the enthalpic (reported above) and entropic components (Table IV-1). For T539A these values were also calculated for positive potentials +40 to +120 mV.

The change in free energy (ΔG^0) between open and closed common gate states was determined from the difference between the free energies of common gate opening, and of closing, and is presented in Table IV-3.

Table IV-1: Thermodynamic properties of WT and T539A common gate opening and closing transition states at membrane potentials between –40 and –140 mV.

V (mV)	-140	-120	-100	-80	-60	-40
WT-Opening						
$\Delta G^{\ddagger}$ (kJ mol^{-1})	66.1 ± 0.2	66.6 ± 0.1	66.9 ± 0.1	67.3 ± 0.1	67.6 ± 0.1	67.3 ± 0.2
$\Delta H^{\ddagger}$ (kJ mol^{-1})	52.3 ± 9.5	55.7 ± 7.5	49.2 ± 6.6	56.5 ± 5.1	70.1 ± 6.8	56.2 ± 9.2
$\Delta S^{\ddagger}$ (kJ K^{-1} mol^{-1})	-0.05 ± 0.03	-0.04 ± 0.03	-0.06 ± 0.02	-0.04 ± 0.02	0.01 ± 0.02	-0.04 ± 0.03
E_a (kJ mol^{-1})	54.7 ± 9.5	58.1 ± 7.5	51.7 ± 6.6	59.0 ± 5.1	72.6 ± 6.8	58.6 ± 9.2
WT-Closing						
$\Delta G^{\ddagger}$ (kJ mol^{-1})	65.1 ± 0.2	65.7 ± 0.1	66.1 ± 0.1	66.9 ± 0.1	68.5 ± 0.1	70.2 ± 0.2
$\Delta H^{\ddagger}$ (kJ mol^{-1})	107.6 ± 8.8	112.6 ± 6.2	109.5 ± 5.3	124.2 ± 4.4	149.0 ± 5.8	142.6 ± 10.5
$\Delta S^{\ddagger}$ (kJ K^{-1} mol^{-1})	0.14 ± 0.03	0.16 ± 0.02	0.15 ± 0.02	0.19 ± 0.01	0.27 ± 0.02	0.24 ± 0.04
E_a (kJ mol^{-1})	110.1 ± 8.8	115.1 ± 6.2	112.0 ± 5.3	126.7 ± 4.4	151.5 ± 5.8	145.1 ± 10.5
T539A-Opening						
$\Delta G^{\ddagger}$ (kJ mol^{-1})	71.9 ± 0.5	71.9 ± 0.5	71.2 ± 0.3	71.3 ± 0.3	71.6 ± 0.3	72.0 ± 0.2
$\Delta H^{\ddagger}$ (kJ mol^{-1})	91.2 ± 31.9	109.3 ±39.6	85.3 ± 23.8	101.6 ±20.3	119.3 ± 17.4	117.4 ± 10.9
$\Delta S^{\ddagger}$ (kJ K^{-1} mol^{-1})	0.07 ± 0.11	0.13 ± 0.13	0.05 ± 0.08	0.10 ± 0.07	0.16 ± 0.06	0.15 ± 0.04
E_a (kJ mol^{-1})	93.7 ± 31.9	111.7 ± 39.6	87.8 ± 23.8	104.1 ± 20.3	121.8 ± 17.4	119.9 ± 10.9
T539A-Closing						
$\Delta G^{\ddagger}$ (kJ mol^{-1})	65.0 ± 0.5	64.8 ± 0.5	64.1 ± 0.3	64.3 ± 0.3	64.8 ± 0.2	65.8 ± 0.1
$\Delta H^{\ddagger}$ (kJ mol^{-1})	84.3 ± 34.6	100.9 ± 35.3	77.9 ± 22.3	89.5 ± 21.5	112.0 ± 12.0	120.4 ± 9.0
$\Delta S^{\ddagger}$ (kJ K^{-1} mol^{-1})	0.07 ± 0.12	0.12 ± 0.12	0.05 ± 0.08	0.08 ± 0.07	0.16 ± 0.04	0.18 ± 0.03
E_a (kJ mol^{-1})	86.8 ± 34.6	103.3 ± 35.3	80.4 ± 22.3	92.0 ± 21.5	114.5 ± 12.0	122.9 ± 9.0

Table IV-2: Thermodynamic properties of T539A common gate opening and closing transition states at membrane potentials between +40 and +120 mV.

V (mV)	+40	+60	+80	+100	+120
T539A-Opening					
$\Delta G^{\ddagger}$ (kJ mol^{-1})	70.1 ± 0.2	68.7 ± 0.2	67.6 ± 0.2	67.0 ± 0.2	66.6 ± 0.2
$\Delta H^{\ddagger}$ (kJ mol^{-1})	92.8 ± 13.4	90.0 ± 14.2	81.6 ± 13.1	75.3 ± 11.4	67.0 ± 12.0
$\Delta S^{\ddagger}$ (kJ K^{-1} mol^{-1})	0.08 ± 0.05	0.07 ± 0.05	0.05 ± 0.04	0.03 ± 0.04	0.00 ± 0.04
E_a (kJ mol^{-1})	95.3 ± 13.4	92.5 ± 14.2	84.1 ± 13.1	77.8 ± 11.4	69.4 ± 12.0
T539A-Closing					
$\Delta G^{\ddagger}$ (kJ mol^{-1})	70.0 ± 0.1	70.7 ± 0.2	71.8 ± 0.2	73.5 ± 0.3	75.2 ± 0.3
$\Delta H^{\ddagger}$ (kJ mol^{-1})	117.1 ± 10.2	109.7 ± 12.2	95.0 ± 15.8	82.0 ± 20.0	67.4 ± 24.0
$\Delta S^{\ddagger}$ (kJ K^{-1} mol^{-1})	0.16 ± 0.03	0.13 ± 0.04	0.08 ± 0.05	0.03 ± 0.07	-0.03 ± 0.08
E_a (kJ mol^{-1})	119.6 ± 10.2	112.2 ± 12.2	97.4 ± 15.8	84.5 ± 20.0	69.8 ± 24.0

Table IV-3: Calculated ΔG^0 values for the common gating process of WT and T539A ClC-1 channels between −140 and +120 mV (kJ mol^{-1})

V (mV)	-140	-120	-100	-80	-60	-40	40	60	80	100	120
WT	1.03±0.23	0.96±0.17	0.79±0.15	0.33±0.12	-0.92±0.16	-2.87±0.24					
T539A	6.97±0.67	7.07±0.73	7.10±0.45	6.99±0.43	6.77±0.31	6.22±0.21	0.15±0.24	-1.93±0.26	-4.18±0.29	-6.55±0.32	-8.62±0.38

IV-4 Conclusions

Our previous research (Duffield et al., 2003; see Chapter III: Involvement of Helices at the Dimer Interface in ClC-1 Common Gating) suggested that the changes in opening and closing rates of the common gate which were observed in many channels with mutations at the ClC-1 dimer interface were likely to occur as a result of changes in the energies of the open and closed states of the common gate. We were, however, unable to show conclusively that this was the case. To further investigate the mechanism underlying the observed changes in common gating we have therefore investigated the temperature dependence of the T539A mutant, and compared it to that of the WT channel. The T539A mutant was chosen as it shows a significant change in the voltage dependence of the

common gating process, with no change in the fast gating process (Duffield et al., 2003; see Chapter III: Involvement of Helices at the Dimer Interface in ClC-1 Common Gating).

The common gate deactivating time constants for WT and T539A channels became faster with increasing temperature, and showed similar temperature dependence. Both channels also showed no signs of voltage-dependence in the temperature sensitivity of the common gate time constant, over the voltage range investigated.

Whilst there was little difference between the WT and T539A channels in terms of temperature sensitivity of gating time constants, there were differences observed in the temperature dependence of gating open probability. Whilst the WT channel open probability displayed an obvious temperature dependence, with shifts of $V_{½}$ to more positive potentials with increasing temperature, the open probability of the T539A channel showed no temperature dependence. The channel open probability is a product of the open probabilities of the fast and common gates. To further elucidate the reasons for this observed difference in gating between the two channels we separated the open probabilities of these two processes. In WT ClC-1 both the $V_{½}$ and P_{min} of the common gating process were found to be temperature dependent, whilst this dependence was no longer present in the T539A common gating process.

The final step in elucidating the mechanisms underlying the observed differences in WT and T539A common gating were to use the time constants of gating, and the open probabilities of the two gating processes to separate the opening and closing rates of the common gate, and examine their temperature dependencies. From this we were able to extract various thermodynamic parameters – the Gibb's free energy of activation between the open and closed channel states, as well as the entropic and enthalpic components of this, and the absolute change in free energy between the open and closed common gate states.

These results showed that in general the T539A mutant has a greater free energy of activation for common gate opening than the WT channel, combined with a smaller free energy of activation for common gate closing. A greater free energy of activation for common gate opening compared with the WT channel would result in a decrease in the T539A common gate opening rate, which is consistent with characteristics of the T539A channel reported previously (Duffield et al., 2003; see Chapter III: Involvement of Helices at the Dimer Interface in ClC-1 Common Gating). Similarly, the decreased free energy for common gate closing is in agreement with the increased closing rate observed in the T539A channel compared to the wild type channel.

The ΔG^0 value gives a measure of the absolute difference in Gibb's free energy between the open and closed gate states, and is unaffected by the height of the energy barrier between these two states (see Figure IV-9). A positive ΔG^0 value indicates that the closed channel state is at a lower free energy state than the open channel – and hence the channel is more likely to reside in the closed state – whilst a negative ΔG^0 value indicates the opposite. These values clearly show the voltage dependence of the common gating process, with positive ΔG^0 values at more negative potentials indicating a thermodynamic bias for the common gate closed state at these potentials, and negative ΔG^0 values at more positive potentials indicating a shift towards the open state of the common gate. A similar shift towards the common gate open state is observed in the T539A channel, which is expected, given that T539A common gate also opens upon depolarisation. However, this shift occurs over a more positive voltage range in the T539A mutant, which is in agreement with the observed shift in $V_{½}$ of this mutant to more positive potentials (Duffield et al., 2003; see Chapter III: Involvement of Helices at the Dimer Interface in ClC-1 Common Gating).

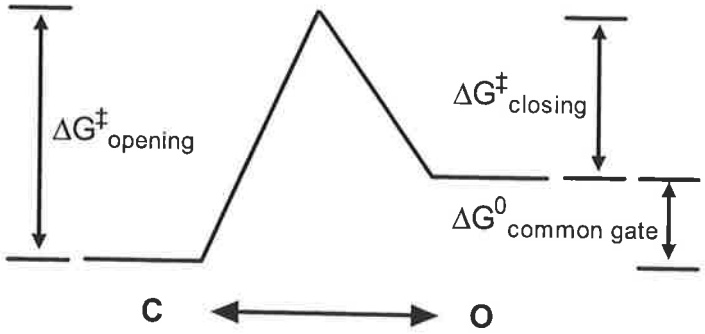

Figure IV-9: Gibb's free energy of activation for channel gating
Illustration of the relationship between the Gibb's free energy of activation for common gate opening ($\Delta G^{\ddagger}_{opening}$), the free energy for channel closing ($\Delta G^{\ddagger}_{closing}$), and the absolute change in Gibb's free energy ($\Delta G^{0}_{common\ gate}$).

The enthalpic component of the free energy of gating is essentially temperature independent. Consequently, the significant difference observed in the temperature dependence of the WT and T539A common gating process must be explained by differences in the entropic components of common gating in each of these channels. In WT ClC-1 the change in entropy observed during the common gate opening process is generally negative, whilst the entropy of the closing process is positive (Table IV-1). This suggests that the entropy of the WT ClC-1 common gate closed state is higher than that of the open state, with the entropy of the transition state somewhere in between (see Figure IV-10*A*). This means that the WT ClC-1 common gate closed state is more disordered, or has more conformational freedom, than either the open or transition substates, and is in agreement with previous work suggesting that the open state of both the WT ClC-1 fast and common gates is more ordered than the closed state (Bennetts et al., 2001). An increase in temperature will therefore tend to shift the channel to a more disordered state, thereby resulting in closure of the WT channel common gate (as indicated by a rightward shift in $V_{½}$ (Figure V-6). At the same time, the entropic components of both the T539A common gate opening and closing processes are positive, and of similar magnitudes (Table IV-1), suggesting that the entropy of the common gate transition state is higher than that of

either the common gate open or closed substates in the T539A channel (Figure IV-10*B*). This means that both T539A open and closed common gate substates are more ordered, or have less conformational freedom, than the transition state. Hence a change in temperature will increase the likelihood of the T539A channel entering the common gate transition substate, but not the relative amounts of time in which the common gate is open or closed. Hence the T539A common gating process is, to all intents and purposes, temperature independent (Figure IV-5).

It therefore appears that the T539A mutation, amongst other things, acts to decrease the entropy of the ClC-1 common gate closed substate. This may mean that the T to A mutation could allow the channel protein to pack together more stably in the common gate closed substate, hence making this state more ordered than in the WT ClC-1 channel.

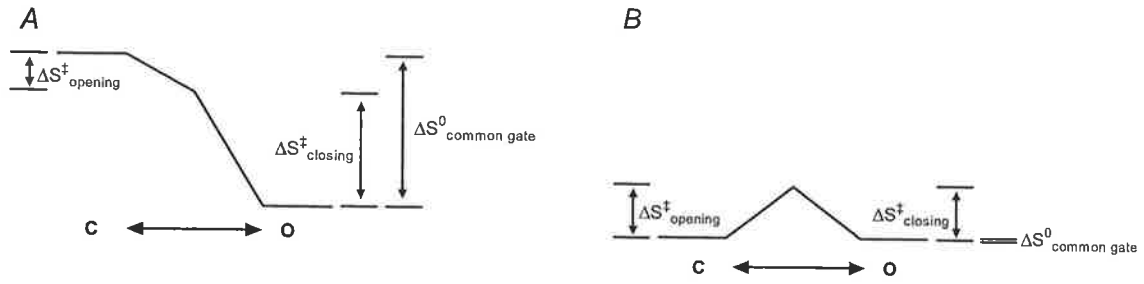

Figure IV-10: Entropy of common gating
Schematic illustrating the relationship between the entropy of activation for common gate opening ($\Delta S^{\ddagger}_{opening}$), common gate closing ($\Delta S^{\ddagger}_{closing}$), and the absolute change in entropy for the common gating process ($\Delta S^{0}_{common\ gate}$), for (*A*) WT ClC-1, and (*B*) T539A.

This study has investigated the temperature dependence of the ClC-1 common gating process in the WT and T539A mutant channels. Results show that the voltage dependence of the WT and T539A channels is caused by a change in the free energy of the open and closed channel states – favouring the open state of the common gate at more positive potentials. We also show that the differences in common gating observed between the WT and T539A channels are due to alterations in the free energy of the opening and closing transitions of the mutant channel.

Chapter V: A Relationship Between Gating and Zinc Inhibition of ClC-1

V-1 Introduction

The ClC-0 common gating process is facilitated in the presence of zinc (Zn^{2+}), such that the common gate closing rate is increased (Chen, 1998; Lin et al., 1999). Earlier research has shown that Zn^{2+} is also able to inhibit the resting conductance of skeletal muscle, most of which is likely to be due to the presence of the ClC-1 channel (Hutter and Warner, 1967; Stanfield, 1970; Bretag et al., 1984), with more recent research demonstrating that Zn^{2+}, and other transition metals, directly inhibit currents through the ClC-1 channel (Kurz et al., 1997; Rychkov et al., 1997; Kurz et al., 1999).

Although the ClC-1 channel is, like the ClC-0 channel, inhibited in the presence of Zn^{2+}, it is not known whether the mechanism of ClC-1 inhibition by Zn^{2+} also involves an interaction with the common gating process, as occurs in ClC-0 (Chen, 1998). The different sensitivities of these two channels to Zn^{2+} (ClC-0 IC_{50} 1 - 3 μM; ClC-1 IC_{50} 200 - 300 μM) suggests that Zn^{2+} may in fact be affecting these two channels through different mechanisms. There are also numerous differences between the common gating processes of ClC-0 and ClC-1, with this gating process showing vastly different time courses and voltage dependence between the two channels (Saviane et al., 1999). This evidence suggests that the inhibition of ClC-1 currents by Zn^{2+} may not occur in the same manner as the Zn^{2+}-mediated inhibition observed in ClC-0.

The current study has set out to elucidate the mechanisms by which Zn^{2+}-mediated inhibition of the ClC-1 channel occurs and, in particular, to investigate any interaction between Zn^{2+} and the ClC-1 common gating process. Our results show that Zn^{2+} is likely to

be acting on ClC-1 by stabilising a closed substate of the ClC-1 common gating process. We also provide evidence that ClC-1 residues C277 and C278 may form part of the ClC-1 Zn^{2+} binding site.

V-2 *Experimental Procedures*

V-2-1 Cell Culture and Transfection

Human embryonic kidney (HEK293) cells were cultured and transfected as previously described (see Chapter II: General Methods).

V-2-2 Electrophysiology

Patch-clamping experiments were performed as described previously (see Chapter II: General Methods)

For treatment with Zn^{2+}, $ZnSO_4$ (1 - 5 mM) was added to standard external solution (see Chapter II: General Methods), and used to perfuse cells. MTSET and MTSEA stock solutions (1 M) were prepared in MQ water and stored frozen. For experiments utilising these compounds a 1 mM solution was prepared from stock, in normal external solution, immediately prior to use, and used to superfuse the cell. The total bath volume was 2 mL, and bath perfusion occurred at a rate of 0.6 mL/min.

For analysis of the temperature dependence of Zn^{2+} inhibition the temperature of the bath was raised from room temperature (23 ± 1 °C) to 30 °C using a Peltier-based device with negative feedback. Standard external solution (see Chapter II: General Methods) was then replaced with external solution containing Zn^{2+}, which was heated to

the same temperature as the bath. Experiments at 30 °C were conducted using a –30 mV holding potential only.

V-2-3 Mutations

This study has looked at the effects of Zn^{2+} on three ClC-1 point mutants, C277S, C278S and V321S. These mutants have been described previously (Accardi et al., 2001; Duffield et al., 2003; see Chapter III: Involvement of Helices at the Dimer Interface in ClC-1 Common Gating). The mutations C277S and C278S were studied as these residues are equivalent to residues C212 and C213 in ClC-0, which have been implicated in ClC-0 common gating and Zn^{2+} block. These residues were mutated to serine as the ClC-0 cysteine to serine mutant C212S shows altered common gating and Zn^{2+} binding (Lin et al., 1999). The mutation V321S was studied as we have shown previously that this mutation is able to affect ClC-1 common gating, whilst having no affect on the ClC-1 fast gating process (Duffield et al., 2003; Chapter III: Involvement of Helices at the Dimer Interface in ClC-1 Common Gating). Site-directed mutagenesis techniques have been described previously (see Chapter II: General Methods).

V-2-4 Data Analysis

The time and voltage dependence of the ClC-1 current inhibition by Zn^{2+} was measured by holding cells at +40, -30 or –60 mV and, every 2 seconds, measuring the instantaneous inward current in response to a 12 ms test pulse to –100 mV. At each holding potential the magnitude of the instantaneous inward current was normalised to the magnitude of the instantaneous inward current observed before the application of Zn^{2+}, and plotted against time.

For analysis of temperature dependence of Zn^{2+} inhibition the half-time for current inhibition in the presence of 1 mM Zn^{2+} was calculated for the –30 mV holding potential, at both room temperature, and at 30 °C, by fitting the current inhibition with a single exponential function. The difference in the values at the two temperatures was then used to calculate a Q_{10} value for the process of Zn^{2+} mediated current inhibition.

V-3 Results

As has been reported previously, exposure of the wild-type ClC-1 channel to Zn^{2+} results in an attenuation of ClC-1 mediated currents (Kurz et al., 1997). The magnitude of the observed currents was decreased, with no significant change seen in current kinetics or channel open probability (Kurz et al., 1997) (Figure V-1). These results provide no evidence for a fast, voltage-dependent block of the ClC-1 pore. In addition, attempts to wash out Zn^{2+} from the perfusion bath showed that the Zn^{2+} mediated attenuation was irreversible (data not shown).

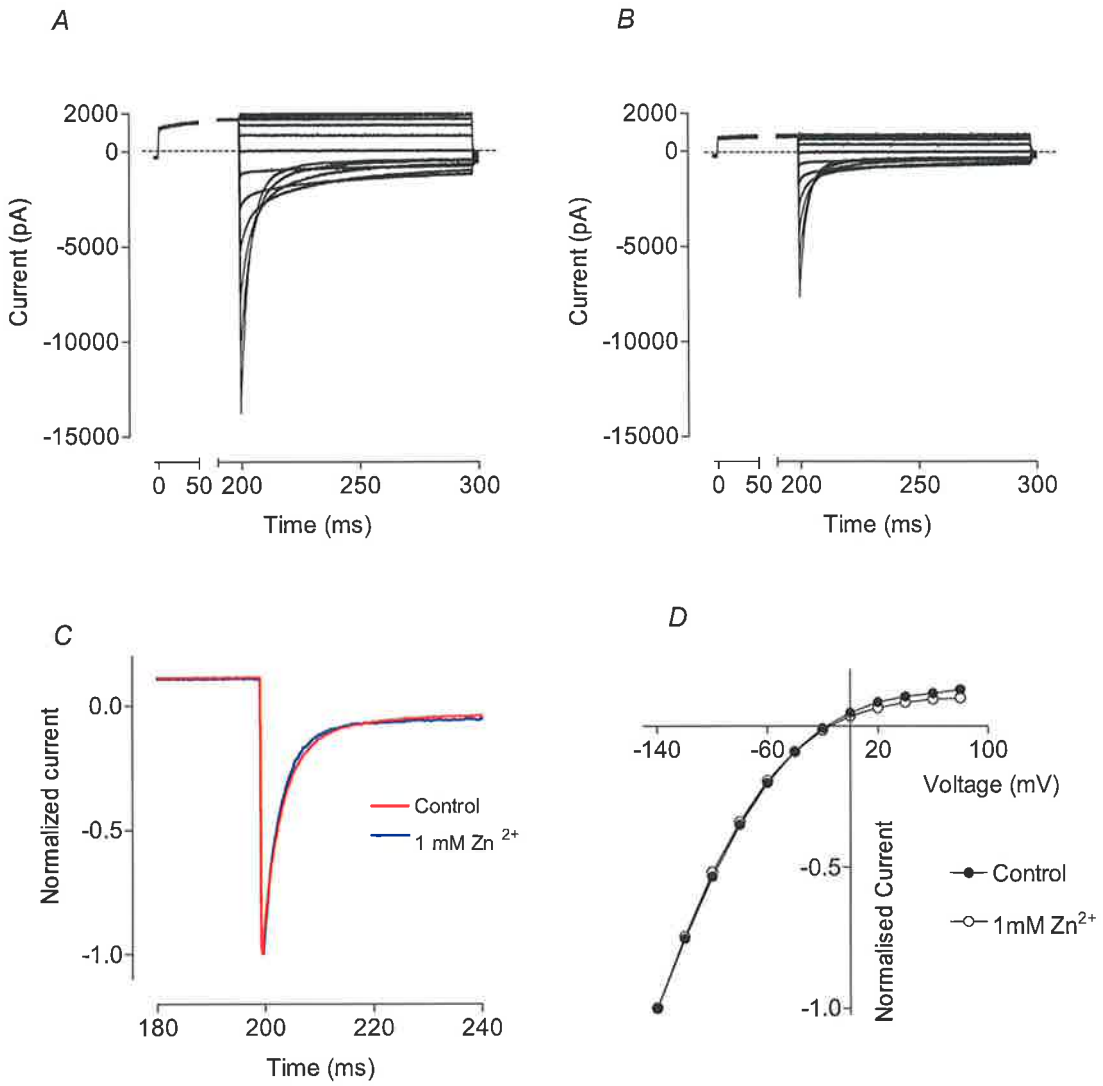

Figure V-1: ClC-1 gating in the presence of Zn^{2+}
(*A* and *B*) WT ClC-1 currents during voltage steps between –140 and +80 mV (20 mV steps), from a holding potential of +40 mV, both (*A*) before and (*B*) after partial block with 1 mM Zn^{2+}. (*C*) Superimposition of normalised currents following a voltage step to –140 mV, in the absence and presence of 1 mM Zn^{2+}. (*D*) Instantaneous inward current at each voltage step, normalised in each case to the instantaneous current measured at step to –140 mV.

To investigate the Zn^{2+}-mediated inhibition of ClC-1, and in particular whether this process is dependent on the state of the channel, we have investigated the current attenuation caused by Zn^{2+} at three different holding potentials. The time course of current attenuation varied dramatically with the holding potential of the cell. Inhibition occurred much more quickly at more hyperpolarised potentials (Figure V-2), where the WT ClC-1 channel is in the closed state. Fitting single exponential functions to the currents observed

at –60 and -30mV suggested that at both potentials the current would plateau at a value of 6 % of the initial current. The half-times for WT current inhibition were 148 s at –60 mV and 355 s at –30 mV. Assuming that the extent of current block would be the same at +40mV, with only the time course of block changing, the half-time of WT current inhibition at +40mV would then be 1081 s. The time dependence of Zn^{2+} attenuation was not simple, with a slight delay, in the region of 30 – 60 seconds, observed between the application of Zn^{2+} solution and occurrence of current attenuation at all holding potentials (Figure V-2). The dependence of Zn^{2+}-mediated inhibition on cell holding potential suggests that Zn^{2+} attenuation of ClC-1 currents is a state-dependent process, acting preferentially on the closed state of the channel. There is no indication of whether Zn^{2+} is acting on the fast or the common gating process.

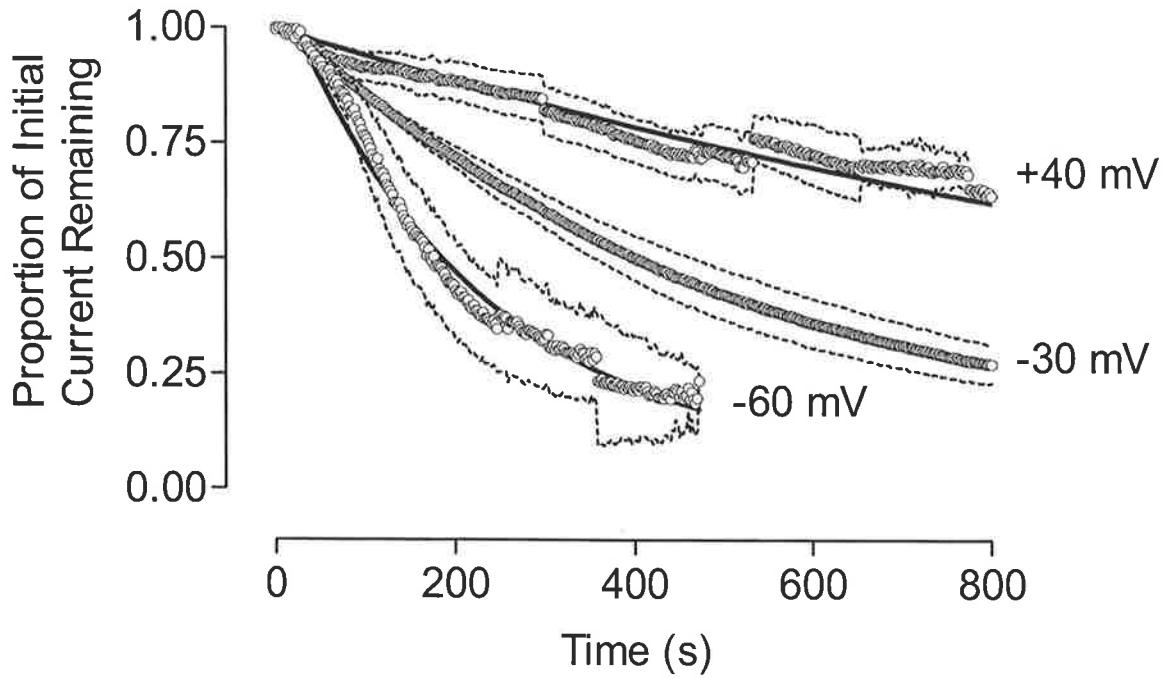

Figure V-2: Zn^{2+}-mediated inhibition of currents through the wild-type ClC-1 channel. Cells were held at either +40 mV, -30 mV or –60 mV, as indicated, throughout the experiment, and stepped to –100 mV for 12 ms at 2 s intervals. Open circles indicate the means at each time-point, with dotted lines indicating ± SEM (n = 3–7 cells). Sudden steps visible in the data are due to a variable number of cells used in the averaging procedure at different time points, due to the difficulty in maintaining seals over the entire time period. Continuous lines represent single-exponential decay functions fitted to the data in order to estimate the half-time of Zn^{2+} block at each potential.

To differentiate between the possibilities of Zn^{2+} acting through pore block, or through an effect on one of the ClC-1 gating processes, we studied the affect of Zn^{2+} on various ClC-1 mutants with altered gating. A mutant which effectively locks the ClC-1 common gating process in the open state, C277S (Accardi et al., 2001; Duffield et al., 2003; see Chapter III: Involvement of Helices at the Dimer Interface in ClC-1 Common Gating), showed little Zn^{2+} block with 1 mM Zn^{2+}, and a maximal current reduction of around 15 % with 5 mM Zn^{2+} (Figure V-3). The C278S mutation causes an increase in the open probability of the fast gating process with little alteration in ClC-1 common gating (Duffield et al., 2003; see Chapter III: Involvement of Helices at the Dimer Interface in ClC-1 Common Gating), and also showed a greatly reduced Zn^{2+} block of around 25% with 5 mM Zn^{2+} (Figure V-3). The third mutation investigated, V321S, doesn't affect the open probability of the ClC-1 fast gating process, but dramatically shifts the common gate open probability to more positive potentials (Duffield et al., 2003; see Chapter III: Involvement of Helices at the Dimer Interface in ClC-1 Common Gating) – meaning that at any given potential the common gate is more likely to be closed than in the WT channel. The V321S mutation also shows a much more prominent 'third gating component' than that seen in WT ClC-1, which is likely to represent a second kinetic component of the ClC-1 common gating process (Accardi et al., 2001; Duffield et al., 2003; see Chapter III: Involvement of Helices at the Dimer Interface in ClC-1 Common Gating). This mutant showed a much faster time course for Zn^{2+} block (Figure V-4). The time course and extent of the block was similar, regardless of whether the channel was held at –30 or +60 mV (Figure V-4). V321S also showed no delay in the onset of Zn^{2+} block, as had been observed with the WT channel (Figure V-2), as well as with the C277S and C278S mutants (Figure V-3).

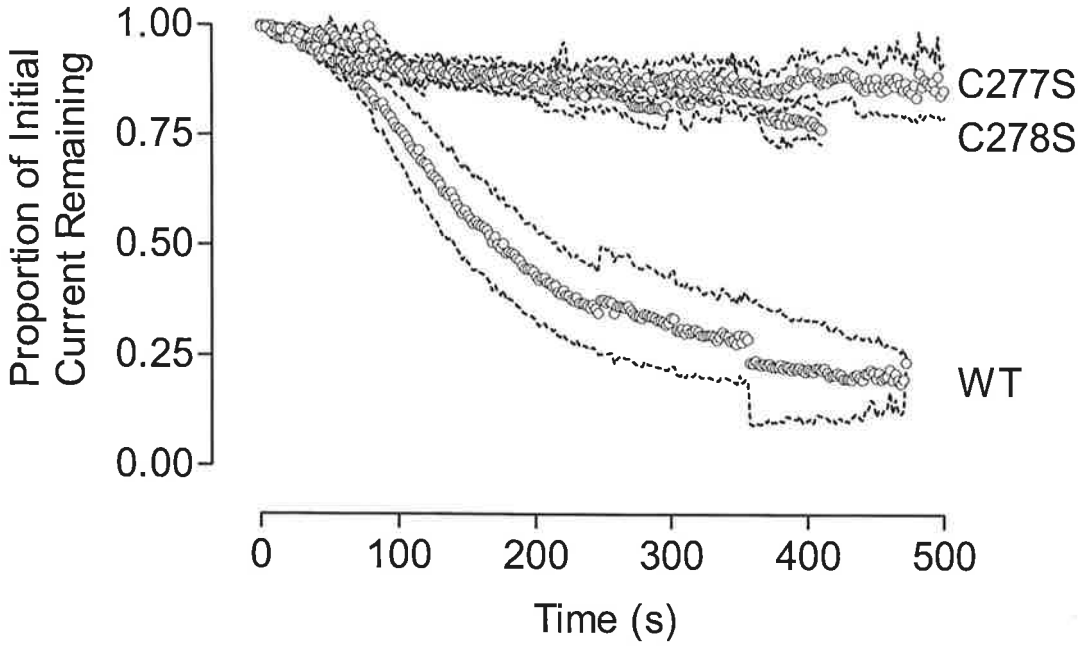

Figure V-3: Inhibition of currents through C277S and C278S ClC-1 channels by 5 mM Zn^{2+}.
Cells were held at –60 mV, and every 2s were stepped to –100 mV for 12 ms. Current inhibition of wild-type (WT) ClC-1 at –60 mV by 1 mM Zn^{2+} is shown for comparison. Open circles indicate the means at each time point, with dotted lines indicating ± SEM (n = 5–6 cells).

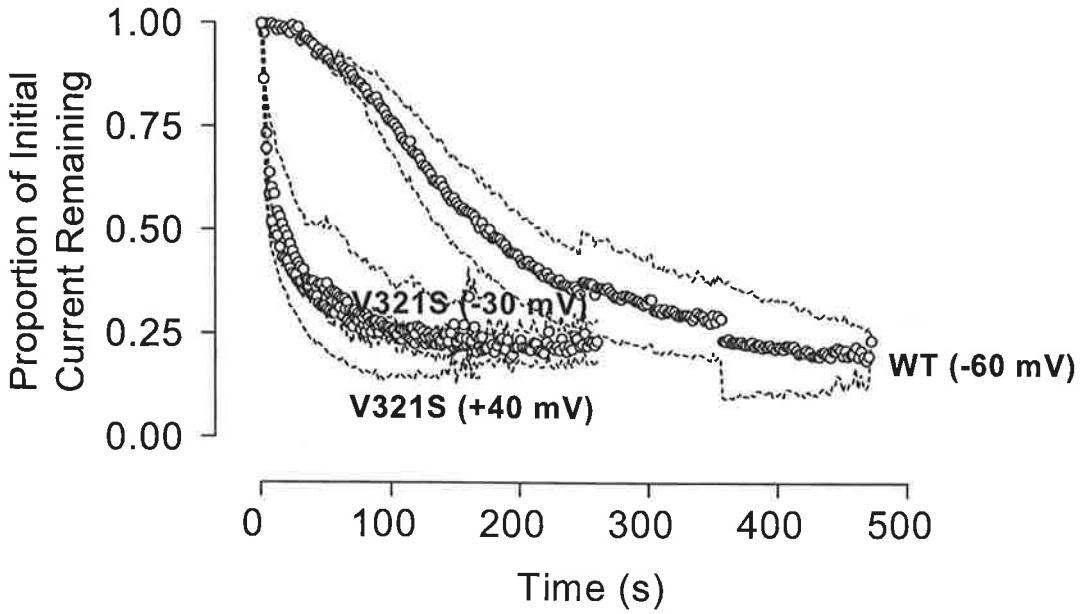

Figure V-4: Inhibition of currents through V321S ClC-1 channels by 1 mM Zn^{2+}.
Cells were held at –30 mV or +40 mV, as indicated, and then stepped to –100 mV for 12 ms every 2 s. Current inhibition of wild-type (WT) ClC-1 at –60 mV by 1 mM Zn^{2+} is shown for comparison. Open circles indicate the means at each time point, with dotted lines indicating ± SEM (n = 3–6 cells).

Zinc binding sites often contain a number of cysteine residues (Karlin and Zhu, 1997; Auld, 2001). To investigate further the possible role of cysteine residues, and their potential movements during channel gating, MTSET and MTSEA reagents, which are able to react with cysteine residues within a peptide (Akabas et al., 1992), were applied to the WT ClC-1 channel. MTSET had no effect on channel currents, even following more than 10 mins of perfusion (Figure V-5), and initial experiments with MTSEA showed similar results.

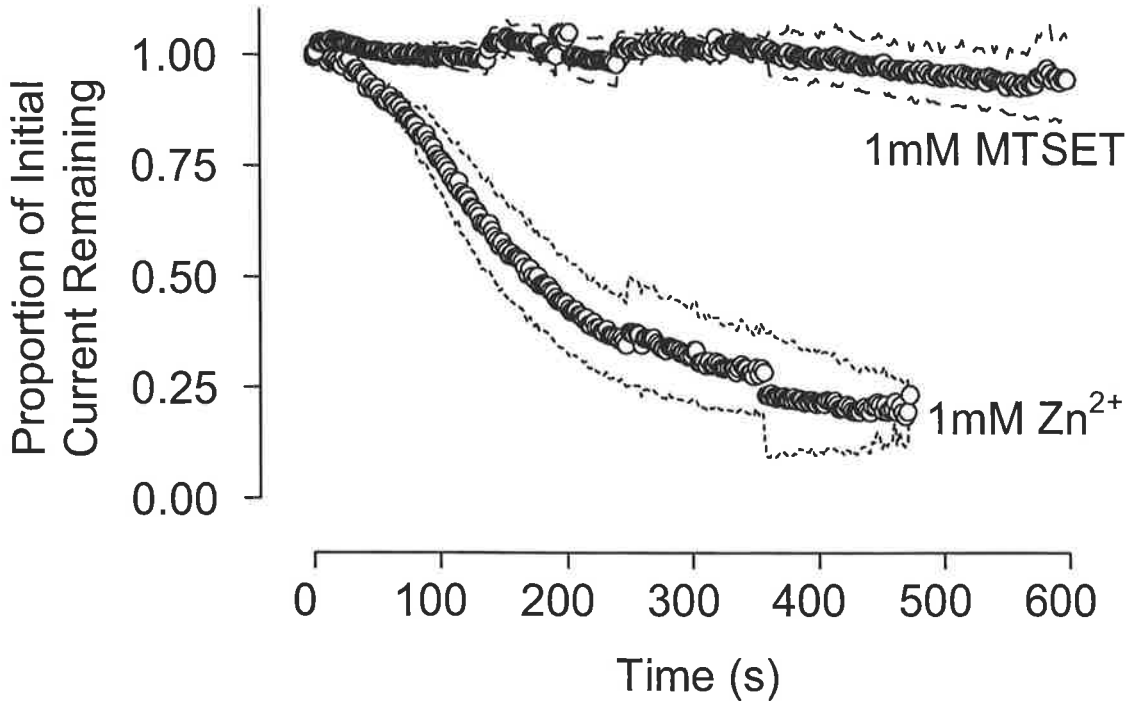

Figure V-5: Effect of 1 mM MTSET on currents through WT ClC-1 channels.
Cells were held at -60 mV and then stepped to –100 mV for 12 ms every 2 s. Current inhibition of wild-type (WT) ClC-1 by 1 mM Zn^{2+} is shown for comparison. Open circles indicate the means at each time point, with dotted lines indicating ± SEM (n = 2–9 cells).

The time constant of ClC-1 common gating is in the range of 1 to 100 ms (Rychkov et al., 1996; Saviane et al., 1999; Accardi and Pusch, 2000), much faster than the time course of current attenuation by Zn^{2+} (Figure V-2, Figure V-3, Figure V-4). This raises the possibility that Zn^{2+} may be interacting with another closed substate of the ClC-1 channel common gate – one which has a much slower time course than that of the whole common

gating process. To further study the process on which Zn^{2+} acts we have investigated the temperature dependence of the Zn^{2+} blocking process. Results show that current inhibition occurs much faster at higher temperatures (Figure V-6). At 24 °C the half-time of current inhibition was 355 ± 1 s, whilst at 30 °C the half-time was 46 ± 1 s. This corresponds to a Q_{10} value for the Zn^{2+} inhibition process of 12.9.

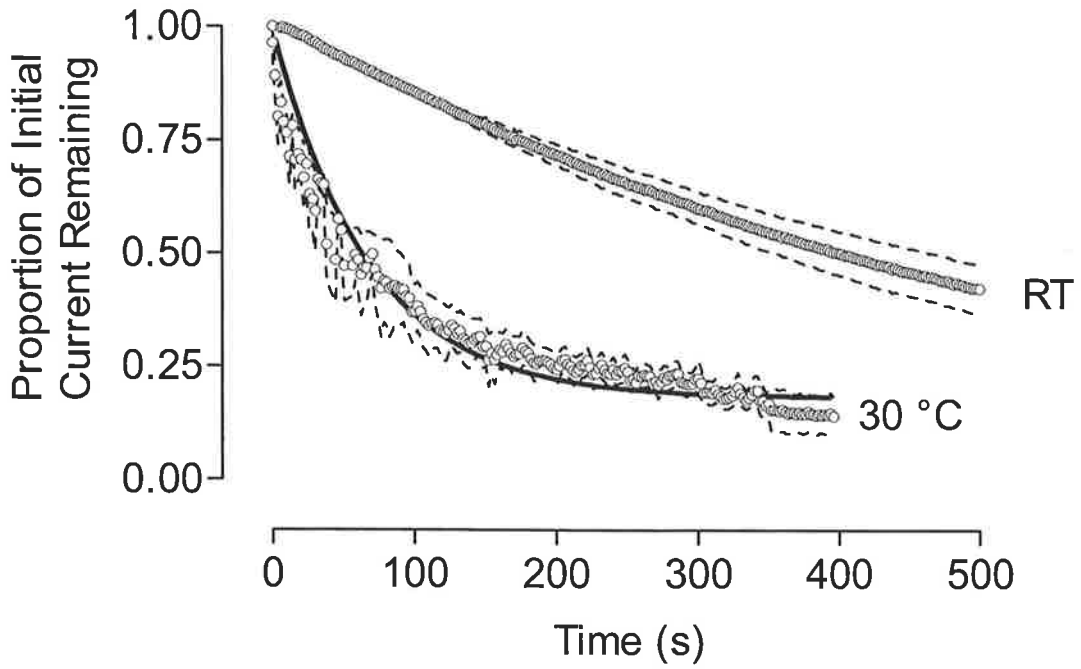

Figure V-6: Temperature dependence of the inhibition of WT ClC-1 current by 1 mM Zn^{2+} Cells were held at –30 mV, and every 2 s were stepped to –100 mV, for 12 ms. During this procedure cells were held at either room temperature (RT), or 30 °C, as indicated. Open circles indicate means at each time point (n = 2-7 cells), with dotted lines indicated ± SEM. Continuous lines represent single-exponential decay functions fitted to the data in order to estimate the half-time of Zn^{2+} block at each potential.

V-4 Discussion

In the WT ClC-1 channel it was observed that Zn^{2+}-mediated inhibition was fastest when cells were held at a hyperpolarised holding potential of –60 mV, and became slower as the holding potential applied was made more depolarised (Figure V-2). Holding potentials more hyperpolarised than –60 mV were not used due to the difficulty in

maintaining seals at these potentials. It is known that at +40 mV (with junction potential correction applied as per Barry, 1994, equivalent to a membrane potential of +25 mV) the WT ClC-1 channel is fully open, at –30 mV (junction potential corrected, –45 mV) the channel open probability is close to 60%, and at –60 mV (junction potential corrected, –75 mV) the channel is significantly more likely to be closed, with an open probability of only 30% (Rychkov et al., 1996). Given that the ClC-1 channel is virtually impermeant to cations (in a NaCl solution ClC-1 equilibrium potential follows [Cl^-]; Rychkov et al., 1998), and with the high potential energy barrier expected for a positively charged Zn^{2+} ion entering the ClC-1 conduction pathway, it appears unlikely that Zn^{2+} is affecting ClC-1 currents through a process involving pore block. It is also seen that the temperature dependence of the inhibition greatly exceeds the temperature dependence of ion diffusion across an energy barrier (DeCoursey and Cherny, 1998), providing further evidence that the Zn^{2+}-mediated inhibition is not related to a pore blocking process. It has also been shown that Zn^{2+} has no affect on ClC-1 kinetics or voltage dependence (Kurz et al., 1997) (Figure V-1), and therefore it is unlikely that Zn^{2+} is simply increasing the closing rate (or decreasing the opening rate) of the open channel state. Instead, it is more likely that Zn^{2+} is binding specifically to the closed state of the ClC-1 channel. Because this binding is irreversible and occurs on a time scale thousands of times slower than ClC-1 gating this results in a decrease in ClC-1 currents, without affecting channel gating parameters. This mechanism of action is quite different to that proposed to occur in the ClC-0 channel, where Zn^{2+} binding is reversible, and causes an increase in the inactivation rate of the common gating process (Chen, 1998). To determine whether Zn^{2+} is also acting on the common gating process of the ClC-1 channel we have utilised ClC-1 mutations that affect only the common gating process. The mutation C277S has been previously characterised (Accardi et al., 2001; Duffield et al., 2003; see Chapter III: Involvement of Helices at the Dimer Interface in ClC-1 Common Gating), and causes a drastic increase in the open

probability of the common gating process, such that at any given potential the common gate is more likely to be open than in the WT ClC-1 channel. The V321S mutation also affects the ClC-1 common gating process (Duffield et al., 2003; see Chapter III: Involvement of Helices at the Dimer Interface in ClC-1 Common Gating), altering the common gate voltage dependence such that at any given potential the common gate is more likely to be closed than in the WT ClC-1 channel. Both C277S and V321S show no change in the fast gating process compared to the WT channel (Accardi et al., 2001; Duffield et al., 2003; see Chapter III: Involvement of Helices at the Dimer Interface in ClC-1 Common Gating).

In the C277S channel it was observed that Zn^{2+}-mediated inhibition was greatly decreased, showing much less inhibition following 10 minutes of Zn^{2+} application when compared to that seen in the WT channel at the same holding potential, even at a Zn^{2+} concentration of 5 mM, 5 times that used for the WT channel (Figure V-3). The V321S channel showed a very different effect, with 1 mM Zn^{2+} causing much faster inhibition than that seen in the WT channel, even at more positive holding potentials. In fact, in the V321S mutant inhibition was equally fast at both +40 mV and –30 mV (Figure V-4).

While the effects of holding potential on the rate of block of WT ClC-1 suggest that Zn^{2+} binds to the closed state of the channel, the results with C277S and V321S extend this by indicating that Zn^{2+} binding is to the closed common gate. The differences observed in the time course of Zn^{2+} inhibition cannot, however, be completely explained by the differences in open probability of the slow gating process. The open probability of the V321S channel common gate at +40 mV is close to 70 % (Duffield et al., 2003; see Chapter III: Involvement of Helices at the Dimer Interface in ClC-1 Common Gating), which is approximately equivalent to the open probability of the WT ClC-1 channel common gate at –60 mV (Duffield et al., 2003; see Chapter III: Involvement of Helices at the Dimer Interface in ClC-1 Common Gating). Nevertheless, the rate of Zn^{2+} inhibition of

the V321S channel at +40 mV is still significantly faster than that seen in the WT channel at –60 mV (Figure V-4). Similarly the rates of Zn^{2+} block seen in V321S are very similar at both holding potentials used, -30 and +40 mV, even though there is a difference of close to 40 % in the open probability of the V321S common gate between these two potentials (Duffield et al., 2003; see Chapter III: Involvement of Helices at the Dimer Interface in ClC-1 Common Gating) (Figure V-4). These observations could reflect the possibility that Zn^{2+} binds to a substate of the ClC-1 common gating process which only contributes minimally to the overall process of common gating, and is therefore not normally visible. A possible model of this is illustrated below:

$$O \overset{\tau_1}{\rightleftharpoons} C_1 \overset{\tau_2}{\rightleftharpoons} C_2$$

where O is the common gate open and conducting state and C_1, C_2 are two closed states of the ClC-1 common gating process. τ_1 and τ_2 indicate the time constants of transitions between O and C_1, and C_1 and C_2, respectively. In this model C_1 is the most commonly occurring common gate closed state, with movement to the C_2 closed conformation only a rare event. When the channel does enter the C_2 conformation, however, Zn^{2+} is able to bind to the channel, and stabilise the closed conformation. Because Zn^{2+} can only bind to an infrequently occurring substate of the common gating process the Zn^{2+}-mediated inhibition therefore takes place over a much slower time course than that of the experimentally observed common gating process.

The presence of additional common-gating substates has been postulated previously (Duffield et al., 2003; see Chapter III: Involvement of Helices at the Dimer Interface in ClC-1 Common Gating), and could explain previously described ClC-1 characteristics, including the presence of a third, slower, component in deactivating WT ClC-1 currents (Rychkov et al., 1996), and the presence of a minor second component in activating WT ClC-1 currents, which was much slower than that reported previously for

the ClC-1 common gate (Duffield et al., 2003; see Chapter III: Involvement of Helices at the Dimer Interface in ClC-1 Common Gating). In a number of ClC-1 mutants, including the V321S mutant, this second activating component was altered compared to the WT channel, becoming slower, as well as much more prominent, in activating ClC-1 currents. Based on the common-gating model postulated above, it therefore seems likely that the V321S mutation increases the probability of the channel occupying the alternate closed substate (C_2), thereby enhancing the ability of Zn^{2+} to block the channel.

The temperature dependence of the Zn^{2+} mediated current inhibition process is also consistent with Zn^{2+} acting on a substate of the ClC-1 common gating process. The Q_{10} value of 12.9 for Zn^{2+} inhibition indicates that the process on which Zn^{2+} inhibition acts is significantly more temperature sensitive than either the ClC-1 fast or common gating processes, which have reported Q_{10} values of ~3 and ~4 respectively (Bennetts et al., 2001). The higher temperature dependence of this transition may suggest that this process is related to the ClC-0 common gating process, which also has an extremely high Q_{10}, in the range of 40 (Pusch et al., 1997). Additionally, the high temperature dependence suggests that this particular substate transition may involve significant protein rearrangement, possibly allowing the formation of a Zn^{2+} binding site from residues which are more removed from each other in the open, or other closed ClC-1 channel substates.

Therefore it is possible that the ClC-1 common gating process may contain at least one additional substate transition (denoted in the model above as C_2), which is more temperature sensitive than the overall gating process, and to which Zn^{2+} can bind, stabilising the ClC-1 channel in the non-conducting state.

The final mutant channel investigated in this study was the C278S mutant. This mutant has also been previously characterised (Duffield et al., 2003; see Chapter III: Involvement of Helices at the Dimer Interface in ClC-1 Common Gating), and displays an increased open probability of the fast gating process, with little effect on the common

gating process. A mutation at the equivalent residue in the ClC-0 channel, C213, causes a slight decrease in the Zn^{2+} sensitivity of that channel (Lin et al., 1999).

Investigation of the Zn^{2+}-mediated current inhibition in the C278S mutant channel revealed a similar pattern of inhibition to that previously observed for the C277S mutation. The Zn^{2+}-mediated current inhibition was greatly decreased compared with the WT channel, even when using a 5 mM concentration of Zn^{2+} instead of the 1 mM concentration used with the WT channel. As the C278S mutation has no affect on the ClC-1 common gate such an effect appears to contradict the evidence that Zn^{2+} inhibition occurs through Zn^{2+} binding and stabilisation of the common gating process. Given the importance, however, of cysteine residues in formation of Zn^{2+} binding domains (Karlin and Zhu, 1997; Auld, 2001) it is also possible that C278 has no direct involvement in the common gating process, but rather forms part of the Zn^{2+} binding domain in ClC-1. This is also a possible explanation for the reduced Zn^{2+} inhibition observed in the C277S mutant. A final possibility is that the C278S mutation alters the Zn^{2+}-binding substate of the common gate, but without affecting the overall common gating process (which is unaltered in C278S – see Chapter III: Involvement of Helices at the Dimer Interface in ClC-1 Common Gating).

Previous investigations of Zn^{2+}-mediated inhibition of the ClC-1 channel have looked at the possible involvement of cysteine and histidine residues in formation of a Zn^{2+} binding site (Kurz et al., 1999). Such a site is likely to consist of four or more cysteine or histidine residues, or a combination of both (Karlin and Zhu, 1997; Auld, 2001), which would be in close proximity to each other in the 3-dimensional channel structure, allowing coordination of the Zn^{2+} cation. These previous studies have particularly identified the cysteine at position 546 in ClC-1 as being important in Zn^{2+} binding. Looking at the ClC crystal structure (Dutzler et al., 2002), there do not appear to be obvious groupings of Cys and His residues that could form a Zn^{2+} binding site. However, C546 and C278, which may both be involved in Zn^{2+} binding (Kurz et al., 1999) (present study) do lie on the dimer

interface of the channel, suggesting that these four residues (C278 and C546 from each subunit) could form the Zn^{2+} binding site of the ClC-1 channel. The position of these residues at the dimer interface (Figure V-7), which is likely to be involved in the ClC-1 common gating process (Duffield et al., 2003; see Chapter III: Involvement of Helices at the Dimer Interface in ClC-1 Common Gating), also fits with the evidence suggesting that Zn^{2+} acts on the common gating process. These residues may form a binding site that can only coordinate Zn^{2+} when the channel assumes a closed substate – thereby allowing Zn^{2+} to bind and lock the channel into the closed state. Although the crystal structure shows that these residues are probably too far apart to coordinate a Zn^{2+} ion (a maximum of around 30 Å between the two C278 residues; see Figure V-7), the crystal structure is that of a bacterial ClC channel, not of ClC-1, and so it is likely that there are some differences in structure between the two channels. There is also almost certainly movement of the channel as it opens and closes, and such movement at the dimer interface could bring these residues closer together than seen in the crystal structure. The high temperature dependence of the Zn^{2+}-mediated inhibition observed in this study supports this argument, suggesting that Zn^{2+} inhibition may be closely related to major movements in channel structure.

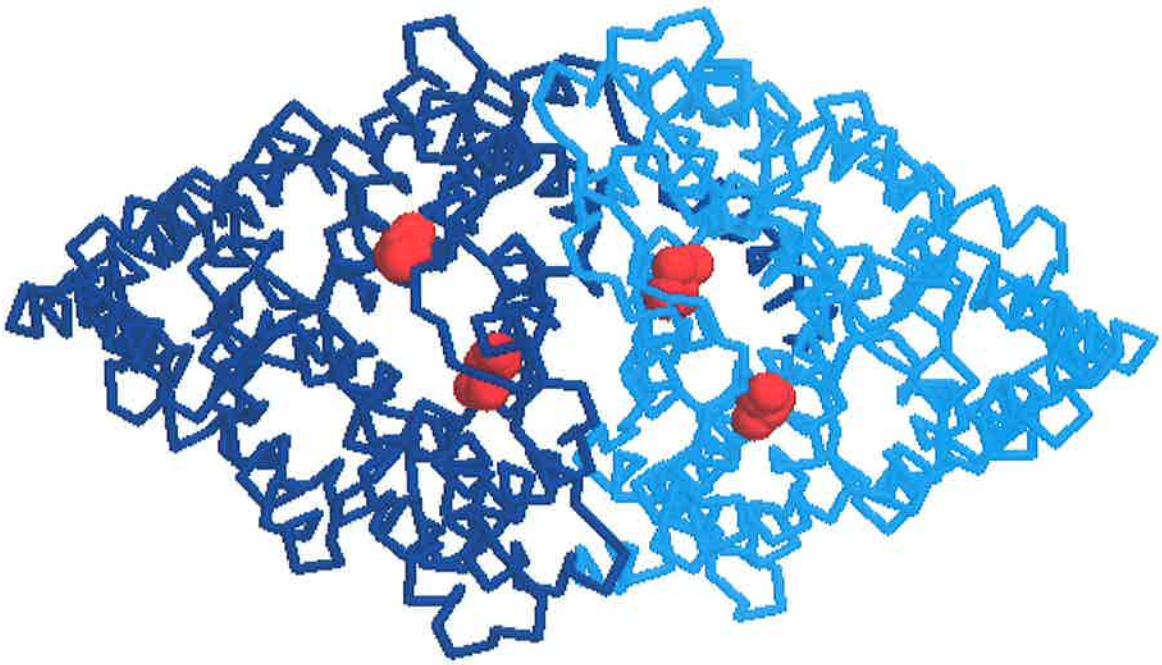

Figure V-7: Crystal structure of ClC
Bacterial ClC crystal structure (adapted from Dutzler et al., 2002), viewed from extracellular side. The backbone structure of each ClC monomer is shown in a different shade of blue, whilst the locations of residues equivalent to ClC-1 residues C278 and C546 are shown in red.

Previous mutagenesis studies have also suggested that the residues C242 and C254 are important in formation of a ClC-1 Zn^{2+} binding site (Kurz et al., 1999), based on the reduced Zn^{2+} affinity observed in ClC-1 channels with mutations at these residues. However, the reduction in Zn^{2+} affinity observed with mutations at these residues is significantly less than that observed with mutations at the C546 residue (Kurz et al., 1999). In addition, mutations such as R304E have been shown to reduce the affinity of divalent cations for ClC-1 by an amount comparable with that seen with C242 and C254 mutations (Rychkov et al., 1997; Kurz et al., 1999). Arginine residues, however, do not participate in Zn^{2+} binding (Karlin and Zhu, 1997; Auld, 2001). It therefore seems unlikely that residues such as R304, C242 and C254 are principal residues in formation of the ClC-1 Zn^{2+} binding site. Any mutations, however, which alter ClC-1 common gating, are likely to alter the affinity of Zn^{2+} for the channel without interacting directly with the Zn^{2+} binding site.

The failure of the methanthiosulphonate reagents MTSEA and MTSET to alter channel kinetics agrees with the findings of Fahlke et al., 1997c, but differs from those of Kurz et al., 1997, who found that 1mM MTSET significantly inhibited WT ClC-1 currents. The underlying reason for this difference in experimental findings is not obvious, and will certainly require further investigation. If indeed methanthiosulphonate reagents do not affect ClC-1 currents then this may indicate that residues other than cysteines coordinate Zn^{2+} binding, although it could also reflect an inaccessibility of the ClC-1 Zn^{2+} binding site to such reagents.

Another interesting observation of this study was the delay, in the range of 30 – 60 seconds, between the commencement of Zn^{2+} perfusion and the onset of inhibition. This delay was observed with the WT channel (Figure V-2), the C277S and C278S mutants (Figure V-3), but not the V321S mutant (Figure V-4). A similar delay is shown, but not discussed, in a previous study investigating Zn^{2+} inhibition of ClC-1 (Kurz et al., 1997). This delay is unlikely to represent delays caused by experimental set-up, such as a slow perfusion of Zn^{2+} onto the cells, as the delay is not observed with the V321S mutant. It is therefore likely that this delay is in fact representative of an underlying mechanism occurring during Zn^{2+}-mediated current inhibition. Although at this stage it is only possible to speculate as to what such a mechanism might be, it is possible that the delay is representative of an underlying co-operativity, or two state process, required for Zn^{2+} inhibition to occur. Thus Zn^{2+} may not bind at the coordinating site in a single step process, but may bind firstly to part of the binding site, and then bind the remaining residues only as the channel enters a second closed substate, hence locking the channel into that closed state. Such a process could explain the delay observed, due to the presence of a delay between the initial Zn^{2+} binding step, and the secondary, irreversible, 'locking' step. Mutations which not only affect the common gating process, but which also increase the

rate at which the channel is able to enter this further locked substate, would therefore show a decreased delay between Zn^{2+} application and block, as observed with V321S.

This study has further investigated the ability of Zn^{2+} ions to inhibit currents through the ClC-1 channel. Our results indicate that Zn^{2+} is able to inhibit currents through ClC-1, not by direct obstruction of the ion-conducting pathway, but through binding and stabilisation of the ClC-1 closed state. In fact it appears likely that Zn^{2+} acts by stabilising a closed substate of the ClC-1 common gate. Furthermore, our results provide evidence that residues C278, and possibly C277, may form part of the Zn^{2+} binding site in ClC-1.

Chapter VI: Discussion

Whilst significant advances have been made toward understanding the structure and function of ClC channels, many questions still remain to be answered. The research described in this thesis provides significant novel information on the process of gating in the ClC-1 channel, and in particular on the common gating process, which to date has been poorly understood. This information is likely to enhance our knowledge of the structure-function relationship for common gating in the ClC-1 channel, and of gating in the ClC channel family in general.

This research has identified helices positioned at the interface of the ClC dimer, these being the G, H, I, P and Q helices, as structures likely to be involved in ClC common gating. Site-directed mutagenesis of residues positioned within these helices in the ClC-1 channel produced mutations which altered the common gating process, whilst having little or no effect on fast gating. This has provided the first evidence that helices at the dimer interface of ClC channels may play an important functional role in the common gating process of these channels.

Further analysis of mutations at the ClC-1 dimer interface led to the suggestion that these mutations were able to alter the common gating process by altering the opening rate, the closing rate, or both rates, of common gating. Such changes would most likely occur due to changes in the energy of the open or closed common gate states. We therefore went on to investigate this possibility by investigating the temperature dependence of one of these dimer interface mutations in comparison to the WT ClC-1 channel. These results indicated that the variations observed in the common gating of this mutant channel could be explained by alterations in the free energy of common gate opening and closing.

We have also utilised the divalent Zn^{2+} cation in our analysis of ClC-1 gating. Although Zn^{2+} had previously been found to interact with the common gating process of the ClC-0 channel, its mechanism of inhibiting ClC-1 currents has not otherwise been characterised. Through the investigation of Zn^{2+} mediated current block of WT and common-gating mutant ClC-1 channels we have been able to show that Zn^{2+} inhibits ClC-1 currents through irreversible binding to the closed ClC-1 common gate. Analysis of the kinetics and temperature dependence of ClC-1 Zn^{2+} block suggest the presence of an additional ClC-1 common gate substate, not previously described, which is the target of Zn^{2+} binding. Additionally, we have identified the location of a number of cysteine residues that may form part of the ClC-1 Zn^{2+} binding site. The location of these residues on the ClC-1 dimer interface further reinforces the relationship seen between Zn^{2+} inhibition and the ClC-1 common gating process.

This research, therefore, has further extended our knowledge of ClC-1 gating through a further characterisation of the ClC-1 common gating process and its interaction with the Zn^{2+} cation. In addition, we have identified a structure-function relationship between the helices lining the ClC dimer interface and the ClC-1 common gating process, and shown the thermodynamic process by which mutations in this region alter channel gating.

Whilst residues at the dimer interface have now been implicated in ClC-1 common gating (see Chapter III: Involvement of Helices at the Dimer Interface in ClC-1 Common Gating), an intriguing question which is yet to be investigated is the role of a cluster of dominant myotonic mutations which does not occur at the dimer interface (see cluster of residues to the left hand side of Figure III-1). It is most likely that these mutations are part of a pathway responsible for communicating common gating movements between the dimer interface and the ClC pore. A detailed investigation of mutations in this region could provide valuable information on the precise structural pathway of ClC-1 common gating,

including whether the common gating process acts through a simultaneous closing of both individual protopore fast gates, or through an independent gating structure. An interesting possibility is that of using a technique such as Φ-value analysis (for example, see Cymes et al., 2002) to gain insight into the structural movements of ClC-1 during the common gating transition. Such a technique could provide information on whether common gating begins at the dimer interface and progresses outwards to each monomer simultaneously, or begins with structural rearrangements in one monomer, which subsequently progress to the other monomer.

A technique which hasn't been explored in this thesis, but which may also prove valuable to our understanding of ClC-1 gating, is the use of concatermeric channels. The use of such constructs in conjunction with techniques used here, such as analysis of temperature dependence and Zn^{2+} inhibition, could enable a much greater understanding of the way in which a mutation in one ClC-1 monomer is able to have a dominant negative affect on the whole channel dimer. Of particular interest would be an investigation of the extent to which dimer interface mutations, such as those described in Chapter III: Involvement of Helices at the Dimer Interface in ClC-1 Common Gating, affect the common gating process when inserted into only a single ClC-1 monomer.

The techniques used for analysing Zn^{2+} mediated ClC-1 channel inhibition (see Chapter V: A Relationship Between Gating and Zinc Inhibition of ClC-1) have highlighted the importance of ClC gating components other than the traditional fast and common gates. Whilst evidence for additional components of ClC-1 gating has been observed previously (Rychkov et al., 1996), these processes remain to be properly investigated. If indeed Zn^{2+} interacts with a substate of the ClC-1 common gate then this provides a valuable pharmacological technique for investigation of these previously ignored components of gating. A thorough investigation utilising this technique, in conjunction with temperature dependence and site-directed mutagenesis, will enable a better understanding of the nature

of this gating component. In particular, it would be of interest to determine whether this component is related to the ClC-0 common gating process, or to the hyperpolarisation activated gating process of ClC-1 (see I-5-2: ClC Common Gating).

It is hoped that future research will be able to determine the precise structural movements responsible for ClC-1 common gating, and how these interact with ion conduction and with the ClC-1 fast gating process. Using the information obtained from the current research it should also be possible to assess more fully the structural reasons for the thermodynamic impact of dimer interface mutations on ClC-1 common gating. This would lead to a more thorough understanding of the changes in ClC-1 gating occurring in dominant myotonia. Further research into the interaction of Zn^{2+} with ClC-1 should also elucidate the substate of common gating which has been identified in this research, as well as identifying the precise site of Zn^{2+} binding. This would provide valuable information on the mechanism of drug interactions with ClC-1 common gating, which may lead to possible treatments for ClC-1 related disorders.

It is likely that the mechanism of common gating in ClC-1 is shared in some way across other members of the ubiquitous ClC channel family. Hence, understanding of common gating in ClC-1 channels may provide information that is also applicable to other members of the ClC family. This information may therefore also be useful in discovering treatments for some of the kidney, bone and other disorders which result from mutations in various ClC channel proteins.

Appendix I: Bibliography

Accardi A., Ferrera L. and Pusch M. (2001). Drastic reduction of the slow gate of human muscle chloride channel (ClC-1) by mutation C277S. *J. Physiol. (Lond).* **543**:745-752.

Accardi A. and Miller C. (2004). Secondary active transport mediated by a prokaryotic homologue of ClC Cl^- channels. *Nature* **427**:803-807.

Accardi A. and Pusch M. (2000). Fast and slow gating relaxations in the muscle chloride channel CLC-1. *J. Gen. Physiol.* **116**:433-444.

Adachi S., Uchida S., Ito H., Hata M., Hiroe M., Marumo F. and Sasaki S. (1994). Two isoforms of a chloride channel predominantly expressed in thick ascending limb of Henle's loop and collecting ducts of rat kidney. *J. Biol. Chem.* **269**:17677-17683.

Aggarwal S.K. and MacKinnon R. (1996). Contribution of the S4 segment to gating charge in the Shaker K^+ channel. *Neuron* **16**:1169-1177.

Akabas M.H., Stauffer D.A., Xu M. and Karlin A. (1992). Acetylcholine receptor channel structure probed in cysteine-substitution mutants. *Science* **258**:307-310.

Aromataris E.C., Astill D.S., Rychkov G.Y., Bryant S.H., Bretag A.H. and Roberts M.L. (1999). Modulation of the gating of CIC-1 by S-(-) 2-(4-chlorophenoxy) propionic acid. *Br. J. Pharmacol.* **126**:1375-1382.

Aromataris E.C., Rychkov G.Y., Bennetts B., Hughes B.P., Bretag A.H. and Roberts M.L. (2001). Fast and slow gating of ClC-1: Differential effects of 2-(4- chlorophenoxy) propionic acid and dominant negative mutations. *Mol. Pharmacol.* **60**:200-208.

Astill D.S., Rychkov G., Clarke J.D., Hughes B.P., Roberts M.L. and Bretag A.H. (1996). Characteristics of skeletal muscle chloride channel ClC-1 and point mutant R304E expressed in Sf9 insect cells. *Biochim. Biophys. Acta* **1280**:178-186.

Auld D.S. (2001). Zinc coordination sphere in biochemical zinc sites. *Biometals* **14**:273-313.

Barry P.H. (1994). JPCalc, a software package for calculating liquid junction potential corrections in patch-clamp, intracellular, epithelial and bilayer measurements and for correction junction potential measurements. *J. Neurosci. Methods* **51**:107-116.

Bateman A. (1997). The structure of a domain common to archaebacteria and the homocystinurua disease protein. *Trends Biochem. Sci.* **22**:12-13.

Bauer C.K., Steinmeyer K., Schwarz J.R. and Jentsch T.J. (1991). Completely functional double-barreled chloride channel expressed from a single *Torpedo* cDNA. *Proc. Natl. Acad. Sci. U. S. A.* **88**:11052-11056.

Beck C.L., Fahlke C. and George A.L., Jr. (1996). Molecular basis for decreased muscle chloride conductance in the myotonic goat. *Proc. Natl. Acad. Sci. U. S. A.* **93**:11248-11252.

Bennetts B., Roberts M.L., Bretag A.H. and Rychkov G.Y. (2001). Temperature dependence of human muscle ClC-1 chloride channel. *J. Physiol. (Lond).* **535**:83-93.

Bettoni G., Loiodice F., Tortorella V., Conte Camerino D., Mambrini M., Ferrannini E. and Bryant S.H. (1987). Stereospecificity of the chloride ion channel: The action of chiral clofibric acid analogues. *J. Med. Chem.* **30**:1267-1270.

Bezanilla F. (2002). Voltage sensor movements. *J. Gen. Physiol.* **12-**:465-473.

Bezanilla F. and Armstrong C.M. (1977). Inactivation of the sodium channel: 1. Sodium current experiments. *J. Gen. Physiol.* **70**:549-566.

Birkenhäger R., Otto E., Schürmann M.J., Vollmer M., Ruf E.M., Maierlutz I., Beekmann F., Fekete A., Omran H., Feldmann D., Milford D.V., Jeck N., Konrad M., Landau D., Knoers N.V.A.M., Antignac C., Sudbrack R., Kispert A. and Hildebrandt F. (2001). Mutation of *BSND* causes Bartter syndrome with sensorineural deafness and kidney failure. *Nat. Genet.* **29**:310-314.

Blaustein R.O. and Miller C. (2004). Shake, rattle or roll? *Nature* **427**:499-500.

Bretag A.H. (1987). Muscle chloride channels. *Physiol. Rev.* **67**:618-724.

Bretag A.H., Fietz M.J. and Bennet R.R.J. (1984). The effects of zinc and other transition metal ions on rat skeletal muscle. *Proc. Aust. Physiol. Pharmacol. Soc.* **15**:146P.

Brugnoni R., Galantini S., Confalonieri P., Balestrini M.R., Cornelio F. and Mantegazza R. (1999). Identification of three novel mutations in the major human skeletal muscle chloride channel gene (CLCN1), causing myotonia congenita. *Hum. Mutat.* **14**:447.

Bryant S.H. and Morales-Aguilera A. (1971). Chloride conductance in normal and myotonic muscle fibres and the action of monocarboxylic aromatic acids. *J. Physiol. (Lond).* **219**:367-383.

Buyse G., Voets T., Tytgat J., De Greef C., Droogmans G., Nilius B. and Eggermont J. (1997). Expression of human pICln and ClC-6 in *Xenopus* oocytes induces an identical endogenous chloride conductance. *J. Biol. Chem.* **272**:3615-3621.

Chang G., Spencer R.H., Lee A.T., Barclay M.T. and Rees D.C. (1998). Structure of the MscL homolog from *Mycobacterium tuberculosis*: A gated mechanosensitive ion channel. *Science* **282**:2220-2226.

Chen T.Y. (1998). Extracellular zinc ion inhibits ClC-0 chloride channels by facilitating slow gating. *J. Gen. Physiol.* **112**:715-726.

Chen T.Y. and Miller C. (1996). Nonequilibrium gating and voltage dependence of the ClC-0 Cl^- channel. *J. Gen. Physiol.* **108**:237-250.

Clark S., Jordt S.-E., Jentsch T.J. and Mathie A. (1998). Characterization of the hyperpolarization-activated chloride current in dissociated rat sympathetic neurons. *J. Physiol. (Lond).* **506**:665-678.

Conte Camerino D., Mambrini M., De Luca A., Tricarico D., Bryant S.H., Tortorella V. and Bettoni G. (1988a). Enantiomers of clofibric acid analogs have opposite actions on rat skeletal muscle chloride channels. *Pflugers Arch.*

Conte Camerino D., Tortorella V., Bettoni G., Bryant S.H., De Luca A., Mambrini M., Tricarico D. and Grasso G. (1988b). A stereospecific binding site regulates the Cl^- ion channel in rat skeletal muscle. *Pharmacol. Res. Commun.* **20**:1077-1078.

Conte-Camerino D., Tortorella V., Ferranini E. and Bryant S.H. (1984). The toxic effects of clofibrate and its metabolite on mammalian skeletal muscle: An electrophysiological study. *Arch. Toxicol.* **7**:482-484.

Corringer J.-P., Le Novère N. and Changeux J.-P. (2000). Nicotinic receptors at the amino acid level. *Annu. Rev. Pharmacol. Toxicol.* **40**:431-458.

Corringer P.J., Bertrand S., Galzi J.L., Devillers-Thiéry A., Changeux J.P. and Bertrand D. (1999). Mutational analysis of the charge selectivity filter of the α7 nicotnic acetylcholine receptor. *Neuron* **22**:831-843.

Cymes G.D., Grosman C. and Auerbach A. (2002). Structure of the transition state of gating in the acetylcholine receptor channel pore: A Φ-value analysis. *Biochemistry (Mosc).* **41**:5548-5555.

Dani J.A. and Mayar M.L. (1995). Structure and function of glutamate and nicotinic acetylcholine receptors. *Curr. Opin. Neurobiol.* **5**:310-317.

De Luca A., Tricarico D., Wagner R., Bryant S.H., Tortorella V. and Conte Camerino D. (1992). Opposite effects of enantiomers of clofibric acid derivative on rat skeletal muscle chloride conductance: Antagonism studies and theoretical modelling of two different receptor site interactions. *J. Pharmacol. Exp. Ther.* **260**:364-368.

DeCoursey T.E. and Cherny V.V. (1998). Temperature Dependence of Voltage-gated H^+ Currents in Human Neutrophils, Rat Alveolar Epithelial Cells, and Mammalian Phagocytes. *J Gen Physiol* **112**:503-522.

Dick G.M., Bradley K.K., Horowitz B., Hume J.R. and Sanders K.M. (1998). Functional and molecular identification of a novel chloride conductance in canine colonic smooth muscle. *Am. J. Physiol.* **275**:C940-950.

Doyle D.A., Cabral J.M., Pfuetzner R.A., Kuo A., Gulbis J.M., Cohen S.L., Chait B.T. and MacKinnon R. (1998). The structure of the potassium channel: Molecular basis of K^+ conduction and selectivity. *Science* **280**:69-77.

Dromgoole S., Campion D. and Peter J. (1975). Myotonia induced by clofibrate and sodium chlorophenoxy isobutyrate. *Biochem. Med.* **14**:238-240.

Duan D., Cowley S., Horowitz B. and Hume J.R. (1999). A serine residue in ClC-3 links phosphorylation-dephosphorylation to chloride channel regulation by cell volume. *J. Gen. Physiol.* **113**:57-70.

Duan D., Winter C., Cowley S., Hume J.R. and Horowitz B. (1997). Molecular identification of a volume-regulated chloride channel. *Nature* **390**:417-421.

Duffield M., Rychkov G., Bretag A. and Roberts M. (2003). Involvement of helices at the dimer interface in ClC-1 common gating. *J. Gen. Physiol.* **121**:149-161.

Dutzler R., Campbell E.B., Cadene M., Chait B.T. and MacKinnon R. (2002). X-ray structure of a ClC chloride channel at 3.0 Å reveals the molecular basis of anion selectivity. *Nature* **415**:287-294.

Dutzler R., Campbell E.B. and MacKinnon R. (2003). Gating the selectivity filter in ClC chloride channels. *Science* **300**:108-112.

Eberstein A., Goodgold J. and Johnston R. (1978). Clofibrate-induced myotonia in the rat. *Experientia* **34**:1607.

Enz R., Ross B.J. and Cutting G.R. (1999). Expression of the voltage-gated chloride channel ClC-2 in rod bipolar cells of the rat retina. *J. Neurosci.* **19**:9841-9847.

Estevez R., Boettger T., Stein V., Birkenhäger R., Otto E., Hildebrandt F. and Jentsch T.J. (2001). Barttin is a Cl^- channel beta-subunit crucial for renal Cl^- reabsorption and inner ear K^+ secretion. *Nature* **414**:558-561.

Estévez R., Schroeder B.C., Accardi A., Jentsch T.J. and Pusch M. (2003). Conservation of chloride channel structure revealed by an inhibitor binding site in ClC-1. *Neuron* **38**:47-59.

Fahlke C., Durr C. and George A.L.J. (1997a). Mechanism of ion permeation in skeletal muscle chloride channels. *J. Gen. Physiol.* **110**:551-564.

Fahlke C., Knittle T., Gurnett C.A., Campbell K.P. and George A.L.J. (1997b). Subunit stoichiometry of human muscle chloride channels. *J. Gen. Physiol.* **109**:93-104.

Fahlke C., Rhodes T.H., Desai R.R. and George A.L.J. (1998). Pore stoichiometry of a voltage-gated chloride channel. *Nature* **394**:687-690.

Fahlke C., Rudel R., Mitrovic N., Zhou M. and George A.L.J. (1995). An aspartic acid residue important for voltage-dependent gating of human muscle chloride channels. *Neuron* **15**:463-472.

Fahlke C., Yu H.T., Beck C.L., Rhodes T.H. and George A.L.J. (1997c). Pore-forming segments in voltage-gated chloride channels. *Nature* **390**:529-532.

Fong P., Rehfeldt A. and Jentsch T.J. (1998). Determinants of slow gating in ClC-0, the voltage-gated chloride channel of *Torpedo marmorata*. *Am. J. Physiol.* **274**:C966-973.

Furman R.E. and Barchi R.L. (1978). The pathophysiology of myotonia produced by aromatic carboxylic acids. *Ann. Neurol.* **4**:357-365.

Furukawa T., Ogura T., Katayama Y. and Hiraoka M. (1998). Characteristics of rabbit ClC-2 current expressed in *Xenopus* oocytes and its contribution to volume regulation. *Am. J. Physiol.* **274**:C500-512.

Galzi J.-L. and Changeux J.-P. (1994). Neurotransmitter-gated ion channels as unconventional allosteric proteins. *Curr. Opin. Struct. Biol.* **4**:554-565.

Galzi J.L., Devillers-Thiéry A., Hussey N., Bertrand S., Changeux J.P. and Bertrand D. (1992). Mutations in the channel domain of a neuronal nicotinic receptor convert ion selectivity from cationic to anionic. *Nature* **359**:500-505.

Gandhi C.S. and Isacoff E.Y. (2002). Molecular models of voltage sensing. *J. Gen. Physiol.* **120**:445-463.

Goldberg A.F. and Miller C. (1991). Solubilization and functional reconstitution of a chloride channel from *Torpedo californica* electroplax. *J. Membr. Biol.* **124**:199-206.

Gründer S., Thiemann A., Pusch M. and Jentsch T.J. (1992). Regions involved in the opening of the ClC-2 chloride channel by voltage and cell volume. *Nature* **360**:759-762.

Hamill O.P. and Martinac B. (2001). Molecular basis of mechanotransduction in living cells. *Physiol. Rev.* **81**:685-740.

Hanke W. and Miller C. (1983). Single chloride channel from *Torpedo* electroplax: Activation by protons. *J. Gen. Physiol.* **82**:25-45.

Hille B. (2001a). Ionic channels of excitable membranes. Sunderland, MA, Sinauer Associates: 406-407, 410.

Hille B. (2001b). Ionic channels of excitable membranes. Sunderland, MA, Sinauer Associates: 503-537.

Ho S.N., Hunt H.D., Horton R.M., Pullen J.K. and Pease L.R. (1989). Site-directed mutagenesis by overlap extension using the polymerase chain reaction. *Gene* **77**:51-59.

Holmgren M., Jurman M.E. and Yellen G. (1996). N-type inactivation and the S4-S5 region of the Shaker K^+ channel. *J. Gen. Physiol.* **108**:195-206.

Horn R. (2002). Coupled movements in voltage-gated ion channels. *J. Gen. Physiol.* **120**:449-453.

Hoshi T., Zagotta W.N. and Aldrich R.W. (1990). Biophysical and molecular mechanisms of *Shaker* potassium channel inactivation. *Science* **250**:533-538.

Hutter O.F. and Warner A.E. (1967). Action of some foreign cations and anions on the chloride permeability of frog muscle. *J. Physiol. (Lond).* **189**:445-460.

Isacoff E.Y., Jan Y.N. and Jan L.Y. (1991). Putative receptor for the cytoplasmic inactivation gate in the *Shaker* K^+ channel. *Nature* **353**:86-90.

Jentsch T.J. (1996). Chloride channels: A molecular perspective. *Curr. Opin. Neurobiol.* **6**:303-310.

Jentsch T.J., Stein V., Weinreich F. and Zdebik A.A. (2002). Molecular structure and physiological function of chloride channels. *Physiol. Rev.* **82**:503-508.

Jentsch T.J., Steinmeyer K. and Schwarz G. (1990). Primary structure of *Torpedo marmorata* chloride channel isolated by expression cloning in *Xenopus* oocytes. *Nature* **348**:510-514.

Jiang Y., Lee A., Chen J., Cadene M., Chait B.T. and MacKinnon R. (2002a). Crystal structure and mechanism of a calcium-gated potassium channel. *Nature* **417**:515-522.

Jiang Y., Lee A., Chen J., Cadene M., Chait B.T. and MacKinnon R. (2002b). The open pore conformation of potassium channels. *Nature* **417**:523-526.

Jiang Y., Lee A., Chen J., Ruta V., Cadene M., Chait B.T. and MacKinnon R. (2003a). X-ray structure of a voltage-dependent K^+ channel. *Nature* **423**:33-41.

Jiang Y., Ruta V., Chen J., Lee A. and MacKinnon R. (2003b). The principle of gating charge movement in a voltage-dependent K^+ channel. *Nature* **423**:42-48.

Karlin A. (1993). Structure of nicotinic acetylcholine receptors. *Curr. Opin. Neurobiol.* **3**:299-309.

Karlin A. (2002). Emerging structure of the nicotinic acetylcholine receptors. *Nature Rev. Neurosci.* **3**:102-114.

Karlin S. and Zhu Z.Y. (1997). Classification of mononuclear zinc metal sites in protein structures. *Proc. Natl. Acad. Sci. U. S. A.* **94**:14231-14236.

Kawasaki M., Fukuma T., Yamauchi K., Sakamoto H., Marumo F. and Sasaki S. (1999). Identification of an acid-activated Cl^- channel from human skeletal muscles. *Am. J. Physiol.* **277**:C948-954.

Kawasaki M., Uchida S., Monkawa T., Miyawaki A., Mikoshiba K., Marumo F. and Sasaki S. (1994). Cloning and expression of a protein kinase C-regulated chloride channel abundantly expressed in rat brain neuronal cells. *Neuron* **12**:597-604.

Keramidas A., Moorhouse A.J., French C.R., Schofield P.R. and Barry P.H. (2000). M2 pore mutations convert the glycine receptor channel from being anion- to cation-selective. *Biophys. J.* **78**:247-259.

Keramidas A., Moorhouse A.J., Pierce K.D., Schofield P.R. and Barry P.H. (2002). Cation-selective mutations in the M2 domain of the inhibitory glycine receptor channel reveal determinants of ion-charge selectivity. *J. Gen. Physiol.* **119**:393-410.

Kieferle S., Fong P., Bens M., Vandewalle A. and Jentsch T.J. (1994). Two highly homologous members of the ClC chloride channel family in both rat and human kidney. *Proc. Natl. Acad. Sci. U. S. A.* **91**:6943-6947.

Koch M.C., Steinmeyer K., Lorenz C., Ricker K., Wolf F., Otto M., Zoll B., Lehmann-Horn F., Grzeschik K.H. and Jentsch T.J. (1992). The skeletal muscle chloride channel in dominant and recessive human myotonia. *Science* **257**:797-800.

Kornak U., Kasper D., Bösl M.R., Kaiser E., Schweizer M., Schulz A., Friedrich W., Delling G. and Jentsch T.J. (2001). Loss of the ClC-7 chloride channel leads to osteopetrosis in mice and men. *Cell* **104**:205-215.

Kubisch C., Schmidt-Rose T., Fontaine B., Bretag A.H. and Jentsch T.J. (1998). ClC-1 chloride channel mutations in myotonia congenita: Variable penetrance of mutations shifting the voltage dependence. *Hum. Mol. Genet.* **7**:1753-1760.

Kurz L., Wagner S., George A.L.J. and Rudel R. (1997). Probing the major skeletal muscle chloride channel with Zn^{2+} and other sulfhydryl-reactive compounds. *Pflugers Arch.* **433**:357-363.

Kurz L.L., Klink H., Jakob I., Kuchenbecker M., Benz S., Lehmann-Horn F. and Rudel R. (1999). Identification of three cysteines as targets for the Zn^{2+} blockade of the human skeletal muscle chloride channel. *J. Biol. Chem.* **274**:11687-11692.

Kwiecinski H. (1978). Myotonia induced with clofibrate in rats. *J. Neurol.* **219**:107-116.

Kwiecinski H., Lehmann-Horn F. and Rudel R. (1988). Drug-induced myotonia in human intercostal muscle. *Muscle Nerve* **11**:576-581.

Langer T. and Levy R.I. (1968). Acute muscular syndrome associated with administration of clofibrate. *N. Engl. J. Med.* **279**:856-858.

Lehmann-Horn F. and Rüdel R. (1997). Channelopathies: Their contribution to our knowledge about voltage-gated ion channels. *News Physiol. Sci.* **12**:105-112.

Lester H.A. (1992). The permeation pathways of neurotransmitter-gated ion channels. *Annu. Rev. Biophys. Biomol. Struct.* **21**:267-292.

Lin Y.W., Lin C.W. and Chen T.Y. (1999). Elimination of the slow gating of ClC-0 chloride channel by a point mutation. *J. Gen. Physiol.* **114**:1-12.

Lindenthal S., Schmieder S., Ehrenfeld J. and Wills N.K. (1997). Cloning and functional expression of a ClC Cl^- channel from the renal cell line A6. *Am. J. Physiol.* **273**:C1176-1185.

Lipicky R.J. and Bryant S.H. (1966). Sodium, potassium and chloride fluxes in intercostal muscle from normal goats and goats with hereditary myotonia. *J. Gen. Physiol.* **50**:89-111.

Lipicky R.J., Bryant S.H. and Salmon J.H. (1971). Cable parameters, sodium, potassium, chloride, and water content, and potassium efflux in isolated external intercostal muscle of normal volunteers and patients with myotonia congenita. *J. Clin. Invest.* **50**:2091-2103.

Lloyd S.E., Pearce S.H., Fisher S.E., Steinmeyer K., Schwappach B., Scheinman S.J., Harding B., Bolino A., Devoto M., Goodyer P., Rigden S.P., Wrong O., Jentsch T.J., Craig I.W. and Thakker R.V. (1996). A common molecular basis for three inherited kidney stone diseases. *Nature* **379**:445-449.

Lopez G.A., Jan Y.N. and Jan L.Y. (1994). Evidence that the S6 segments of the *Shaker* voltage-gated K^+ channel comprises part of the pore. *Nature* **367**:179-182.

Lorenz C., Pusch M. and Jentsch T.J. (1996). Heteromultimeric CLC chloride channels with novel properties. *Proc. Natl. Acad. Sci. U. S. A.* **93**:13362-13366.

Ludewig U., Pusch M. and Jentsch T.J. (1996). Two physically distinct pores in the dimeric ClC-0 chloride channel. *Nature* **383**:340-343.

Ludewig U., Pusch M. and Jentsch T.J. (1997). Independent gating of single pores in CLC-0 chloride channels. *Biophys. J.* **73**:789-797.

MacKinnon R., Aldrich R.W. and Lee A.W. (1993). Functional stoichiometry of *Shaker* potassium channel inactivation. *Science* **262**:757-759.

Meyer-Kleine C., Steinmeyer K., Ricker K., Jentsch T.J. and Koch M.C. (1995). Spectrum of mutations in the major human skeletal muscle chloride channel gene (CLCN1) leading to myotonia. *Am. J. Hum. Genet.* **57**:1325-1334.

Middleton R.E., Pheasant D.J. and Miller C. (1994). Purification, reconstitution, and subunit composition of a voltage-gated chloride channel from *Torpedo* electroplax. *Biochemistry (Mosc).* **33**:13189-13198.

Middleton R.E., Pheasant D.J. and Miller C. (1996). Homodimeric architecture of a ClC-type chloride ion channel. *Nature* **383**:337-340.

Miller C. (1982). Open-state substructure of single chloride channels from *Torpedo electroplax. Philos. Trans. R. Soc. Lond. B. Biol. Sci.* **299**:401-411.

Miller C. and White M.M. (1984). Dimeric structure of single chloride channels from *Torpedo electroplax. Proc. Natl. Acad. Sci. U. S. A.* **81**:2772-2775.

Miller G. (2003). The puzzling portrait of a pore. *Science* **300**:2020-2022.

Mindell J.A., Maduke M., Miller C. and Grigorieff N. (2001). Projection structure of a ClC-type chloride channel at 6.5Å resolution. *Nature* **409**:219-223.

Miyazawa A., Fujiyoshi Y. and Unwin N. (2003). Structure and gating mechanism of the acetylcholine receptor pore. *Nature* **423**:949-955.

Palade P.T. and Barchi R.L. (1977). On the inhibition of muscle membrane chloride conductance by aromatic carboxylic acids. *J. Gen. Physiol.* **69**:879-896.

Perozo E., Cortes D.M., Sompornpisut P., Kloda A. and Martinac B. (2002). Open channel structure of MscL and the gating mechanism of mechanosensitive channels. *Nature* **418**:942-948.

Ponting C.P. (1997). CBS domains in ClC chloride channels implicated in myotonia and nephrolithiasis (kidney stones). *J. Mol. Med.* **75**:160-163.

Pusch M. (2002). Myotonia caused by mutations in the muscle chloride channel gene CLCN1. *Hum. Mutat.* **19**:423-434.

Pusch M., Accardi A., Liantonio A., Ferrera L., De Luca A., Camerino D.C. and Conti F. (2001). Mechanism of block of single protopores of the *Torpedo* chloride channel ClC-0 by 2-(*p*-chlorophenoxy)butyric Acid (CPB). *J. Gen. Physiol.* **118**:45-62.

Pusch M., Accardi A., Liantonio A., Guida P., Traverso S., Camerino D.C. and Conti F. (2002). Mechanisms of block of muscle type CLC chloride channels (Review). *Mol. Membr. Biol.* **19**:285-292.

Pusch M., Jordt S.E., Stein V. and Jentsch T.J. (1999). Chloride dependence of hyperpolarization-activated chloride channel gates. *J. Physiol. (Lond).* **515 (Pt 2)**:341-353.

Pusch M., Liantonio A., Bertorello L., Accardi A., De Luca A., Pierno S., Tortorella V. and Camerino D.C. (2000). Pharmacological characterization of chloride channels belonging to the ClC family by the use of chiral clofibric acid derivatives. *Mol. Pharmacol.* **58**:498-507.

Pusch M., Ludewig U. and Jentsch T.J. (1997). Temperature dependence of fast and slow gating relaxations of ClC-0 chloride channels. *J. Gen. Physiol.* **109**:105-116.

Pusch M., Ludewig U., Rehfeldt A. and Jentsch T.J. (1995a). Gating of the voltage-dependent chloride channel CIC-0 by the permeant anion. *Nature* **373**:527-531.

Pusch M., Steinmeyer K. and Jentsch T.J. (1994). Low single channel conductance of the major skeletal muscle chloride channel, ClC-1. *Biophys. J.* **66**:149-152.

Pusch M., Steinmeyer K. and Jentsch T.J. (1995b). Mutations in dominant human myotonia congenita drastically alter the voltage dependence of the CLC-1 chloride channel. *Neuron* **15**:1455-1463.

Rees D.C., Chang G. and Spencer R.H. (2000). Crystallographic analyses of ion channels: Lessons and challenges. *J. Biol. Chem.* **275**:713-716.

Rudel R. and Lehmann-Horn F. (1985). Membrane changes in cells from myotonia patients. *Physiol. Rev.* **65**:310-356.

Rychkov G., Pusch M., Roberts M. and Bretag A. (2001). Interaction of hydrophobic anions with the rat skeletal muscle chloride channel ClC-1: Effects on permeation and gating. *J. Physiol. (Lond).* **530**:379-393.

Rychkov G.Y., Astill D.S., Bennetts B., Hughes B.P., Bretag A.H. and Roberts M.L. (1997). pH-dependent interactions of Cd^{2+} and a carboxylate blocker with the rat C1C-1 chloride channel and its R304E mutant in the Sf-9 insect cell line. *J. Physiol. (Lond).* **501**:355-362.

Rychkov G.Y., Pusch M., Astill D.S., Roberts M.L., Jentsch T.J. and Bretag A.H. (1996). Concentration and pH dependence of skeletal muscle chloride channel ClC-1. *J. Physiol. (Lond).* **497**:423-435.

Rychkov G.Y., Pusch M., Roberts M.L., Jentsch T.J. and Bretag A.H. (1998). Permeation and block of the skeletal muscle chloride channel, ClC-1, by foreign anions. *J. Gen. Physiol.* **111**:653-665.

Sakamoto H., Kawasaki M., Uchida S., Sasaki S. and Marumo F. (1996). Identification of a new outwardly rectifying Cl^- channel that belongs to a subfamily of the ClC Cl^- channels. *J. Biol. Chem.* **271**:10210-10216.

Saviane C., Conti F. and Pusch M. (1999). The muscle chloride channel ClC-1 has a double-barreled appearance that is differentially affected in dominant and recessive myotonia. *J. Gen. Physiol.* **113**:457-468.

Scheinman S.J. (1998). X-linked hypercalciuric nephrolithiasis: Clinical syndromes and chloride channel mutations. *Kidney Int.* **53**:3-17.

Schmidt-Rose T. and Jentsch T.J. (1997a). Reconstitution of functional voltage-gated chloride channels from complementary fragments of CLC-1. *J. Biol. Chem.* **272**:20515-20521.

Schmidt-Rose T. and Jentsch T.J. (1997b). Transmembrane topology of a CLC chloride channel. *Proc. Natl. Acad. Sci. U. S. A.* **94**:7633-7638.

Scott J.W., Hawley S.A., Green K.A., Anis M., Stewart G., Scullion G.A., Norman D.G., Hardie D.G. and Kemp B.E. (2004). CBS domains form energy-sensing modules whose

binding of adenosine ligands is disrupted by disease mutations. *J. Clin. Invest.* **113**:274-284.

Seoh S.A., Sigg D., Papazian D.M. and Bezanilla F. (1996). Voltage-sensing residues in the S2 and S4 segments of the Shaker K^+ channel. *Neuron* **16**:1159-1167.

Stanfield P.R. (1970). The differential effects of tetraethylammonium and zinc ions on the resting conductance of frog skeletal muscle. *J Physiol (Lond)* **209**:231-256.

Starace D.M. and Bezanilla F. (2004). A proton pore in a potassium channel voltage sensor reveals a focused electric field. *Nature* **427**:548-553.

Steinmeyer K., Klocke R., Ortland C., Gronemeier M., Jockusch H., Gründer S. and Jentsch T.J. (1991a). Inactivation of muscle chloride channel by transposon insertion in myotonic mice. *Nature* **354**:304-308.

Steinmeyer K., Lorenz C., Pusch M., Koch M.C. and Jentsch T.J. (1994). Multimeric structure of ClC-1 chloride channel revealed by mutations in dominant myotonia congenita (Thomsen). *EMBO J.* **13**:737-743.

Steinmeyer K., Ortland C. and Jentsch T.J. (1991b). Primary structure and functional expression of a developmentally regulated skeletal muscle chloride channel. *Nature* **354**:301-304.

Steinmeyer K., Schwappach B., Bens M., Vandewalle A. and Jentsch T.J. (1995). Cloning and functional expression of rat CLC-5, a chloride channel related to kidney disease. *J. Biol. Chem.* **270**:31172-31177.

Sukharev S.I., Blount P., Martinac B. and Kung C. (1997). Mechanosensitive channels of *Escherichia coli*: The MscL gene, protein, and activities. *Annu. Rev. Physiol.* **59**:633-657.

Thiemann A., Gründer S., Pusch M. and Jentsch T.J. (1992). A chloride channel widely expressed in epithelial and non-epithelial cells. *Nature* **356**:57-60.

Uchida S., Sasaki S., Furukawa T., Hiraoka M., Imai T., Hirata Y. and Marumo F. (1993). Molecular cloning of a chloride channel that is regulated by dehydration and expressed predominantly in kidney medulla. *J Biol Chem* **268**:3821-3824.

von Weikersthal S.F., Barrand M.A. and Hladky S.B. (1999). Functional and molecular characterization of a volume-sensitive chloride current in rat brain endothelial cells. *J. Physiol. (Lond).* **516**:75-84.

Weinreich F. and Jentsch T.J. (2001). Pores formed by single subunits in mixed dimers of different CLC chloride channels. *J. Biol. Chem.* **276**:2347-2353.

Wollnik B., Kubisch C., Steinmeyer K. and Pusch M. (1997). Identification of functionally important regions of the muscular chloride channel ClC-1 by analysis of recessive and dominant myotonic mutations. *Hum. Mol. Genet.* **6**:805-811.

Wood J.M. (1999). Osmosensing by bacteria: Signals and membrane-based sensors. *Microbiol. Mol. Biol. Rev.* **63**:230-262.

Wrong O.M., Norden A.G. and Feest T.G. (1994). Dent's disease: A familial proximal renal tubular syndrome with low-molecular-weight proteinuria, hypercalciuria, nephrocalcinosis, metabolic bone disease, progressive renal failure and a marked male predominance. *Q. J. Med.* **87**:473-493.

Wu F., Roche P., Christie P.T., Loh N.Y., Reed A.A., Esnouf R.M. and Thakker R.V. (2003). Modeling study of human renal chloride channel (hCLC-5) mutations suggests a structural-functional relationship. *Kidney Int.* **63**:1426-1432.

Wu F.F., Ryan A., Devaney J., Warnstedt M., Korade-Mirnics Z., Poser B., Escriva M.J., Pegoraro E., Yee A.S., Felice K.J., Giuliani M.J., Mayer R.F., Mongini T., Palmucci L., Marino M., Rudel R., Hoffman E.P. and Fahlke C. (2002). Novel CLCN1 mutations with unique clinical and electrophysiological consequences. *Brain* **125**:2392-2407.

Zagotta W.N., Hoshi T. and Aldrich R.W. (1990). Restoration of inactivation in mutants of *Shaker* potassium channels by a peptide derived from ShB. *Science* **250**:568-571.

Zhang J., Sanguinetti M.C., Kwiecinski H. and Ptacek L.J. (2000). Mechanism of inverted activation of ClC-1 channels caused by a novel myotonia congenita mutation. *J. Biol. Chem.* **275**:2999-3005.